Materials for Well Integrity

Performance of Setting Materials for Well Cementing Operation

by

Mohammadreza Kamali

Thesis submitted in fulfilment of
the requirements for the degree of
PHILOSOPHIAE DOCTOR
(PhD)

Faculty of Science and Technology
Institute of Energy and Petroleum Engineering
Spring 2022

University of Stavanger
NO-4036 Stavanger
NORWAY
www.uis.no

ISBN: 978-82-8439-079-6
ISSN: 1890-1387
PhD: Thesis UiS No. 642

ACKNOWLEDGEMENTS

I would like to express my sincere gratitude to my supervisors Professor Mahmoud Khalifeh and Professor Arild Saasen for their patience and support and for giving me the opportunity to lead this project.

I gratefully acknowledge the Research Council of Norway for financing this project. I would like to thank AkerBP ASA, Equinor ASA, TotalEnergies, Halliburton, Wellcem, Saferock AS, and Altiss Technologies for providing materials and technical information. I also appreciate inputs from Laurent Delabroy, Rune Godøy, Johan Kverneland, Salim Taoutaou, Carl Johnson, Gunnar Lende, Espen Sørensen, Svein Normann, Minli Xie, and Heiko Plack.

A special thanks to all the staff and engineers at the Department of Energy and Petroleum Engineering (IEP), and the Department of Mechanical and Structural Engineering and Material Science (IMBM) for their massive support in my three-year project. I would like to thank Øystein Arild, Hilde Jonsbråten, Mona Minde, Caroline Rudd, Jostein Djuve, Kim Andre Vorland, Inger Johanne Olsen, Caroline Einvik, Ola Ketil Siqveland, Johannes Jensen, Emil Kristiansen, and Samdar Kakay. Without their help, the massive tests in this project would not be possible. I also appreciate Irene Heggstad, Andreas Delimitis, and Wakshum Tucho for helping with the electron microscope.

Finally, and perhaps most importantly, I would like to express my deep gratitude to my wife and my parents for their endless love and support.

Mohammadreza Kamali

Stavanger, Norway - 2022

PREFACE

Primary cementing operation is the process of pumping and placing a cementitious slurry in a well. After setting, the so-called barrier material has to provide zonal isolation in the annular gap behind casing string. After a hundred years of using hydraulic Portland cement as prime material for cementing operation, although the chemistry of the material is well-developed, still shortcomings are reported in short- and long-term properties. Safe and cost-efficient operations have been the motivation for improving the performance of barrier material. Additionally, annual increase of the carbon tax is a driving force for switching to green alternatives to Portland cement.

The present study includes scientific examination of candidate barrier materials for cementing operation. These materials are an industrial class of expansive cement, a non-cement-based pozzolanic material, an inorganic polymer known as geopolymer, and organic thermosetting resin. The materials were assessed aiming to evaluate their performance at equal conditions.

The thesis is divided into two main sections comprising a core that describe the research project and appended papers discussing scientific achievements. The outcome of this study includes strengths and weaknesses of each material, which are published in seven scientific papers: three journals, two peer-reviewed conferences, and two SPE conferences. The papers are included as Appendix and labeled using Roman numerals. In the present review, same numerals are used when referring to the papers.

Paper I includes fluid-state properties of the candidate barrier material. Density, viscosity profile, static fluid-loss, and the pumpability of the materials are tested at bottom-hole circulating temperature.

Paper II presents short-term mechanical properties of Portland cement-based systems and highlights the effect of chemical additives on the mix design. In this study, the mechanical properties of expansive cement and API neat class G cement are included. The samples were cured from one day to fourteen days at bottom-hole static temperature and under elevated pressure.

Paper III includes the mechanical properties of candidate barrier materials. The short-term mechanical properties were tested up to seven days.

Paper IV shows mechanical properties of the materials up to one month. In this paper, uniaxial compressive strength, tensile strength, and Young's modulus are measured and possible correlations between these parameters are investigated. Moreover, sonic strength development rate of the materials is tested by using ultrasonic cement analyzer.

Paper V includes shear bond and hydraulic sealability of cement-based systems and geopolymer. Shear bond strength of these materials is examined at two circumferential surfaces by placing the cementitious material between a pipe and bar. For both shear bond and hydraulic sealability, both clean and rusty steel are considered as casing string representatives.

Paper VI has bond strength and hydraulic sealability of the setting materials. The interface of materials with steel is studied by scanning electron microspore. Morphology and mineralogy of materials at their interface satisfy the behavior of materials in shear bond and hydraulic sealability tests.

Paper VII includes mechanical properties of the materials up to nine months of curing at bottom-hole static temperature and elevated pressure. Additionally, morphology and mineralogy of the materials are tested to support the mechanical behavior of materials.

List of Publications

I. Kamali, M., Khalifeh, M., Saasen, A., Delabroy, L., & Godøy, R. (2022). Materials for Well Integrity–Rheological Behavior Study. Paper is Submitted to the SPE Norway Subsurface Conference. Bergen, Norway.

II. Kamali, M., Khalifeh, M., Saasen, A., & Delabroy, L. (2020). Materials for Well Integrity–Short-Term Mechanical Properties of Cement Systems. Paper presented at the SPE Norway Subsurface Conference. Bergen, Norway. Doi: https://doi.org/10.2118/200739-MS

III. Kamali, M., Khalifeh, M., Saasen, A., & Delabroy, L. (2020). Materials for Well Integrity- Characterization of Short-Term Mechanical Properties. Paper presented at the Proceedings of the ASME 2020 39th International Conference on Ocean, Offshore and Arctic Engineering OMAE2020. Doi: https://doi.org/10.1115/OMAE2020-18623

IV. Kamali, M., Khalifeh, M., Saasen, A., Godøy, R., & Delabroy, L. (2021). Alternative Setting Materials for Primary Cementing and Zonal Isolation–Laboratory Evaluation of Rheological and Mechanical Properties. *Journal of Petroleum Science and Engineering*, 108455. Doi: https://doi.org/10.1016/j.petrol.2021.108455

V. Kamali, M., Khalifeh, M., Eid, E., & Saasen, A. (2021). Experimental Study of Hydraulic Sealability and Shear Bond Strength of Cementitious Barrier Materials. *Journal of*

Energy Resources Technology, 1-33. Doi: https://doi.org/10.1115/1.4051269

VI. Kamali, M., Khalifeh, M., & Saasen, A. (2022). Bonding Mechanism of Zonal Isolation Materials to Casing and Pipe Materials. Under Review at a scientific journal.

VII. Kamali, M., Moreira, P., Khalifeh, M., & Saasen, A. (2022). Long-Term Mechanical Properties of Barrier Materials for Cementing Operations – Analysis of Morphology and Micro-structure. Paper is Accepted at the Proceedings of the ASME 2022 41st International Conference on Ocean, Offshore and Arctic Engineering OMAE2022.

Table of Contents

Table of Figures

List of Tables

NOMENCLATURE

A	Area
API	The American Petroleum Institute
Bc	Bearden unit of consistency
BHCT	Bottom-hole circulating temperature
BHST	Bottom-hole static temperature
BSE	Backscattered electrons
BWOC	By weight of cement
C_3A	Tricalcium aluminate
C_4AF	Tetracalcium aluminoferrite
C_2S	Dicalcium silicate
C_2SH	Dicalcium silicate hydrate
C_3S	Tricalcium silicate
Ca	Calcium
CCUS	Carbon capture, utilization and storage
CH	Calcium hydroxide
CSH	Calcium silicate hydrate
D	Diameter
E	Young’s modulus
EDS	Energy-dispersive X-ray spectroscopy
F	Force
ft	foot
GGBFS	Ground granulated blast furnace slag
GOF	Goodness of fit
GPa	Giga pascal
H	Hydrogen
HSR	High sulfate resistance
K	Consistency factor of the flow
L	Length
lb	Pound mass
Mg	Magnesium
mm	Millimeter
MPa	Mega Pascal
MSR	Medium sulfate resistance
N	Newton
n	Flow index

NCS	Norwegian continental shelf
NORSOK	The Norwegian shelf's competitive position
O	Oxygen
OPC	Ordinary Portland cement
PP&A	Permanent plug and abandonment
ppg	Pound per gallon
PSA	Petroleum Safety Authority
psi	Pound per square inch
Q	API fluid-loss
R_{wp}	Weighted profile R-factor
RAS	Right Angle Set
RNNP	Trends in risk level
RPM	Rotation per minute
SBS	Shear bond strength
SCP	Sustained casing pressure
SE	Secondary electrons
SEM	Scanning electron microscope
sg	Specific gravity
Si	Silicon
SRA	Shrinkage reducing admixture
SSI	Steel-setting material interface
T	Thickness
t	time
TS	Tensile strength
UCA	Ultrasonic cement analyzer
UCS	Uniaxial compressive strength
V	Cumulative volume
WBE	Well barrier elements
Greek	
α	alpha
$\dot{\gamma}$	Shear rate
σ	Compressive stress
σ_t	Tensile stress
τ	Shear stress

1 Introduction

In oil and gas industry, wells are the vital veins delivering hydrocarbons from depths to the surface or injecting fluids to the reservoirs. After reservoir exploration and economic feasibility studies, the geographical location of production well is determined by multiple complex studies over strata. Once the well is designed and the guidelines are set, well construction is commenced.

Initially, the necessary equipment is mobilized to the location and gets ready for drilling. Well construction is commenced by drilling an openhole on the crust or seabed, depending on the location of the well. In drilling operations, regardless of well purpose, either it is oil and gas, geothermal or carbon capture, utilization and storage (CCUS), production or injection optimization depends on appropriate completion and subsequently, maintaining well integrity of primary cement job.

The first cementing operation was performed in 1905 in Lompoc oil field located in California, USA aiming to stop downhole water flow over a sedimentary rock. Followed by placing the cement, the well was shut down for 28 days allowing the cement to set. However, the primary cementing behind casing was patented by Erle P. Halliburton and executed in 1920s to stabilize the borehole in a sandstone formation above a reservoir (Bearden and Lane, 1961). Initially, the wells were cemented by common construction cements and a number of additives to improve performance of the cement in downhole condition. Later, American Petroleum Institute (API) started to study cement for drilling operations and established standards to evaluate the performance of cement and various additives for drilling operations. Nowadays, a tremendous number of additives are available to improve and control the performance of Ordinary Portland Cement (OPC) and this trend is still ongoing to minimize the risk of well integrity failures rooted to OPC. Moreover, the cement industry produces up to 600 kg CO_2 per ton of

cement, accounting for about 7 % of total CO_2 emission (East, 2018). Depending on cement type and class, CO_2 emitted from the calcination process varies. Using supplementary cementitious materials such as fly ash is one of strategies to keep emission at lower rates. Hence, it is expected that the carbon footprint of the drilling application cement is being even higher than the reported numbers (Fantilli et al., 2019). Reducing carbon dioxide emissions may require a shift from Portland cement to environmentally friendly alternatives. Therefore, extensive scientific activities are in progress to develop new materials for cementing operations. The new materials have to cover possible shortcomings of the oil well cement.

1.1 *Well integrity*

Well integrity is defined as technical and operation task that result in consolidation of all elements in the well and consequently, minimize the risk of uncontrolled formation fluid flow during the well's lifecycle (NORSOK-D-010, 2013). In this respect, the barrier elements should be designed or be selected to tolerate chemical, thermal, and mechanical stresses and environmental conditions that they are exposed to at downhole condition. The operational conditions include different parameters such as pressure, temperature, effect of corroding elements, erosion, and fatigue. The status of well barrier elements shall be monitored regularly under the mentioned operational conditions. Therefore, operators are recommended to codify a comprehensive integrity management system for the wells under operation. The general requirements and guidelines related to well integrity are introduced by available standards and recommended practices such as NORSOK D-010 (NORSOK-D-010, 2013), ISO standard in well integrity (International Organization for Standardization, 2014), and Guidelines on Qualification of Materials for the Abandonment of Wells (Oil&GasUK, 2015). These documents address establishing and acceptance criteria of the well barrier elements (WBE).

During the well's lifecycle, well integrity issues may happen at different phases such as well construction, production, testing, intervention, or post abandonment (Khalifeh and Saasen, 2020a). These issues can be formation-induced i.e., pressure and temperature variation or corrosion and erosion due to flow rate or chemistry of the formation fluid flow, or operations induced. If the well is operated beyond the designed limit, one or more elements may fail and result in loss of well integrity. Poor maintenance, improper installation, and failure related to testing are other operationally related integrity issues that can cause leakage in the system. The leakage can occur through completion equipment such as different safety valves (e.g., downhole safety valves, annular safety valve), packers, along cement, or at the interface of cement with casing string or formation.

1.2 *Primary cementing operation – setting material as well barrier element*

In drilling operations, when the hole reaches a certain depth, a casing string is placed in the wellbore. The casing functions to provide stabilized conduit and prevent the wellbore from collapse. Running casing string in the well is followed by cementing operation, in which the drilling fluid is displaced by cement slurry. The cement fills annular gap between the casing and formation or the space between two casing strings. The slurry is then solidified and seals off the annular space. The annular cement has different functions including providing zonal isolation and preventing formation fluid migration between different strata, protecting casing from corrosion, and mechanically holding the casing in place. The role of cement is important to protect the surface aquifer from contamination by hydrocarbons or other fluids and hinder further environmental issues. According to NORSOK D-010, any zonal isolation material should have certain properties (NORSOK-D-010, 2013):

- *Long term integrity* – The material should perform as it is designed during its lifecycle.
- *Impermeable* – It should be capable of preventing formation fluid flow through its matrix structure.
- *Non-shrinking* – Any kind of shrinkage (i.e., chemical, autogenous, and drying) increases the risk of leakage.
- *Ductile* – The material should develop sufficient strength and having some degree of flexibility to withstand mechanical loads.
- *Corrosion resistant* – Being chemically resistant to corrosive substances ensuring safe operations by preventing degradation.
- *Bonding* – It is necessary to have an integrated bonding of the material to casing and formation to prevent micro-path formation at the interface.
- *Compatible to tubular integrity* – The material has a duty to protect casing; therefore, the barrier material and tubular should be chemically consistent.

Amidst these properties, long-term integrity of the zonal isolation material is an issue that requires further development. Although the standards emphasize long-term integrity of barrier materials, there are still shortcomings in a clear description of testing related to several operational factors, such as time, temperature, type and concentration of chemicals, types of loads.

1.3 *Possible difficulties with zonal isolation material*

From the well integrity perspective, wellbore as a unified system consists of several well barrier elements responsible for zonal isolation. The well barrier elements include steel casing, cement, elastomers, and surrounding formation. Among these, cement as the key component seals unintended zones from fluid flow. Failure in cement integrity is critically important and requires immediate action.

The cement-casing/formation interface or the matrix of cement are regarded as potential leak paths. Figure 1.1 shows the schematic of a well and possible leak path scenarios. Considering cement as one of the well barrier elements, permeable structure of cement matrix, crack development, and micro annular channel are the main reasons of loss of well integrity and zonal isolation. Cracks can be formed due to mechanical loads existing at downhole and cyclic changes in pressure and temperature. Insufficient mechanical strength of the cement to tolerate these loads during operation can cause cracks and debonding from adjacent medium and consequently, resulting in sustained casing pressure (SCP). SCP is defined as pressure build-up in the annular gap due to intrusion of formation fluid.

In Norway, Petroleum Safety Authority (PSA) is responsible for the safety and emergency awareness in the petroleum industry. PSA monitors drilling plans from well construction to permanent plug and abandonment (PP&A). They publish the trends in risk level in petroleum activity (RNNP) on an annual basis aiming to have a more integrated picture about the incident risk. The latest report published in 2021 includes the survey of 1292 temporary abandoned wells from 2011 to 2020 (PSA, 2020). It was mentioned that the percentage of healthy wells with no or major issues in integrity has been reduced from 62 % to about 45 %. The failure can occur in different well barrier elements in the well such as casing, annular safety valve, tubing, etc. Among these, shortcoming associate with cement is well known (Kiran et al., 2017).

Several factors can increase the risk of micro annuli formation at the interface. Poor drilling mud removal before pumping the cement slurry, deficiency in casing centralization, irregular wellbore geometry and existence of caves in the annulus, and presence of wax, scale, and pre-existing rust on steel surface prohibit integrated bonding of cement with surrounding medium and leave channels at the interface.

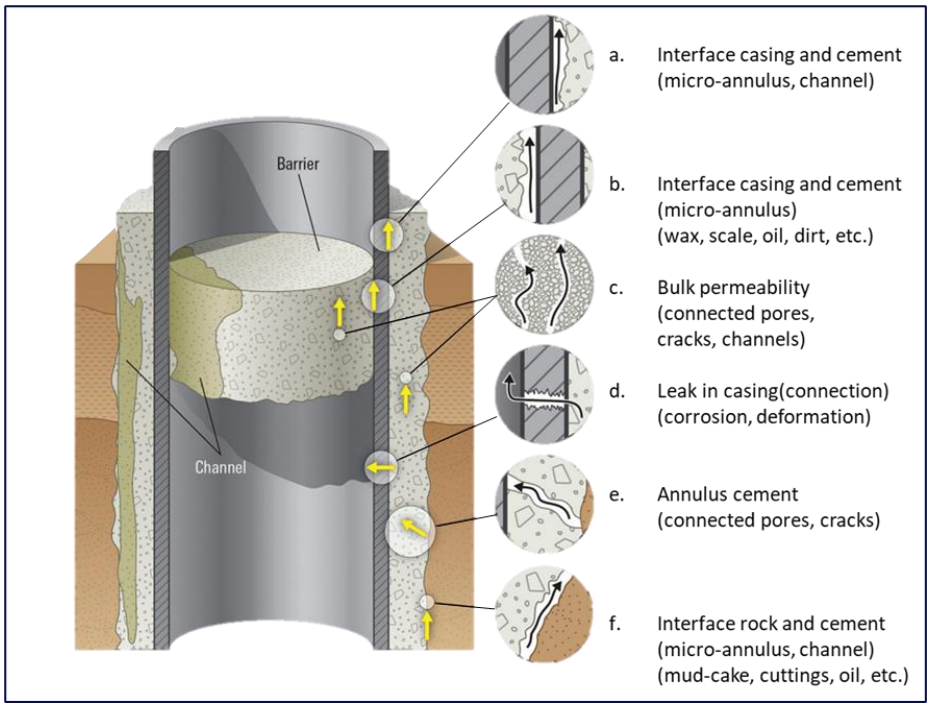

Figure 1.1. Schematic of wellbore cross section including casing, annular barrier, primary cement sheath, cement plug inside casing, and the possible leak paths (Gasda et al., 2004).

Over the hundred years of using Portland cement in drilling operations, although different additives have been introduced to upgrade its properties, still long-term integrity remains an issue for some wells (Trudel et al., 2019). It requires practical collaboration between academia and field engineers to find the gaps and develop safe and cost-efficient solutions for the drilling operations including petroleum applications, geothermal, or CCUS wells (Vrålstad et al., 2019). In addition to Portland cement, there are other materials that can be considered as barrier, depending on operational condition and functional requirements (Khalifeh and Saasen, 2020b; Oil&GasUK, 2015; Vrålstad et al., 2019). Thermosetting and thermoplastic polymers, metal alloys, non-setting grouts, modified in-situ materials, in-situ formation, etc. are some of candidate materials that can be used as a well barrier element.

Amongst these, three alternative setting material are selected for further examination in this study.

In the following, the properties of two Portland based cements and three noncement-based materials are described in the light of the strong chemistry background of Portland cement and high ambition of green shift from OPC to alternative materials. These materials are:

- An industrial class of expansive cement
- Noncement-based pozzolanic material
- Inorganic geopolymer
- Organic thermosetting resin

A Dyckerhoff API neat class G cement was selected as a reference. The neat cement was selected as each chemical additive may have a different impact on the performance of the material depending on material suppliers around the world.

2 Objectives and scope of the study

The scope of this study includes evaluating the candidate materials for cementing operations at equal conditions of pressure and temperature and at laboratory scale. Besides, the test results of each material are compared together to find the corresponding current strengths and shortcomings linked to each mix design. The objectives of this project are summarized as follows:

- Determine the fluid-state properties and rheological behavior of the alternative materials and compare the results with field requirements. The questions are: 1- Are the viscosity profiles of these materials in the range of operational conditions? 2- Are the slurries stable during placement and post-placement when they expose to a porous medium? 3- Are these materials pumpable for sufficient time to be placed in the well?
- Determine the mechanical properties after solidification. The questions are 1- Are the materials able to solidify and develop strength? 2- Are the materials able to maintain their mechanical properties in long-term? 3- Is there any correlations between different mechanical properties? 4- What are the changes in micro-structure and mineralogy of materials and what are their contributions to the mechanical properties?
- Determine the bond strength between barrier materials and steel as a representative for the casing. The questions are: 1- Are these materials able to bond to the steel metal? 2- Is there any correlation between hydraulic sealability and bonding? 3- How is the morphology of the interface of these materials when they are cured in contact with steel?

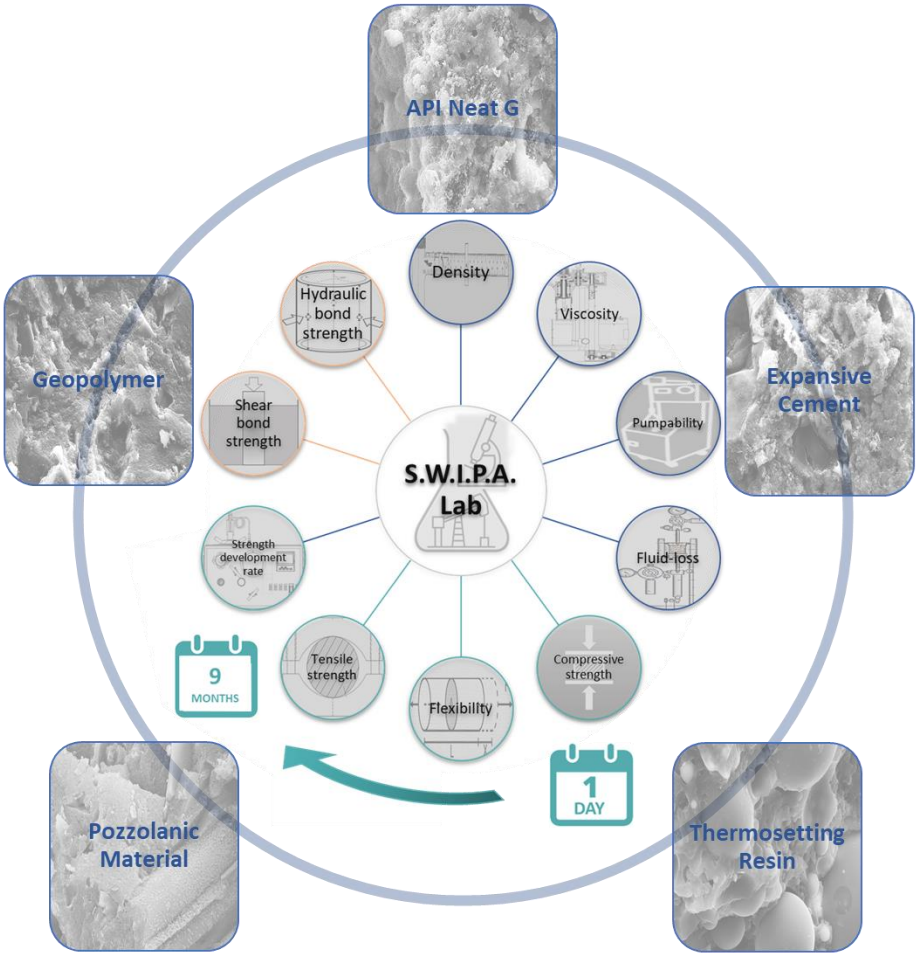

Figure 2.1. Infographic presenting measured properties of candidate barrier materials.

3 Candidate Materials for Cementing Operation - Review

3.1 *API neat class G*

The properties of conventional Portland cement depend on the hydration reaction of minerals in the clinker and the phase of products after solidification. The effect of various mineralogical compositions has been previously studied in detail (Bullard et al., 2011; Taylor, 1997). Mineral phases distribution is the principal criterion in Portland cement classification. Based on API standard, the Portland cement is classified into six different classes depending on the depth of placement and operational condition of pressure and temperature. Table 3.1 shows typical classes of Portland cement and the potential phase composition according to the API standard spec 10 (Americal Petroleum Institute, 2010).

Table 3.1. Cement classes based on API standard. Typical major mineral phases for each class are adopted from API standard spec 10 (Americal Petroleum Institute, 2010).

API class	Potential composition of major phases (wt%)			
	C_3S[1] (Alite)	C_2S[2] (Belite)	C_3A[3] (Aluminate)	C_4AF[4] (Ferrite)
A	45	27	11	8
B	44	31	5	13
C	53	19	11	9
D	28	49	4	12
G	50	30	5	12
H	50	30	5	12
1 – Tricalcium silicate 2 – Dicalcium silicate 3 – Tricalcium aluminate 4 – Calcium aluminoferrite				

In offshore drilling operations, classes G and H are selected as basic well cement. They are mainly available in moderate sulfate resistance (MSR)

and high sulfate resistance (HSR). In this project, an HSR API neat class G cement manufactured by Dyckerhoff was used as the reference. The chemical composition of the material is summarized in Table 3.2.

Table 3.2. Chemical composition of the Dyckerhoff class G cement.

Composition	MgO	SO_3	Na_2O	C_3S	C_3A	C_4AF	Insoluble residue	LOI
Amount wt %	1	2.7	0.61	51	2.4	17	0.49	1.5

3.2 *Expansive cement*

Shrinkage is a well-known phenomenon for Portland cement, and it is subcategorized into three main types: a) chemical shrinkage, b) autogenous shrinkage, and c) drying shrinkage (Panchmatia et al., 2020). In cement hydration reaction, the volume of products is less than the sum of the volume of reactants. The decrease in volume due to hydration reaction is referred to as chemical shrinkage. When the cement hardened in a sealed container and the structure is formed, the unreacted particles consume the pore solution trapped inside the bulk and the hydration reaction continues, which results in empty pores behind. Pore water consumption and the corresponding volume reduction cause capillary pressure development and introducing extra tension within the cement matrix. Volume shrinkage due to capillary pressure development of empty pores is referred to as autogenous shrinkage of cement. Drying shrinkage occurs when the moisture leaves cement matrix. Empty pores induce a negative capillary pressure to the matrix and causes volume reduction. However, this type of shrinkage is not applicable in downhole condition due to presence of humidity.

When the cement is solidified inside a well, the inner or outer circumferences are under extra tension due to changes in temperature and pressure. Hence, enhancing the chemical reaction of cement to reduce shrinkage induce stresses will help to improve the mechanical properties of cement during the well's lifecycle. Shrinkage reducing admixtures

(SRA) (Zhan and He, 2019) and expanding agents (Ghofrani and Plack, 1993) are used in application to mitigate the cement shrinkage. Generally, the SRAs are glycol-based chemicals used for reducing the drying shrinkage of cement or concrete by decreasing the surface tension of pore water. The expanding agents have a role to compensate autogenous shrinkage, especially at early ages.

There are two main expansion mechanisms for cement and concrete (Nelson and Guillot, 2006):

1- Expansion by gas generation: In this method, aluminum, zinc, or magnesium powders is used as an additive and hydrogen gas is generated as a result of reaction with alkaline elements in cement.
2- Expansion by crystal growth: This method relies on the crystal growth of a certain mineral within the cement matrix. Alkaline oxides of magnesium (MgO) and calcium (CaO) are the common additives, which dry blended with cement. The crystal hydroxides of these elements ($Mg(OH)_2$ and $Ca(OH)_2$) have higher volume and, therefore, mitigate the cement shrinkage to some extent.

Both methods mentioned above require to be engineered to have a controlled expansion. In the first method, hydrogen bubbles generated as the result of reaction may coalesce and form micro channels in the matrix. Similarly, for the crystal growth mechanism, the corresponding expansion should take place when the shrinkage arises. Obviously, early expansion is not effective for shrinkage compensation and very late expansion can form cracks in the matrix and compromise zonal isolation. Parameters such as downhole operational condition, the particle size of expanding agent, and the effective dosage have a critical role in short- and long-term zonal isolation.

Among the mentioned methodologies, utilization of MgO has been well established for oil and gas applications and compared to CaO, it is more efficient for temperatures above 80 °C (Van et al., 2019). Nano-MgO

expanding agents with different particle sizes are under development for oil and gas applications (Jafariesfad et al., 2017). It provides diverse reactivity levels to form crystals at the right time and with the right size to avoid expansion-induced crack in the matrix.

In this project, an industrial expansive cement, which is used for P&A applications is considered and tested for primary cementing operations. The cement is dry blended with MgO as expanding agent by about 2 % by weight of cement (BWOC). Other commercial chemical additives are recommended by the material supplier to enhance performance of the cement. The mixing procedure and chemicals are introduced in detail in the next section.

3.3 *Pozzolanic material*

Pozzolan is the name some of silica-rich materials that have no cementitious properties on their own, but they can react with alkaline hydroxide (such as $Ca(OH)_2$) and present cementitious properties. Pozzolans are considered as an important group of cement extenders. Extenders are used to reduce the cement slurry's density. Pozzolans also reduce the cement permeability by reacting with $Ca(OH)_2$ and forming calcium-silicate-hydrate (CSH) compounds through pozzolanic reaction (McCarthy and Dyer, 2019). Besides, a zeolite structure of the set pozzolan based material can act as an ion exchange component in corrosive environments and prevent chemical deterioration of the solidified cement (Papadakis et al., 1992).

Utilization of pozzolanic materials as a cement-free binder has been of interest of researchers. Slag, rice husk ash, palm oil fuel ash, and fly ash are well-known sources of pozzolanic components that can be activated with a calcium hydroxide based activator solution (Karim et al., 2017). In the current study, a non-cement pozzolanic material is selected as a candidate material for zonal isolation. This is an alkali activated commercial material that is used as a spacer in drilling operations to

separate the drilling mud and cement. It is a cement-compatible material and if mixes with cement, it will contribute to strength development and proper zonal isolation. Besides, the material has adjustable rheological properties, and it is capable of solidifying with time. The application of the material as an individual well barrier element in cementing operation was investigated. The chemical composition of the material is patented and unfortunately, no detailed information is available for ingredients used in mixing.

3.4 *Geopolymer*

Geopolymers are a class of alkali activated materials, consisting of long-chain aluminosilicate molecules. The solid precursor can be from a natural source such as thermally activated kaolin or rock-based material, or from industrial sources including fly ash, granulated blast furnace slag, rice husk (Hajimohammadi et al., 2011; Khalifeh, 2016). The liquid activator, also known as hardener, is an alkaline solution based on sodium or potassium involving silicate species. Geopolymerization reaction consists of various mechanisms. First, the dissolution of solid amorphous precursors starts when it is mixed with an alkaline solution in the presence of hydroxyls. In this phase, active monomers connected silanol groups (Si-O-H) start to form in the slurry. As the concentration of active monomers reached a specific level, the silicate species start to reposition themselves and reconnect. Polycondensation and crosslinking are followed by the reaction when monomers and small oligomers form three-dimensional networks and make tetrahedral aluminosilicate structure gels. After solidification, the geopolymer structure is a function of curing temperature and pressure, source of solid phase and reactivity of particles, alkali elements in liquid hardener, and silica/alkali molar ratio (Davidovits, 2013; Hajimohammadi et al., 2011; Khalifeh, 2016; Provis and van Deventer, 2009).

Nowadays, geopolymers as a green alternative for cement have attracted significant attention. It is believed that it has a lower carbon footprint

and it can reduce the CO_2 emission up to about 70 % compared to Portland cement (Paiva et al., 2018). Application of geopolymers in oil and gas market is seriously under study and researchers are in close collaboration with engineers to adjust the properties based on field requirements (Eid et al., 2021; Khalifeh et al., 2019; Paiva et al., 2018). Similar to other cementitious materials, the pumpability of geopolymers is reduced as the temperature increased (Salehi et al., 2019). Introducing the chemical admixtures to retard the geopolymerization affects the early strength development of geopolymers (Chamssine et al., 2021). A decent understanding of geopolymerization reaction is the key to success for controlling fluid-state and mechanical properties after solidification.

In this project, a naturally occurring rock was used as the source of aluminosilicate in geopolymerization reaction. The chemical composition of the solid precursor was normalized by adding ground granulated blast furnace slag (GGBFS) and microsilica. Table 3.3 summarizes the chemical composition of the solid precursor. The activator was potassium silicate solution. Sugar was used as a retarder for the slurry to make the material pumpable at the specified bottom-hole circulation temperature.

Table 3.3. Chemical composition of the geopolymer solid precursor.

Major element oxides	SiO_2	Al_2O_3	Fe_2O_3	MgO	CaO	Na_2O	K_2O	TiO_2	MnO	Other elements	LOI
wt %	56.63	12.47	1.09	6.23	16.45	1.77	2.87	1.16	0.29	0.45	0.58

3.5 *Thermosetting resin*

Thermosetting resin is an organic polymer available as a particle-free liquid. The material is non-reactive at room condition, while triggered by temperature, it turns into a solid phase (Todorovic et al., 2016). In drilling operations, such properties have made this material suitable for remedial operations and stop leakage through casing cement (Sanabria et al., 2016). The liquid resin penetrates ditches and leak paths and then

solidified at downhole temperature. Temperature, pressure, monomer units, and inter molecular forces are the main variables that control the solidification reaction. Glass transition temperature is an important parameter for amorphous polymers, and it is related to macro-molecules dynamic. It is a temperature limit beyond which, the long-change molecules start to decompose, and the polymer loses its elastic performance and behaves as a plastic material.

Thermosetting resins have higher strength and flexibility compared to the Portland cement-based systems. Previous studies mentioned that the compressive strength of thermosetting resins can reach six times more than the strength of Portland cement (Beharie et al., 2015). The rheological and fluid properties of thermosetting resins can be adjusted depending on the operational condition and application.

Thermosetting resins have limitations in operation. They have a higher coefficient of thermal expansion compared to other cementitious materials and steel. For the operational conditions with a wide range of temperature fluctuations, the thermal instability may compromise long-term integrity of the material. Besides, exposure to brine chemically deteriorates the material. Volume shrinkage and exothermic reaction after solidification are also highlighted in the literature (Dahlem et al., 2017; Todorovic et al., 2016).

In this project, a unique thermosetting resin was designed for primary cementing operations. However, the slurry contains glass beads as a weighting agent and hence, it is not considered as a particle-free system anymore.

4 Analytical Methods

The barrier material which is going to be used for cementing operation is first designed by chemists and material experts. Although the designed cement is going to be pumped in the wellbore, first it must be qualified through tests at cement laboratory. Therefore, the laboratory tests on the barrier materials are considered a critical process for well integrity assessment. In the following sections, the methodology for testing materials is described in detail, from mixing and slurry preparation to performing the corresponding test to measure a particular feature of each material.

4.1 *Testing conditions*

In well construction, the temperature at the bottom of the well is reduced due to continuous fluid circulation. This temperature is called bottom-hole circulating temperature (BHCT). The temperature of the formation at the bottom of the well under undisturbed conditions is the bottomhole static temperature (BHST). Generally, the fluid-state properties of cement are measured at BHCT and the mechanical properties after solidification are measured at BHST. In this project, the BHCT and BHST are 65 and 90 °C, respectively. The working pressure is about 170 bar (2500 psi). This condition covers the environment at intermediate casing for the majority of well on the Norwegian continental shelf (NCS).

4.2 *Slurry preparation*

The primary step in sample preparation is mixing the slurry. API has a recommended practice for mixing oil well cement at laboratory (American Petroleum Institute, 2013). In this procedure, depending on the density and desired rheological and mechanical properties, the water and other liquid additives are prepared and placed in a mixing container.

Accordingly, the solid phase including the required cement powder and solid additives are weighted. The mixing procedure comprises mixing the slurry with the rotation rate of 4000 RPM ±250 RPM for 15 seconds, where the solid phases are added to the liquid mix. Then, the slurry is sheared for 35 more seconds at 12000 RPM ±250 RPM. In slurry mixing, depending on the particle size and reactivity of the cement and additives, the shear rate and time of shearing are critical factors. Previous studies showed that varying these parameters may have a critical effect on rheological properties and mechanical behavior after solidification (Hodne et al., 2000; Saleh and Teodoriu, 2017).

The API class G cement, expansive cement, pozzolanic material, and geopolymer were mixed with API high-speed WARING blender. For the thermosetting resin, Heidolpth overhead stirrer was used with PR 32 Ringed Pitched-Blade Impeller. The thermosetting resin was mixed under 600 RPM following the sequence mentioned in the next section.

4.3 *Mix designs*

API neat class G cement – A class G cement manufactured by Dyckerhoff was mixed with 44 % BWOC of water in accordance with the API specification (Americal Petroleum Institute, 2010).

Industrial expansive cement – The solid phase was API class G cement manufactured by Dyckerhoff dry blended with expanding agent by the material supplier. Magnesium oxide (MgO) was used as expanding agent. Industrial chemicals including retarder, fluid-loss controller, cement dispersant, and antifoam were added to the water before mixing. Microsilica solution (50 wt%) was added to the liquid phase and mixed for 5 seconds at 4000 RPM. The solid phase was added to the liquid following the API standard (American Petroleum Institute, 2013).

Pozzolanic material – Release of the exact composition of this material is prohibited from the material supplier due to the commercialization of

the product. The slurry was received "ready-to-test" and all slurry design was made by the supplier for the same wellbore conditions of this study. A premixed activator was added to the slurry prior to delivery for the tests.

Geopolymer – The rock-based aluminosilicate precursor normalized by introducing ground granulated blast furnace slag (GGBFS). The potassium silicate solution with a Si/K mole ratio of 1.14 was used as the activator for the solid phase. To make the slurry pumpable at BHCT, sugar (4.3 % by weight of solid precursor) was used as retarder. The sugar was added to the liquid phase and mixed for 5 seconds before adding the solid phase.

Thermosetting resin – The liquid organic resin was mixed with a reaction imitator for 10 minutes and a viscosifier was added to the liquid and stirred for 15 more minutes. Glass bead powder as weighting agent was added stepwise to the liquid to increase the density. The whole system was mixed for 30 minutes to get a homogeneous slurry.

Conditioning is performed to simulate the conditions that the slurry encounters during placement. In all tests, materials were conditioned after mixing. The temperature ramp-up rate was selected to be 1 °C/min from room temperature to BHCT and the addition of 30 minutes hold for conditioning. OFITE model 60 atmospheric consistometer was used as a tool for conditioning.

In all experiments, it was attempted to stick to the common standards available for testing cement for oil and gas applications aiming to make reproducible results. The standards are mentioned in each test method. For the tests that have no common standard to the procedure, the methodology is described in detail.

4.4 ***Fluid-state properties***

4.4.1 *Density*

The density of each slurry was measured after conditioning. Pressurized mud balance was used for density measurement. The operational procedure for testing density is described in API RP 10B-2 (American Petroleum Institute, 2013).

4.4.2 *pH measurement of slurry*

The pH of slurries was measured after mixing and before doing conditioning. The pH of slurries was measured by Mettler Toledo pHmeter model SevenCompact^{TM} pH S210. The pH electrode was model LE438.

4.4.3 *Viscosity*

The conditioned slurries were poured into the viscometer cup for viscosity measurements. The viscosity was measured by rotational viscometer Fann 35. The cup was equipped with a heater to keep the temperature constant. The dial readings are extracted from equipment at rotational speeds of 3, 6, 30, 60, 100, 200, and 300 RPM, first in ascending and later in descending orders and the dial reading is reported as an average at each rotation speed (American Petroleum Institute, 2013).

Herschel-Bulkley viscosity model (Eq. 4.1) is one of the general constitutive models accepted in petroleum industry. This model gives a reasonable estimation of the behavior of cementitious fluids. The equation is:

$$\begin{aligned} \tau &= \tau_y + K\dot{\gamma}^n, \quad & \tau > \tau_y \\ \dot{\gamma} &= 0, & \tau \leq \tau_y \end{aligned} \tag{4.1}$$

where τ_y is the yield stress and n is the flow index, both are unique values and depend on the composition of the slurry. K is consistency factor and depends on the flow index. However, the dependency of K on the curvature component, n, hinders comparison of the model for different fluids. Various combinations of K and n can provide a reasonable model fit for the same data set. Saasen and Ytrehus (Saasen and Ytrehus, 2018) presented an approach by re-arranging the model parameters and using the surplus shear stress τ_s, and surplus shear rate $\dot{\gamma}_s$, which both are unique for each fluid. In this model, the equation is defined as follows:

$$\tau = \tau_y + \tau_s \left(\frac{\dot{\gamma}}{\dot{\gamma}_s}\right)^n \tag{4.2}$$

where $\tau_s = \tau - \tau_y$ at $\dot{\gamma} = \dot{\gamma}_s$ and τ_y is approximated by Eq. 4.6 (Power and Zamora, 2003):

$$\tau_y = 2\tau_3 - \tau_6 \tag{4.3}$$

where τ_3 and τ_6 are shear stress at 3 and 6 RPM, respectively. In cementing operation of 9 5/8 in. casing, the slurry is pumped by the rate of about 1300 L/min, which is equal to the shear rate of 102.2 s^{-1} in the annular gap between the casing and 12 ¼ in. borehole. This shear rate is identical to 60 RPM in the rotational viscometer. To determine the curvature components of the equation, two ranges are considered: one at the shear rates below the surplus shear rates (n_{ls}), and one for the higher ranges (n_{hs}). Shear rates at the rotational speeds of 30 and 200 RPM are considered for determination of curvature components (Eq. 4.7):

$$n_{ls} = \frac{\ln\left(\frac{\tau_{30} - \tau_y}{\tau_s}\right)}{\ln\left(\frac{\dot{\gamma}_{30}}{\dot{\gamma}_s}\right)} \tag{4.4}$$

$$n_{hs} = \frac{\ln\left(\frac{\tau_{200} - \tau_y}{\tau_s}\right)}{\ln\left(\frac{\dot{\gamma}_{200}}{\dot{\gamma}_s}\right)}$$

4.4.4 *Static fluid loss*

The conditioned slurries were poured in the high pressure – high temperature fluid loss cell. Filter paper (2.7 μm) was in the cell. The differential pressure of 4.5 MPa (650 psi) was adjusted on top of the cell and the leached liquid was measured for 30 minutes. API standard (American Petroleum Institute, 2013) recommends that the final static fluid loss shall be reported as the cumulative leached liquid multiplicated by two. For the cases in which breakthrough occurs before 30 minutes, the following equation can be used:

$$Q = 2V_t\sqrt{\frac{30}{t}} \qquad 4.5$$

where Q is the API fluid loss, V_t is the cumulative volume of leached liquid in milliliters from time 0 to the time at with the breakthrough occurs, and t is the time of breakthrough in seconds.

4.4.5 *Pumpability*

Pumpability or consistency of slurries was measured by both atmospheric and pressurized consistometers. After mixing, the slurries were poured into the corresponding cell of equipment and the temperature ramp-up rate of 1 °C/min was applied until BHCT was reached and then, held constant. For the pressurized consistometer, the pressure rate was set at 1.7 MPa/min and pumpability was tested at 17 MPa (2500 psi). OFITE model 60 and OFITE and OFITE Model 2040 were used for atmospheric and pressurized consistometers, respectively.

4.5 *Mechanical Properties after solidification*

4.5.1 *Uniaxial compressive strength (UCS) and Young's modulus*

All slurries were poured into cylindrical plastic molds after 30 minutes of conditioning. The samples were cured at BHST (90 °C) for the UCS test. The curing pressure was 170 bars and was supplied by an ISCO pump connected to the curing autoclave. Water was used as medium for pressurizing and curing the samples. Although the common API 10B-2 standard recommends for cubic samples with a diameter of 2 in., it declared that the results can be used only to ensure sufficient strength of cement to resume drilling operation (American Petroleum Institute, 2017). For annular cement integrity simulations, it is recommended to use cylindrical molds with a slenderness ratio (height /length) of 2. Besides, cylindrical samples were preferred due to the availability of cylindrical autoclaves for curing samples. After curing, the samples were removed from the oven to cool down to the ambient temperature. After removing from plastic molds, both ends of the samples were smoothened to eliminate the ending effect under loading.

The equipment used for the UCS test was Toni Technik-H mechanical tester linked to the TestXpert v7.11 software. The tests were performed at a constant load rate of 35 MPa/min (American Petroleum Institute, 2013). The materials were cured for 1, 3, 5, 7, 28, 90, 180, and 270 days. Three samples were provided per each material at different due times. UCS was calculated by Eq 4.6.

$$\sigma = \frac{F}{A} \qquad 4.6$$

where σ is the uniaxial stress in mega pascal (MPa), F is the maximum force before cracking of specimen in Newton (N), and A is the contact area of the specimen to loading frame in square millimeters (mm^2).

The modulus of elasticity, or Young's modulus, was calculated by measuring the slope of the axial stress–strain curve in the elastic region (Eq. 4.7):

$$YM = \frac{\frac{F}{A}}{\frac{\Delta L}{L}} \qquad 4.7$$

where YM is Young's modulus in giga pascal (GPa), F is the on the specimen in N, A is the contact area of the specimen to loading frame in mm^2, and L and ΔL are the initial height and the height change, both in millimeters (mm).

4.5.2 *Sonic strength development*

A Chandler ultrasonic cement analyzer (UCA) model 4265-HT was used to measure the sonic strength development of materials at downhole conditions. The slurry was poured into the UCA cell. The equipment continuously measures the transit time of the sonic wave throughout the sample by transducers located at both ends of the cell. Then the transit time is converted to the compressive strength by the means of pre-defined algorithms. Such algorithms are generated based on correlations for cement slurries. Since the transit time of the sonic wave is unique and it depends on the chemistry of materials, a new algorithm is required for each material in this project. The new algorithms were generated by utilizing the results from UCS tests at different time intervals and the corresponding transit time measured by the equipment. A polynomial equation was developed by plotting UCS data versus transit time.

4.5.3 *Tensile strength*

Brazilian test is a method to indirectly measure the tensile strength of cementitious materials. The same curing procedure for the UCS test was followed. Cylindrical samples after demolding were cut in disk shapes with a thickness to diameter ratio of about 0.6 (American Society for

Testing and Materials, 2015). The disk shape specimens were placed vertically between curved jaws and a compression load of 50 N/s was applied for the test (Figure 4.1). Four specimens were tested per each material at different due times. The tensile strength was calculated by Eq. 4.8.

$$\sigma_t = 1.272\frac{F}{\pi TD} \qquad 4.8$$

where σ_t is the tensile stress in MPa, F is the maximum force before cracking of the specimen in N, T is the thickness, and D is the diameter of the specimen, both in mm.

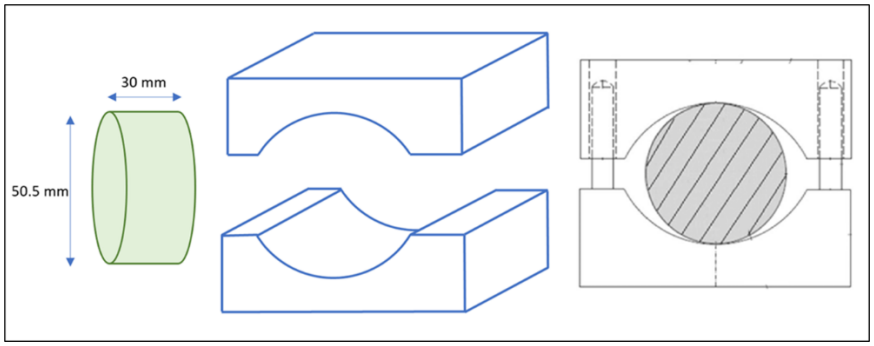

Figure 4.1. Schematic of the samples and testing jaws for indirect tensile strength (Brazilian test) measurement

4.6 *Morphology and micro-structure analysis*

4.6.1 *Scanning Electron Microscopy (SEM)*

Morphology of the solid materials was examined after 7, 28, 30, 180, and 270 days of curing using a Scanning Electron Microscope. The SEM tests were performed on crushed samples in UCS tests. The samples after UCS test were dried under vacuum for 1 more day and then coated with palladium plasma to prevent charging. Additionally, energy-dispersive X-ray spectroscopy (EDS) were used together with SEM intending to identify element distribution on the surface layers of the materials.

Morphology study and EDS analysis was performed using the secondary electrons (SE) mode of the microscope. Scanning Electron Microscope model Gemini Supra 35VP (ZEISS) was used for SEM analysis.

When the sample is exposed to the electron beam for imaging, a variety of signals is generated (Figure 4.2). Low-energy Secondary Electrons are reflected from the surface or near-surface of samples. They are originated from an inelastic interaction between the sample's surface and primary electron of the beam. Therefore, SE is useful for surface topography studies. However, the backscattered electrons (BSE) carry a higher level of energy and they are originated from deeper zones of the sample. They are reflected after elastic interaction of primary electron beam and atoms in the sample. Such collision results in a change in the trajectory of electrons. Generally, larger atoms scatter electrons stronger than lighter atoms, which results in a stronger signal. In this case, the zones with heaver elements are brighter than light elements (Vernon-Parry, 2000).

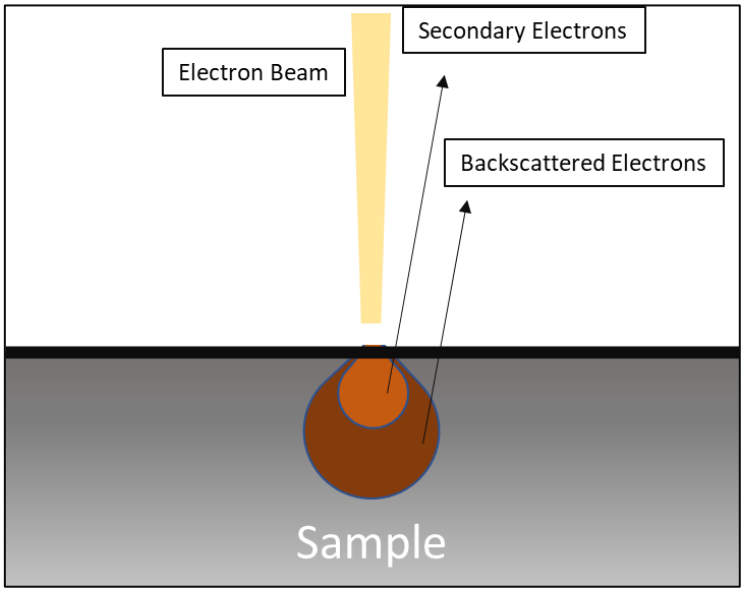

Figure 4.2. Signals emitted from a sample. The image shows the Secondary electrons and backscattered electrons emissions.

4.6.2 *XRD*

X-ray diffraction (XRD) is a technique that is used to identify phase changes and crystallography of precursors. This method was employed to identify the phase of minerals and monitor the change in the phases after each time interval. Bruker D8 Advance micro-diffractometer was used as equipment, and the patterns were extracted in the 2θ range of 5-90 ° at the step of 1 °/min with rotation (15 RPM) of samples.

4.7 ***Bond strength***

The bond strength between cement barrier and casing steel can be divided into three different categories (Figure 4.3): a) shear bond strength, b) hydraulic bond strength and c) tensile bond strength. The scope of this part of project is to establish the effect on shear bond strength and hydraulic bond strength at the steel-setting material interface (SSI). Analysis of the tensile bond strength is outside the scope of the current study.

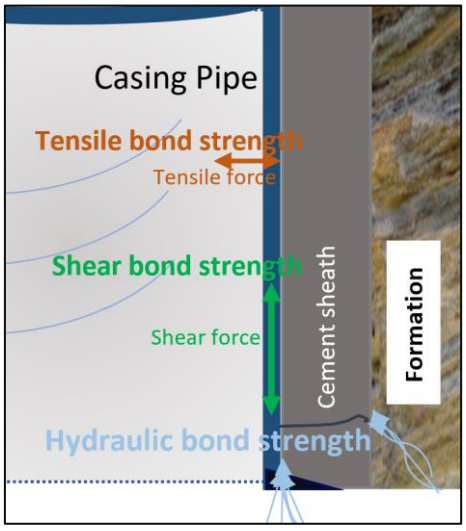

Figure 4.3. Schematic of casing - barrier material system at downhole condition. Shear force, tensile force and hydraulic sealability at the interface of casing pipe and surrounded cementitious material are highlighted.

4.7.1 *Shear bond strength (SBS)*

Shear bond strength (SBS) expresses the maximum force that the interface of casing-cement can handle before the casing starts to move. In laboratory, SBS is measured by the push-out test, in which a bar or pipe is placed inside a cement slurry and the system is cured under desired operational conditions. For the push-out test, the middle bar is pushed by the means of compression load. The maximum force at which the bar initiates moving in the cement is reported as a force to break cement bond (Bearden and Lane, 1961). To have a correlation with various specimens' dimensions, the contact area between the cement and steel bar should be considered. The SBS is calculated by Eq. 4.9:

$$SBS = \frac{F_{max}}{A} \qquad 4.9$$

where F_{max} is the maximum force before debonding in N, and A is the contact area between cementitious material and steel bar in mm^2.

In this study, a test setup was designed for measuring SBS at two different circumferences of cementitious materials and steel including a solid bar with the OD of 50 mm inside a cement slurry, and a pipe with the ID of 150 mm surrounded the materials. Figure 4.4 shows the schematic of SBS test samples setup. Due to technical limitations and market availability, two different steel grades were used for representing casing steel. The middle bar had equal material to AISI 4140 P110 and the outer pipe was a carbon non-alloy P235TR1 steel. The chemical composition of steels is provided in Table 4.1. The tests were conducted on clean and rusted steel surfaces. To make rusted steel pipes and bars, they were immersed in seawater for 14 days. Three samples were considered and tested per each combination of steel and barrier material.

Table 4.1. Type of steels used in shear bond strength, hydraulic sealability, and interface analysis tests.

Steel Type	Application	Chemical Composition % (Max)											
		C	Mn	Mo	Cr	Ni	Cu	Ti	P	S	Si	V	Al
4140 P110	SBS bar – HBS pipe	0.41	0.91	0.23	1.06	0.15	0.2	-	0.011	0.002	0.3	0.013	0.027
P235TR1	SBS outer pipe	0.16	1.2	0.08	0.3	0.3	0.3	0.04	0.025	0.02	0.35	0.02	-
4140 L80	Surface study	0.43	0.91	0.2	0.9	0.25	0.35	-	0.025	0.025	0.3	-	-

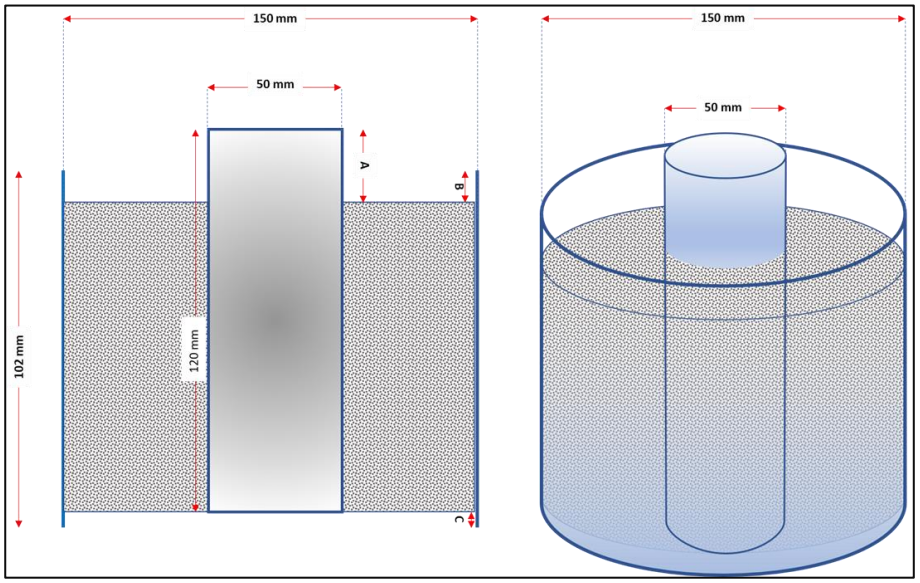

Figure 4.4. Schematic of shear bond strength test setup including a solid steel bar placed in center and a steel pipe around the sample. The cementitious slurry after mixing is poured in the annular gap between the bar and pipe. A, B, and C parameters were measured for every sample to find the correct contact area between the steels and barrier materials.

The samples were cured for seven days under elevated temperature and pressure of 90 °C and 34 bar (500 psi), respectively. The SBS samples were cured at lower pressure mainly due to technical limitations in the size and design of available autoclaves. Zwick/Roell Z050 was used as equipment to apply load on samples and the loading rate was 50 N/S. For the expansive cement and thermosetting resin combined with rusted

steel, Toni Technik-H mechanical tester was used since the bond strength was beyond the capacity of machine.

4.7.2 *Hydraulic sealability*

Hydraulic bond strength is defined as the integrity of cement and casing at the interface that prevents fluid flow (Figure 4.3). There is no common standard nor test procedure for measuring hydraulic sealability. A pre-design test setup was considered for testing the sealing performance of selected barrier materials and steel. The steel pipes used for hydraulic sealability were equal to the material used as the inner bar for shear bond strength. The pipe had a length of 120 mm and an OD of 51 mm. Three holes as injection points were improvised in the middle of the pipe with an orientation of 120 degrees. The pipes had a thickness of 7 mm to avoid any ballooning effect during injection. Both clean and rusted steel pipes were considered for the sealability test, and the rusty surface was provided similar to SBS test steels. For the hydraulic sealability test, three samples were considered per material and steel type.

The conditioned slurries were poured in the annular gap, and the system was cured for seven days at 90 °C and 170 bar. After gradually cooling down, the samples were connected to an ISCO pumped which was able to log the injected flow rate (Figure 4.5)

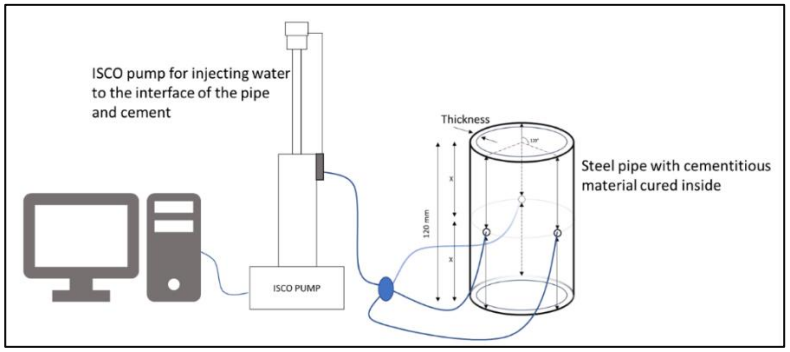

Figure 4.5. Schematic of hydraulic sealability test setup including sample, ISCO pump, and computer for logging data. The injection was done at the cement-steel interface.

The injection pressure was increased at different steps using the following sequence. It is worth noting that higher injection pressure tests were avoided due to safety reasons. The applied procedure was as follows:

- Increase the injection pressure from ambient to 6.8 bar (100 psi) in 1 minute.
- Hold the pressure for 10 minutes.
- Increase the pressure from 6.8 bar to 10.2 bar (150 psi) in 1 minute.
- Hold the pressure for 10 minutes.
- Increase the pressure from 10.2 bar to 13.6 bar (200 psi) in 1 minute.
- Hold the pressure for 5 minutes (where neat G cement started to leak significantly).
- Increase the pressure from 13.6 bar to 20.4 bar (300 psi) in 1 minute.
- Hold the pressure for 5 minutes.
- Increase the pressure from 20.4 bar to 27.2 bar (400 psi) in 1 minute.
- Hold the pressure for 5 minutes.
- Increase the pressure from 27.2 bar to 34 bar (500 psi) in 1 minute.
- Hold the pressure for about 20 minutes.

4.8 *Steel – setting material interface*

To understand the interface properties of cementitious materials and steel pipe from SBS and hydraulic sealability tests, a different test setup and procedure were designed and performed. The objective of this test is to characterize possible interaction at the boundaries by checking the morphology and minerals at the surface.

A semi-cube steel metal was cut from a 9 5/8 in. steel casing pipe grade L-80 with 53 lb/ft (Figure 4.6). This is a common steel for well

construction. On side of the metal was polished with sandpaper grit 2500 to get a smooth surface. The chemical composition of steel is presented in Table 4.1. The steel was immersed inside a slurry and cured under the same condition for SBS and hydraulic sealability test for seven days. After colling down, the steel surface and the corresponding setting material were separated, and both were kept under vacuum and inside a desiccator for one day. The samples were then transferred for SEM test after coating with palladium. Energy-dispersive x-ray spectroscopy (EDS) analysis was performed in parallel to SEM to identify element distribution in the surface layers of the materials.

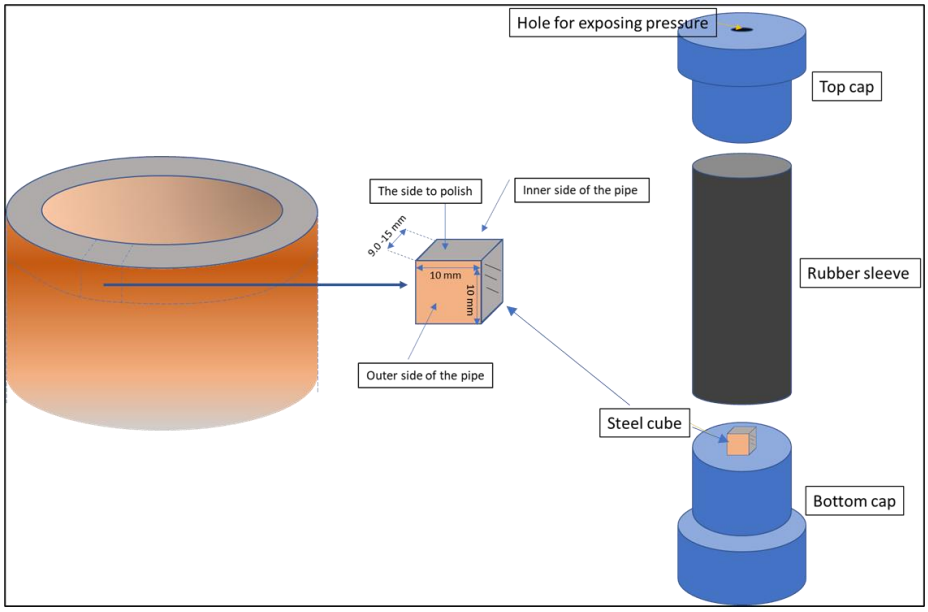

Figure 4.6. The setup and sample preparation for interface analysis. A semi-cube piece was cut from a 9 5/8 in. L-80 (53 lb/ft) casing pipe. One side was completely polished and then immersed inside a slurry.

5 Results & Discussion

5.1 *Fluid-state behavior*

5.1.1 *Viscosity, density, and gel strength*

For any material, viscosity is defined as its resistance to flow. The flow properties of material can be estimated by viscous properties; for example, when it is stirred or pumped. Different parameters such as solid content, carrier fluid or hardener, temperature, pressure, and conditioning time have a direct impact on the viscous behavior of slurry. Figure 5.1 shows the shear stress vs. shear rate of setting materials after pre-conditioning at BHCT (I, IV). All materials present yield stress to various extent; therefore, they are non-Newtonian fluids at 65 °C and atmospheric pressure. The yield stress was estimated based on the model suggested by Powe and Zamora (2003). The model was introduced in Section 4.4.3. The fluid parameters are summarized in Table 5.1. The curvature components of viscosity model parameters (n_{ls} & n_{hs}) were determined as less than unity, which is indication of further shear thinning behavior. The measured API class G cement experienced a sharp bend at shear rates close to 100 s^{-1}. The slurry was conditioned for 30 minutes at 65 °C. Since no retarder was added to the mix, it is likely that the hydration reaction progressed to form weak gel structures in the slurry and therefore, at specific shear rates the gel breaks and results in a sharp decrease in viscosity of the material (II).

The pozzolanic material and thermosetting resin showed the lowest yield stress among materials. However, the viscosity of resin was higher compared to other materials, where the dial reading at 300 RPM was not possible. The weighting agents introduced during mixing caused high viscosity for the thermosetting resin. The viscosity profiles for the geopolymer and expansive cement were almost close to each other. However, at the same shear rates, geopolymer had lower shear stress

compared to the expansive cement. Depending on the wellbore temperature, rheological properties of drilling fluid/spacer present in the well, the viscosity and yield stress of the slurry are needed to engineered. This helps to have a proper placement of the setting material and reduce the risk of mud cake formation at cement-casing/formation interface resulting from poor mud displacement (Taghavi et al., 2012).

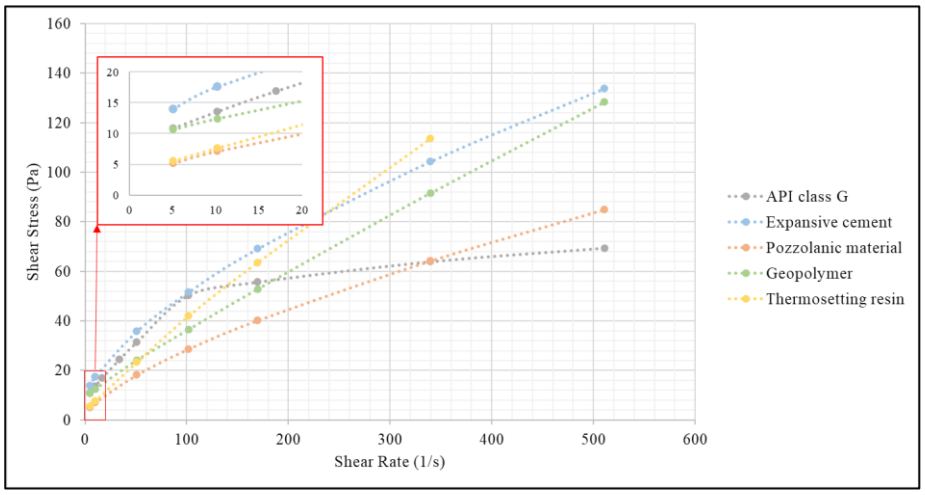

Figure 5.1. Viscosity profile of the materials at 65 °C. Non-Newtonian behavior is concluded for all materials since they showed yield stress and shear-thinning behavior (I, IV).

The 10-second and 10-minute gel strength tests of slurries are taken at 3 RPM. The test procedure is well described in the API standard (American Petroleum Institute, 2013). The results are presented in Table 5.1. Gel strength is due to structure development at static conditions. The gel strength of the expansive and neat class G cements after 10 minutes was considerably higher than other materials (I, II). The pozzolanic material had the lowest gel strength.

The density of slurries was measured after conditioning at BHCT using pressurized mud balance. The density of was in the range 1.65 to 1.95 sg. (13.7 to 16.2 ppg). The thermosetting resin and pozzolanic materials had a lower density compared to other materials.

Table 5.1. Fluid properties including density, pH, gel strength, viscosity model parameters, fluid loss and pumpability of materials (I, IV).

	Density (sg.)	pH	Gel Strength (Pa)		Viscosity model parameters				API Fluid Loss (ml)	Pumpability (min)	
			10-sec	10-min	ty	t_s	n_{ls}	n_{hs}		ATM	PRS
Neat class G	1.9	13.6	11.75	69.5	6.13	31.68	0.98	0.29	821.04	132	96
Expansive cement	1.95	13.2	12.2	40.3	7.4	44.2	0.64	0.65	21	462.5	338.5
Pozzolanic material	1.68	13.3	3.57	5.11	2.04	26.65	0.72	0.70	18.8	N/A	N/A
Geopolymer	1.95	13.4	12.2	23	7.78	28.11	0.95	0.87	0	120	110
Thermosetting resin	1.65	N/A	3.5	19.4	3.32	38.58	0.844	0.82	183.76	293	263.5
N/A: Not Applicable											

5.1.2 *Static fluid loss test*

In cementing operation and during cement placement, when the slurry reaches a porous formation behind casing, the formation may act as a filter that passes the carrier fluid or hardener while stopping the particles. This phenomenon has negative impacts on wellbore control, which are summarized as following:

1- Loss of liquid phase results in solid particle bridging in the annulus and reducing hydrostatic pressure above the cement column. If the hydrostatic pressure falls below the pore pressure of formation, formation fluid can penetrate the annuli and form channels in the cement sheath.
2- Cement fluid loss contributes to an increase in viscosity of the slurry. Hence, a higher pumping pressure may be required to compensate the pressure loss due to high viscosity. In weak formations, high pumping pressure can induce fractures. It is followed by loss of slurry to the formation and therefore, top of cement may not achievable.
3- The liquid portion that left the slurry may have a critical role for solidification reaction after placement. Thus, the chemical

reaction for solidification can be disrupted at a high fluid loss and the mechanical properties are compromised.

Figure 5.2 and Table 5.1 summarize the static fluid loss test results of selected barrier materials in absence of filtration control additives. The neat class G cement encountered a breakthrough after almost 2 minutes from starting the test. Thermosetting resin could hold the pressure for about 7 minutes before breakthrough occurs. Although the thermosetting resin is considered as particle-free system, the current mix design includes glass beads as a weighting agent to increase the density of slurry. Hence, it is not a particle-free system. The expansive cement and pozzolanic material had about 10 ml of fluid loss after 30 minutes, while the geopolymer slurry had no loss during the testing period (I, IV).

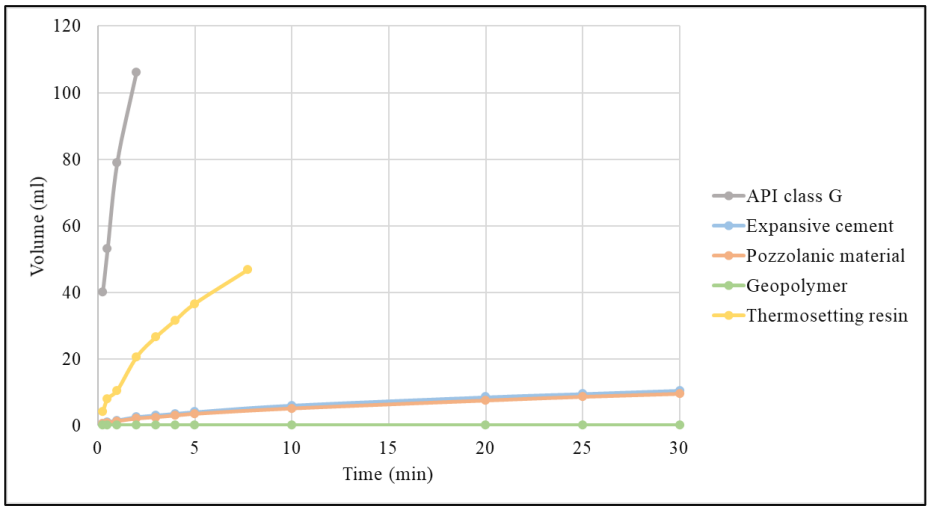

Figure 5.2. Static fluid loss test results of materials (I, IV).

Depending on the geology of drilling environment, different operators have specific criteria on acceptable fluid loss for cement slurries. Generally, values below 50 ml in 30 minutes are desired for primary cementing operations (Bensted, 1998).

5.1.3 *Pumpability and consistency*

In cement laboratory, the consistency of cement slurry is examined by measuring the torques of spring connected to a paddle that continuously shears the slurry. For cementitious materials, pumping time, also known as workability, is an indication of how long the fluid is pumpable before the gelation starts. The test is performed at the BHCT of 65 °C, and the temperature ramp-up rate should follow a specific schedule of individual wells. The instrument measures the consistency of slurry in the Bearden unit of consistency (Bc). The upper limit of pumpability depends on the operators' criteria. Commonly, the consistency above 70 Bc is considered as unpumpable fluid.

Figure 5.3 shows the consistency profiles of the materials at atmospheric and elevated pressure of 170 bar (I, IV). Since two different measuring devices were used for this test, one extra test was conducted for the neat class G cement using a pressurized consistometer but at atmospheric pressure (dash line in Figure 5.3 A). The reason was to check reliability of the atmospheric consistometer. Since no significant difference was observed in the results, atmospheric pressure tests were performed using an atmospheric consistometer. Increasing pressure accelerates the gelation of materials to various extents. The reduction in pumping time was about 25 % for both the neat class G cement and expansive cement. Right-angle-set (RAS) is a manner of cementitious material that shows how quickly the gelation phase occurs and follows in solidification. Besides, right-angle-set can be an indication of early strength development. This behavior is apparent in expansive cement, while the neat class G has a longer gelation period.

The pozzolanic material had a constant trend of consistency for almost 23 hours and the trend started to develop gradually. After 28 hours, the consistency was peaked at around 40 Bc, and followed by reduction in consistency (see Figure 5.3. C). The test was stopped at this point. A few seconds after removing the sample, a strong gel was formed which

was difficult to remove from the consistometer's blade. It is evident that dynamic and static conditions have influences on fluid behavior. Consistency of the geopolymer was less affected by pressure since the consistency curves were almost matched for the atmospheric and elevated pressure tests. Introducing sucrose to the mix design as a retarder could not make the slurry pumpable for more than two hours. The thermosetting resin's pumping time was pressure-dependent, and the pumping time was reduced by 10 % when the consistency was measured under pressure. The test was stopped when the consistency was reached at about 50 Bc, as it was recommended by the material supplier because the resin has a flash setting behavior and it may damage the equipment after solidification.

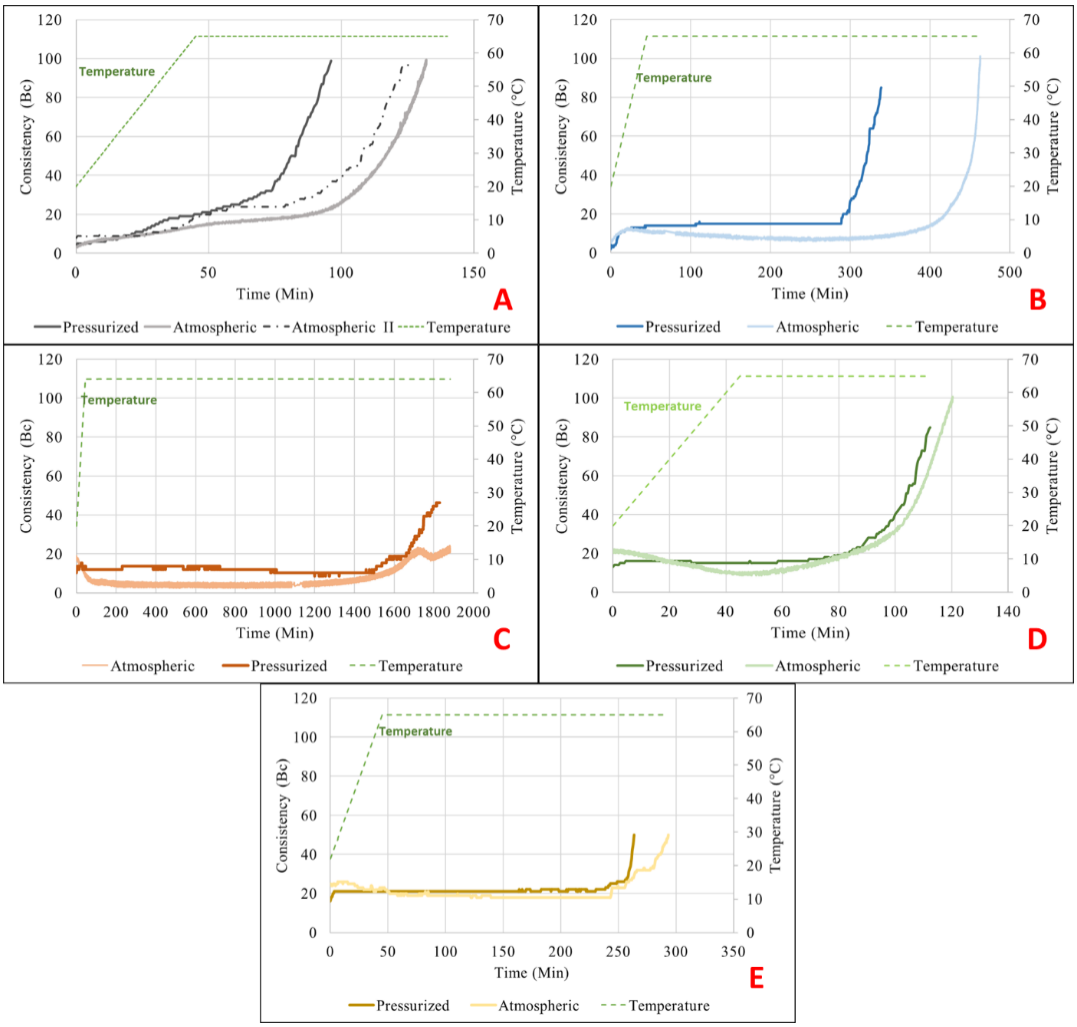

Figure 5.3. Consistency profile for A) API class G cement, B) expansive cement, C) pozzolanic material, D) geopolymer, and E) thermosetting resin. The consistency was tested at both atmospheric pressure and 170 bar (I, IV).

5.1.4 *Conclusion*

The density of slurries was within the desired range of 1.65 to 1.95 sg. (13.7 to 16.2 ppg). The summary and conclusion of fluid-state tests are presented in the following:

1- Yield stress for the thermosetting resin and pozzolanic material was lower than the geopolymer and Portland cement-based systems, which may increase the risk of segregation before solidification.
2- Considering the fact that the selected operational condition may fit for production casing cementing operation (normally 9 5/8 in. to 12 ¼ in. annulus), under a normal pumping rate of about 10 – 12 bbl/min (shear rates below 200 s^{-1}), the viscosity profile for all materials showed an acceptable behavior.
3- Static fluid loss test results show that the weighting agents used for thermosetting resin are not perfectly attached to the liquid resin. High fluid loss can compromise the application of thermosetting resin. Similar to the expansive cement, a chemical additive is required to increase the yield stress and minimize fluid loss.
4- All materials were pumpable to a various extent at the selected BHCT. The pozzolanic material remained in liquid until the slurry was shearing. Quick gelation was observed when the equipment was stopped.

5.2 *Mechanical behavior*

5.2.1 *Uniaxial compressive strength and Young's modulus*

Figure 5.4 shows the average compressive strength of materials from day one and up to nine months of curing at BHST of 90 °C and 170 bars of pressure (VII). The pozzolanic material and geopolymer were not able to develop strength after one day of curing. The compressive strength of pozzolanic material reached about 13 MPa after one week and remained constant for rest of the test period. As it was mentioned in the introduction of materials, the pozzolanic material is already used as spacer to clean the hole before pumping cement. Spacers are normally

not a setting material, but this pozzolanic material can stay in the wellbore and solidify. Hence, the setting time can be adjusted depending on the wellbore environment. The UCA test results in Section 5.2.3 show that the material starts to develop strength after 2 days. In the same Section, the UCA results of geopolymer showed strength development after 2.5 days. The pumpability of geopolymers is temperature sensitive and it requires a proper retarder to prolong pumpability. Sucrose as a retarder in this mix design negatively affected strength development at early ages. Sucrose can cover the aluminosilicate source in the geopolymer precursor and seal it off to be engaged in nucleation reaction (Rattanasak et al., 2011). However, the high concentration of silicate in the hardener was suspected to start polycondensation of silicates in the slurry and initiate gel formation. The compressive strength of geopolymer was increased gradually and reached 15 MPa after one month. The UCS was increased by more than 80 %, from 13 MPa (7-day) to 23 MPa after three months. The UCS reached 58 MPa in sixth month and declined by 37 % after nine months. The GGBFS source was changed during the project and the nine-month-old samples were mixed with the new GGBFS batch. This could be one reason for the reduction in compressive strength.

The thermosetting resin reached a maximum compressive strength in the short-term, more than 120 MPa after one week (III). However, the strength started to decline afterward. The UCS was declined by 40 % after one month, and 72 % after three months compared to one-week results. The compressive strength after six months was only 22 MPa and the material showed a severe plastic behavior. The compressive strength after nine months was not achievable due to hydrothermal degradation. Deterioration of mechanical properties is not intended for a barrier material candidate. Besides, the achieved results of the current thermosetting resin highlight the necessity of long-term evaluation of alternative setting materials (VII).

For the Portland cement-based systems, the compressive strength was measured to be almost constant the test period. The neat class G cement reached maximum strength of 40 MPa after one week and the strength was slightly declined up to six months and reached 35 MPa. After nine months, the strength was reduced to 26 MPa, which was 35 % less than the maximum of its strength during this period. The expansive cement followed the same trend, and the compressive strength was reduced by 24 % after peaking at 45 MPa in one week to 34 MPa in nine months. The curing temperature was 90 °C, which is close to the 110 °C landmark for strength retrogression (Nelson and Guillot, 2006). To minimize the retrogression, an extra source of silica (between 35 to 40 % BWOC) is normally introduced to the cement powder (de Sena Costa et al., 2017).

The UCS results up to nine months provided an overview of the mechanical behavior of materials over time. Although the change of mechanical properties for these mix designs of thermosetting resin and pozzolanic material can give a full picture of their behavior under elevated pressure and temperature, the geopolymer and both cements may need more time to reach a plateau in compressive strength trend over time (VII).

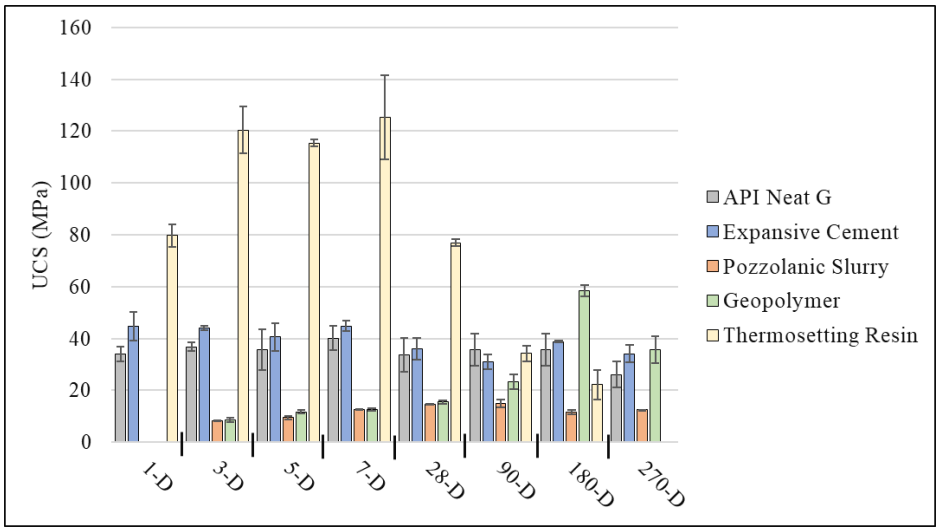

Figure 5.4. UCS test results of the materials at different time intervals; cured at 90 °C and 170 bars (VII).

Figure 5.5 shows Young's modulus of the materials calculated at the elastic region of stress-strain curve, and it is an indication of the flexibility of materials. At the same compressive strength, a higher Young's modulus means a less flexible material. Young's modulus of the materials followed almost the same trend as compressive strength after each time interval. Among all samples, the thermosetting resin test results cured after 90 days may not be reliable data, since the material was entered into plastic region immediately after applying the load. However, the thermosetting resin had a higher compressive strength and higher flexibility compared to other materials up to one week of curing (III).

When studying the mechanical properties of brittle materials such as cement, it is essential to consider both strength and flexibility of materials. In fact, a material with higher flexibility and lower strength may dampen the external stress and survive better than a stronger material with less flexibility. Therefore, the ratio of UCS to Young's modulus (UCS/YM) was calculated for all materials (Figure 5.6). The

calculated ratio for the thermosetting resin was significantly higher than the other materials (around 17×10^{-3}). Hence, the right vertical axis was allocated to thermosetting resin. The ratio is a dimensionless parameter, and the higher values are representing a higher performance. The ratio for the pozzolanic material was slightly higher in long-term. The geopolymer started to show better performance compared to the cement system, from three months to the end of nine months. The performance of the pozzolanic material and the geopolymer during the test period was partially better than the cement system (VII).

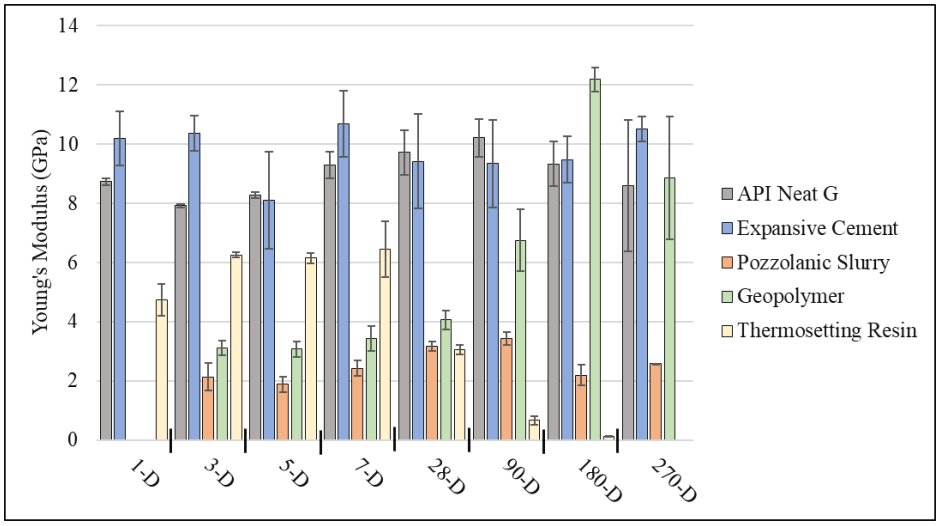

Figure 5.5. Young's modulus test results of the materials at different time intervals; cured at 90 °C and 170 bars (VII).

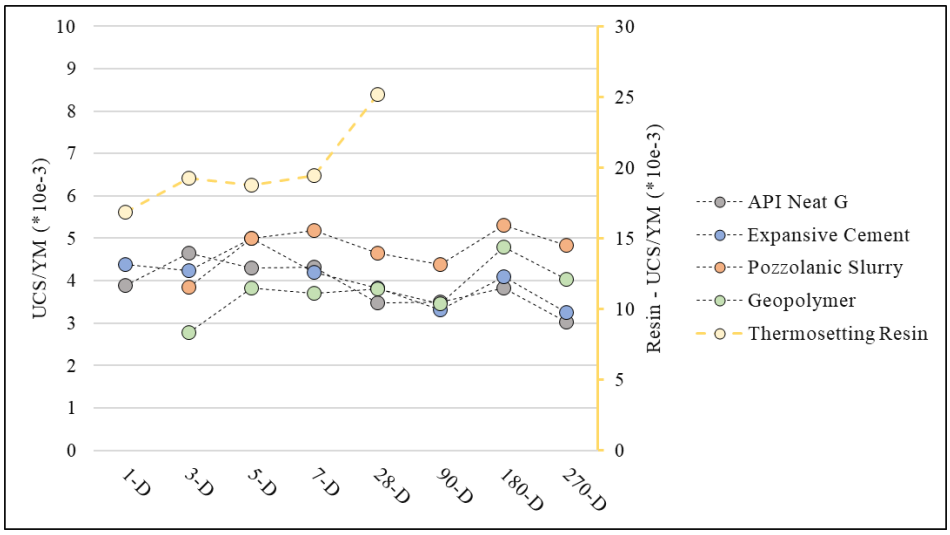

Figure 5.6. UCS/YM of the materials. The right vertical axis shows the ratio for thermosetting resin. Vertical axis is a dimensionless parameter (VII).

5.2.2 *Tensile strength*

The tensile strength was measured indirectly by applying Brazilian test. Figure 5.7 shows tensile strength of the barrier materials (VII). The thermosetting resin had an average tensile strength of 9.5 MPa, which was the highest tensile strength up to one month (IV). The reliability of data for a three-month-old sample and on, is under question due to a significant increase in flexibility of the material. The tensile strength of pozzolanic material was measured to be almost constant, and it was about 1 MPa ± 0.25. The average tensile strength of the geopolymer was 0.8 MPa for the first three months. However, the tensile strength increased by 170 % after six months and remained almost constant at 1.75 MPa up to nine months (VII).

Tensile strength for the expansive cement was increased by 30 %, from 1.5 to 2 MPa in the first seven days. The strength was reduced by 40 % for this material after one month and reached 1.2 MPa. The tensile strength was then increased after six months and reached 2.2 MPa and

remained constant after nine months curing. This trend was almost the same for the class G cement. The material had tensile strength of 2.8 MPa after nine months, which was about 27 % higher than the strength of the material after during the first week of curing. A detail discussion is provided in Appendix (VII).

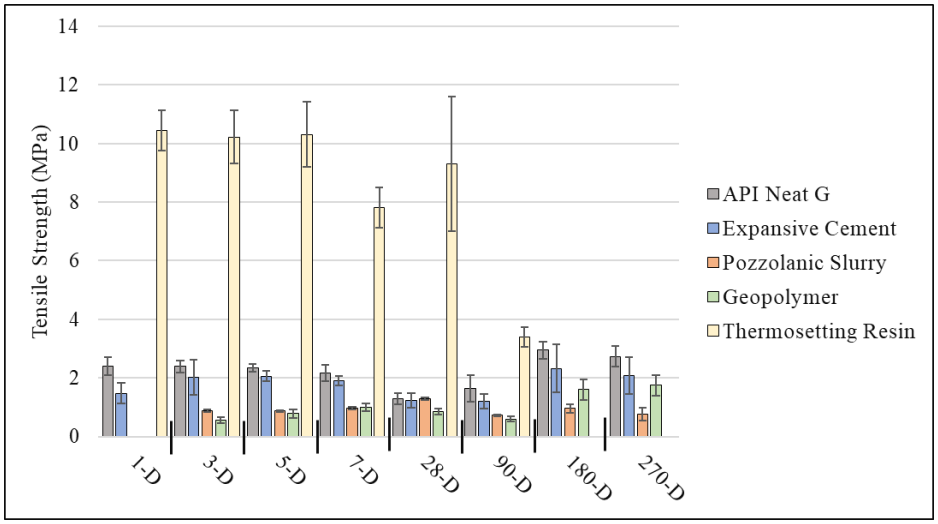

Figure 5.7. Indirect tensile strength of the materials at different time intervals; cured at 90 °C and 170 bars (VII).

5.2.3 *Sonic strength development*

In oil field applications, UCAs are used to measure the strength development of cement. In this method, transit time of the sonic wave is the direct measurement, which is the function of the material's chemistry and structure. A unique algorithm was developed for each material to convert the transit time to compressive strength. The UCS data was plotted versus the measured transit time. The developed polynomial equations for each material are presented in Table 5.2. The UCA test was conducted up to one month for each material and the results are described in the Appendix (III and IV)

Table 5.2. Generated customized algorithm of the barrier materials for the UCA test based on data up to one month (III, IV).

Material	Polynomial equation	R-square value
Class G cement	y=125.77x2 – 3701.1x + 226795	0.9822
Expansive cement	$y = 190.85x^2 – 5281.6x + 35842$	0.9788
Pozzolanic material	$y = 365.82x^2 – 9880.6x + 65261$	0.9907
Geopolymer	$y = 28.662x^2 – 1310.9x + 12057$	0.995
Thermosetting resin	$y = 250.9x^2 – 9065.9x + 80945$	0.8502

5.2.4 *Conclusion*

1- The change in mechanical properties over the testing period revealed the necessity of long-term evaluation of materials for critical applications.

2- According to the UCS and UCA data, the geopolymer was not able to develop early strength for more than two days, while the consistency curve showed that the material is only pumpable for almost two hours. The retarder used in the mix design to prolong the pumping time negatively affected the strength development. Therefore, the gelation time was longer.

3- For all materials, no correlation was observed between the compressive and tensile strengths. For example, the compressive strength of the geopolymer increased between one month and three months, while its tensile strength remained unchanged in this period. The compressive strength observed between six and nine months curing time was decreased, while its tensile strength did not change.

5.3 *Microstructure analysis*

5.3.1 *SEM and EDS Analysis*

Morphology of the materials was studied by running SEM test on crushed samples in UCS tests. Figure 5.8 shows the SEM image of the barrier materials after seven days, three months, and nine months (VII). The Portland cement after hydration forms calcium – silicate – hydrate (C-S-H) as the major phase. This phase is responsible for the strength development after setting. The plates of calcium hydroxide (CH) were identified in the cement matrix after seven days, while they were not found in the three-month-old samples and later (see green square in Figure 5.8). However, the column structure of portlandite dominate the cement matrix. After nine months, the column structure shifted to the dense compact structure. Besides, lamellar plates that could be the result of phase transformation and strength retrogression were identified in the nine-month-old samples. This observation agrees with the UCS results of the API class G cement after nine months (see Figure 5.4). The BHST is 90 °C, which is close to the 110 °C landmark for strength retrogression (Nelson and Guillot, 2006). The XRD results shown in Section 5.3.2 revealed that in nine-month samples, portlandite phase has been increased and C-S-H phase was reduced as result of phase change. As mentioned in Section 5.2.1, for high temperatures, it is a common practice that 35 to 40 % BWOC silica-rich compound (i.e., silica flour) is added to the cement to reduce the calcium oxide to silicon oxide ratio to about 1.0 (Nelson and Guillot, 2006).

In expansive cement, Mg-based expanding agents serve the material to compensate for the chemical shrinkage through crystal growth. The matrix o the material is denser compared to the API class G cement. The crystals of the expanding agent were detected by EDS element analysis and are highlighted with orange arrows shown in Figure 5.8. In the samples assessed after one-week and three-month curing, the crystals are entirely integrated into the surrounding cement matrix. The crushed

samples after nine months of curing showed cracks at the boundaries of the crystals with nearby cement structure. Nevertheless, the mechanical properties were not significantly affected during the test period and the strength of the material followed almost a constant trend. The microsilica added to the slurry acts as the filler in early stages and becomes part of the structure through pozzolanic reaction. It partially act as a silica source preventing strength retrogression as well as providing a gas-tight structure of the expansive cement (Grinrod et al., 1988).

In the pozzolanic material, the matrix had a zeolitic-like structure. This structure is shown by the light orange arrows. However, the structure was impermeable, and it provided hydraulic sealability (see Section 5.4.2), which proves that the pores exist in the matrix are not connected to each other. Moreover, the spongy structure matches the low compressive strength and high flexibility of the material during the nine months of testing. More information regarding the chemical composition of the evaluated material is prohibited due to commercialization purposes.

The SEM image of the geopolymer shows a dense structure after solidification highlighted by green arrows (Figure 5.8). A spongy structure was identified within the one-week-old sample, which is due to the formation of three-dimensional structures after polycondensation in geopolymerization reaction. The geopolymerization reaction leaves unreacted ingredients in the structure to various extents, while they react at a slower rate with alkaline pore solution until becoming part of the geopolymer matrix (Khalifeh et al., 2013). In this mix design, the unreacted rock-based source of aluminosilicate and GGBFS are indicated by blue and yellow arrows, respectively. The EDS element analysis revealed a significantly lower amount of the rock-based aluminosilicate source in the nine-month-old samples compared to younger ones. The existence of such unreacted particles could act similar

to aggregate in concrete, while entire consumption of them results in formation of geopolymer gels with less strength.

The SEM images of thermosetting resin show spheres widespread on the sample's surface (Figure 5.8). The spheres are glass beads added as a weighting agent to the slurry and they are surrounded by the solidified organic resin. The thermosetting resins were cured for one month and after showed radial expansion. The radial expansion after one month was about 2 %, while after nine months, the diameter was increased by almost 12 %. This expansion cracked the curing molds for six- and nine-month old samples. The images for thermosetting resin did not show any change in the microstructure of the material, neither the solidified resin nor the weighting agents and their interface with the resin. Hence, it requires another technique than SEM analysis for further analysis.

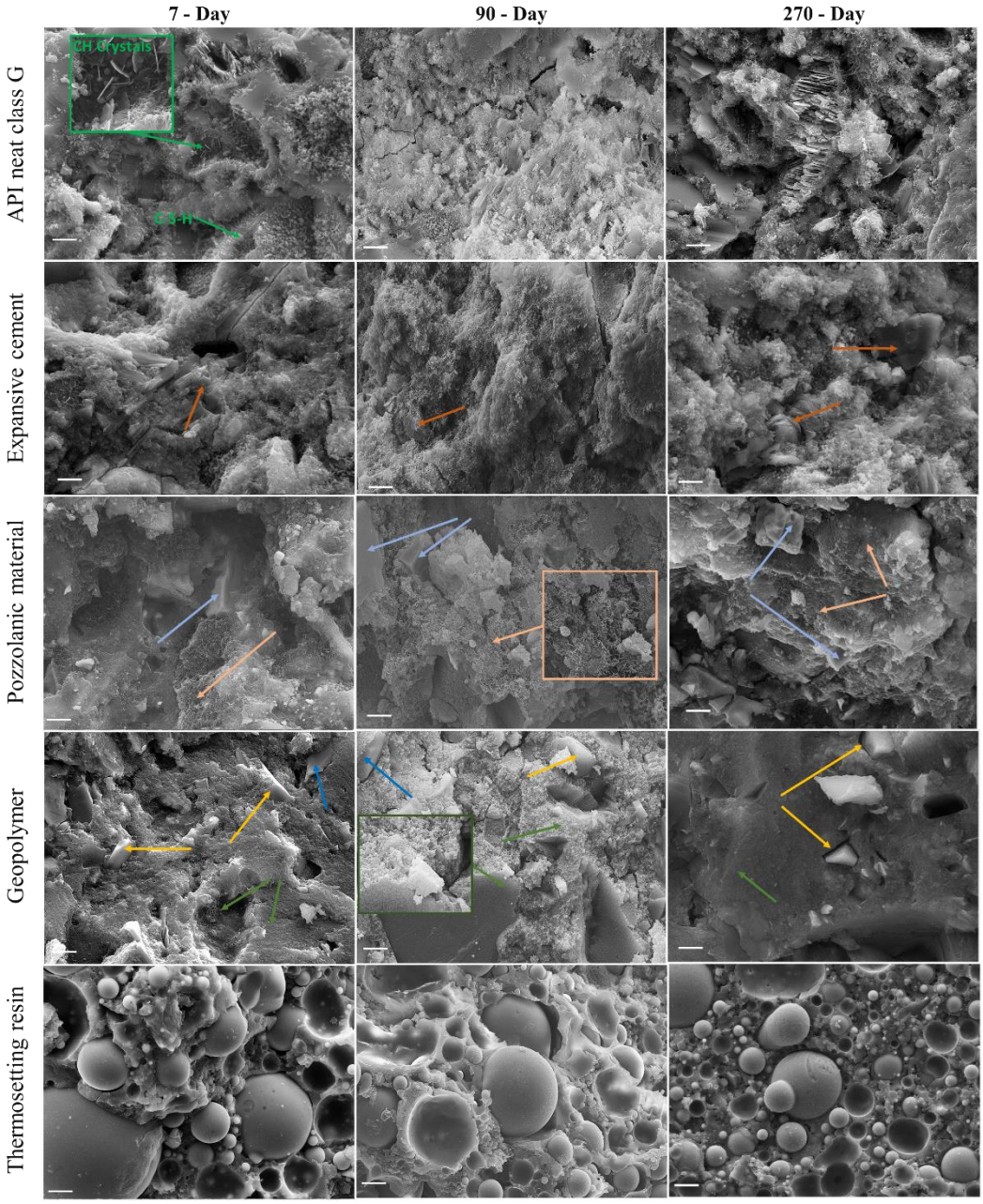

Figure 5.8. SEM images of barrier materials after one week, three months, and nine months. All images, except for the thermosetting resin are taken at the same magnification and the indicated scale bar is 2 µm. For the thermosetting resin, the scale bar is 10 µm (VII).

5.3.2 *XRD-Rietveld determined mineralogy*

The powder X-ray diffraction (XRD) technique was used to study crystallography, phases of the solidified materials, and to relate the possible phase change to behavior of the materials. The samples were collected from UCS crushed specimens, and grinded for XRD analysis. The results of one-month samples for expansive cement and pozzolanic material were discarded due to low intensity in XRD patterns. Rietveld refinement method was used by employing TOPAS software from Bruker to identify and quantify the phases in materials. This method is a powerful technique in which least-squares procedure is applied to quantify phases in the test sample. In this method, the structure of identified phases in XRD test are added to the software and the data is fit to the model. The weighted sum of squared differences between both observed and computed values should be minimized through the algorithm (Toby, 2006). Weighted profile R-factor (R_{wp}) and Goodness-of-fit (GOF) are the terms used to evaluate the Rietveld refinement. The values between 1 and 2 for GOF ($1 < GOF < 2$) and values equal and less than 10 for R_{wp} ($R_{wp} \leq 10$) are considered as good match (Toby, 2006). For all material, GOF are summarized in Table 5.3.

Table 5.3. Goodness of fit and Weighted profile R-factor corresponding to Rietveld refinement.

	7D		1M		3M		6M		9M	
	GOF	R_{WP}	GOF	R_{WP}	GOF	R_{WP}	GOF	R_{WP}	GOF	R_{WP}
Neat class G	1.09	4.44	1.44	4.73	1.12	4.53	1.13	4.55	1.06	4.32
Expan**sive** cement	1.06	3.82	-	-	1.02	4.26	1.04	4.63	1.05	4.24
Pozzolanic material	1.29	5.00	-	-	1.28	5.77	1.31	5.92	1.28	5.42
Geopolymer	1.43	5.72	1.5	5.75	1.42	5.59	1.54	6.09	1.93	7.44

For the expansive and neat class G cements, four major phases were identified (Figure 5.9.A and B). These phases are grouped as clinker and C-S-H phases, while portlandite, α-C_2SH phases are showed separately. The clinker phase includes calcium disilicate, calcium trisilicate, and

calcium aluminoferrite as major elements and it remained almost constant in all samples.

The C-S-H phase is the major product of cement hydration, and it is accountant for the material's strength. In neat G cement, the amount of this phase was constant from seven days to six months. However, this phase was reduced by about 10 % for the nine-month-old samples. This observation agrees with the UCS test results of the material. The compressive strength of the class G cement was reduced after nine months by 35 % compared to six-month-old samples. It was discussed earlier in Section 5.2.1, the curing temperature was 90 °C, which is close to the 110 °C landmark for strength retrogression. During this process, the C-S-H phases converts to a high crystalline phase of alpha dicalcium silicate hydrate (α-C_2SH) at calcium-rich areas. The result is shrinkage of matrix and deterioration in mechanical strength of the material. Although such sharp increase in α-C_2SH was not observed between six- and nine-month-old samples, the general trend is increasing for this phase. Portlandite (CH) crystals are liberated after cement hydration reaction. The refinement results show the portlandite phase was almost constant up to six months; however, the concentration was increased by 5 % after nine months. It satisfies the observation from SEM image of the neat class G cement after nine months, where portlandite crystals were noticed in the structure. Crystal structure growth can increase the formation of cavities in the cement matrix and therefore, reduce the ability of the material to hold higher compression loads.

For expansive cement, the C-S-H was decreased from seven days to nine months, which fits the UCS results. The C-S-H phase was reduced slightly from three months to six months and remained constant up to nine months. Portlandite and α-C_2SH had no major change during the period. Considering the fact that microsilica was added to the mix, the excess source of silica in cement can chemically interact with portlandite through a pozzolanic reaction and form C-S-H phase (Araújo et al., 2019; de Sena Costa et al., 2017). Unlike the neat class G cement that

experienced strength retrogression, expansive cement was backed up by the pozzolanic reaction to maintain its strength after nine months.

Figure 5.9.C shows the XRD refinement of pozzolanic material. Low amount of clinker phase compared to the cement-based materials confirms that pozzolanic material has different ingredient than the Portland cement. However, the identified phases after solidification were like hydrated cement. The material consists of C-S-H phases up to about 90 %, while minor amount of clinker, calcite, α-C_2SH, and quartz were recognized. The identified phases were remained unchanged during the period. This behavior matches the strength profile of the material. Since the pozzolanic material is already patented, further investigation is prohibited by the supplier.

Figure 5.9.D shows the results for geopolymer. Four major phases in solidified materials were C-S-H, plagioclase, microcline and quartz. Considering that the XRD results of the seven-day and nine-month samples include different batch of GGBFS, most of phases follows a trend for one-, three-, and six-month-old samples. During these intervals, the C-S-H phase was increased gradually, which is fitting strength development trend of the material. Besides, the quartz and microcline phases exist in the rock-based aluminosilicate source decreased during this period, which is an indication of ongoing geopolymerization reaction in this material. The XRD results for geopolymer highlights the importance of material source in chemistry of reaction and generated phases after solidification.

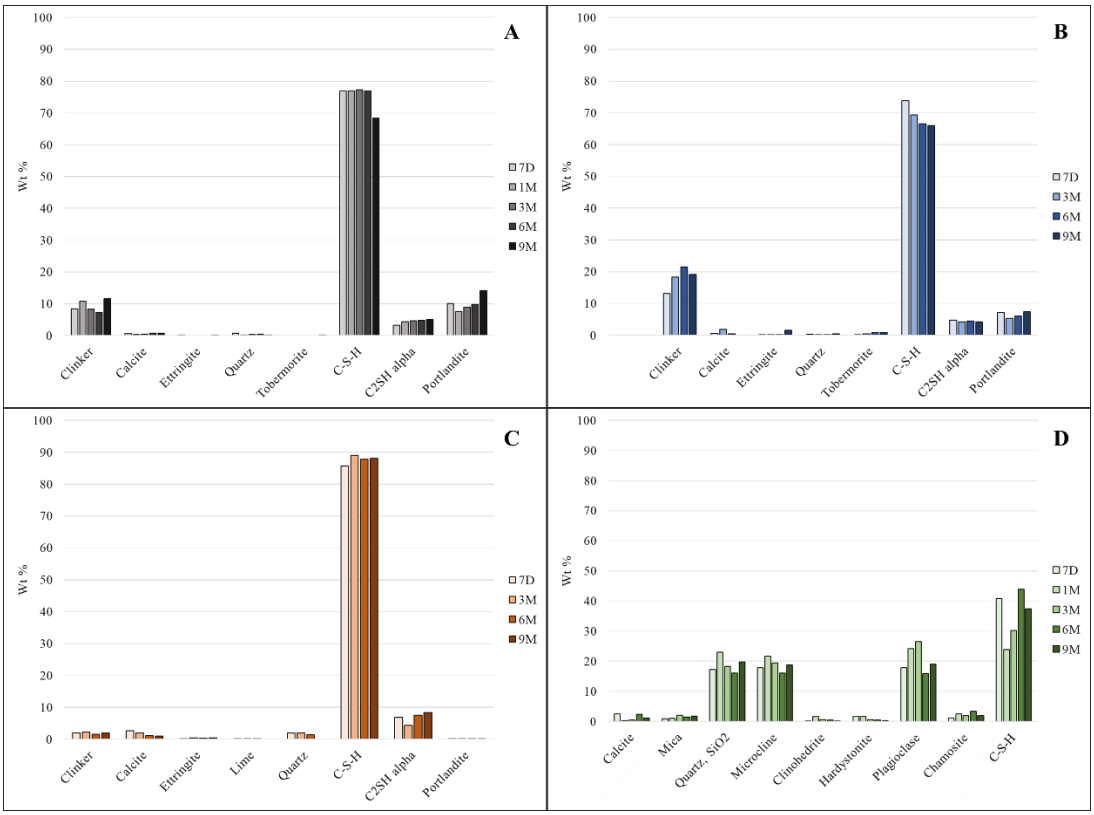

Figure 5.9. Quantification of the major phases using Rietveld refinement method. A) neat class G cement, B) expansive cement, C) pozzolanic material, and D) geopolymer.

5.4 ***Bond strength and interface analysis***

5.4.1 *Shear Bond Strength*

Shear bond strength of materials was tested after curing samples for seven days. Figure 5.10 shows the measured shear bond strength of the materials for clean steel and rusty steel surfaces (V, VI). The shear bond strength at the rusty surface was higher to a different extent compared to that at the clean surface.

The thermosetting resin did not bond to the outer pipe. The samples were cured at elevated temperature of 90 °C and cooled down to the ambient temperature for testing. The coefficient of thermal expansion of thermosetting resin is higher than the steel pipe, therefore, debonding could occur due to excess tension at the interface. On the bar side, the shear bond strength was increased by 100 %, by changing from 2.6 to 5.2 MPa. The main reason is the increase of surface roughness of the rusted pipe. Although it was the highest bond strength measured among all materials, it was significantly touched by its high coefficient of thermal expansion.

The pozzolanic material failed to bond to the clean steel pipe, while the bond strength was 0.25 MPa on the rusty pipe surface. In this case, the surface roughness may have less impact on the shear bond strength. Because if it was the reason, the same impact should be noticed on the bar side. However, the bond strength did not change at the bar side. It is worth noting that the chemical composition of bar and pipe metals are different. The variation in mineralogy and morphology of rust products can directly affect the compatibility and bonding between hardened pozzolanic material and different steel surfaces.

For the geopolymer material, a 100 % increase in shear bond strength was observed when the rusty surface was used compared to the clean surface at both pipe and bar. This increase in SBS is both due to a change in surface roughness and possible chemical interaction between the rust products and geopolymer binder during solidification. For the API class G cement, the bond strength did not change very much neither at the bar or pipe surfaces. The bond strength of expansive cement increased by 140 and 75 % on the bar and pipe, respectively. Similar to the geopolymer, the increase of bond strength of expansive cement may benefit from both roughness and the chemical interaction with rust.

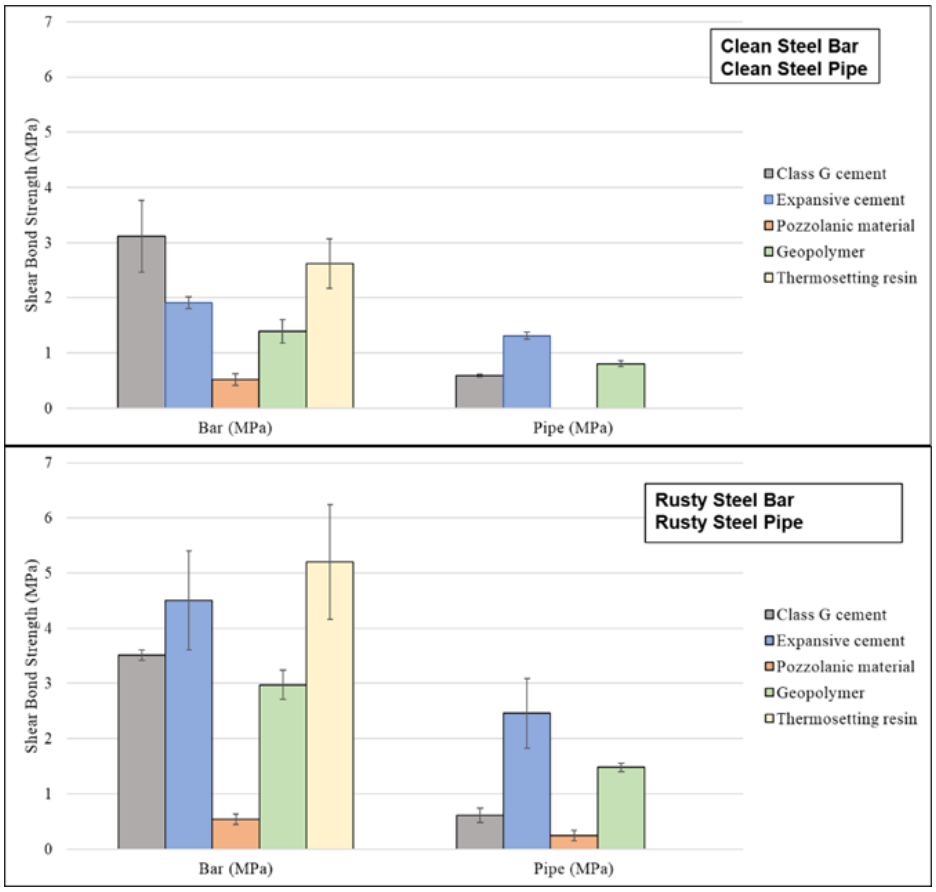

Figure 5.10. Shear bond strength test results from push-out test for clean steel surface (top) and rusty surface (bottom). Samples cured at 90 °C and 34 bars (V, VI).

5.4.2 *Hydraulic sealability*

Figure 5.11 shows the results of hydraulic sealability and hydraulic bond strength of materials (V, VI). These tests were performed at ambient temperature after curing samples at downhole conditions. The thermosetting resin was not able to hold the differential pressure around the sample. This is related to its high coefficient of thermal expansion compared to the steel pipe. The neat class G cement started to leak both at the interface and through the cement matrix. Presence of a rusted

surface had no significant impact on the hydraulic sealability of the cement at its interface with the steel pipe. One reason for the leakage is the autogenous shrinkage of cement matrix after solidification (Nelson and Guillot, 2006). The capillary pressure developed in empty pores of the cement structure introduces excess tension to the structure. Such tensile force at the interface opens micro paths for the fluid to flow and therefore, poor hydraulic sealability.

The expansive cement had better hydraulic sealability compared to the neat class G cement both at the clean and rusty surfaces. The clean steel samples started to leak at pressures above 20 bars, while the rusted surface provided better sealability. Additionally, no leakage was observed through the bulk of the material. The expanding agents introduced in the mix design compensated for the possible shrinkage of the cement matrix. Besides the supplementary materials such as microsilica added to the slurry made a dense structure preventing leakage through the matrix.

The hydraulic sealability profile and the abnormal shape of the pozzolanic material with rusty pipe revealed incompatibility of material and rust products (VI). The material swelled at its interface with a rusted surface which is an indication of a mismatch between the rust products and pozzolanic material that can affect its long-term hydraulic sealability. The injection flow rate for the pozzolanic material was less than the geopolymer. However, the injecting flowrate was higher at rusted surface compared to the clean surface steel.

Hydraulic sealability of geopolymer was better on the clean surface. The rust existed on the steel surface, however improved the shear bond strength properties, but it had a negative impact on the hydraulic bond strength of geopolymer. As the leakage was only observed at the interface of the rusted pipe and not through the matrix, apparently the geopolymerization reaction has deviated due to mixing with rust products and the formation of different minerals at the interface.

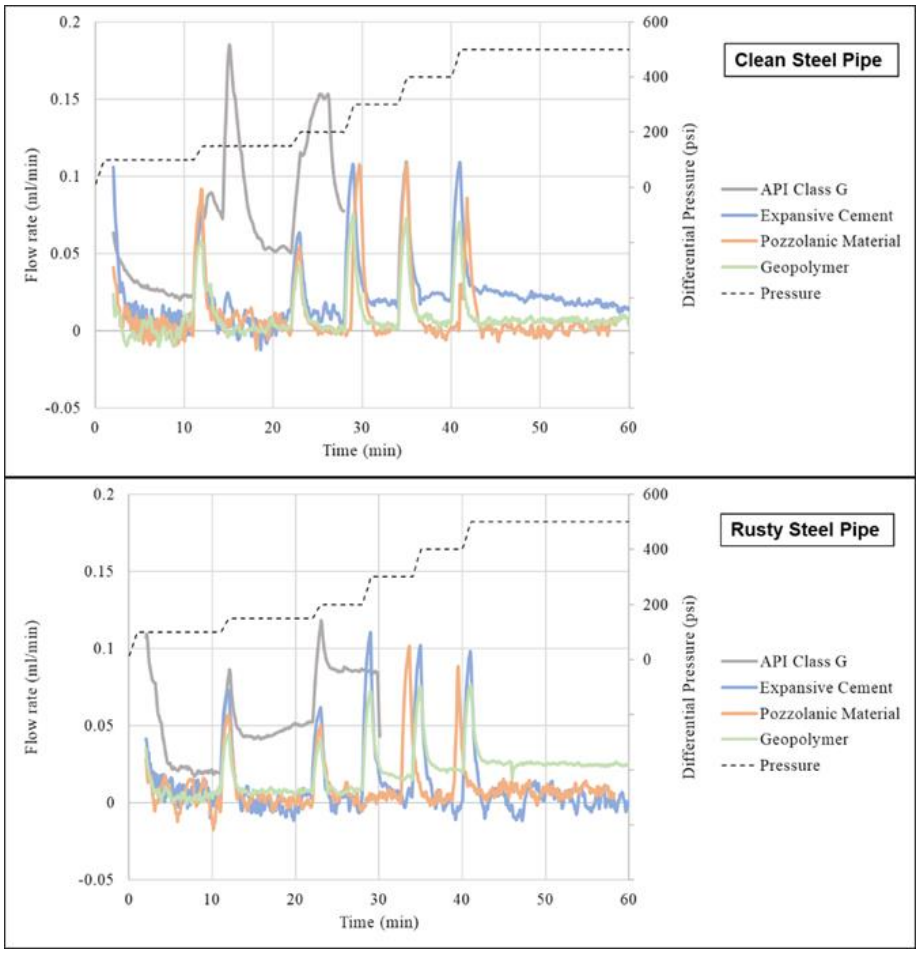

Figure 5.11. Hydraulic sealability test results for clean steel (top) and rusted steel (bottom). Sharp humps in the figures are because of increase in the pressure level across the samples

Overall, hydraulic sealability measurement of a barrier material expresses the potential of material to prevent fluid to flow, either through its matrix or at its boundaries with surrounding medium. In the first scenario, the structure of the material should be impermeable or have very low permeability. In this study, neat class G cement was not able to stop fluid flow within the matrix structure. It is due to the connectivity of the pores in the structure. The injecting water was able to penetrate the material under the applied differential pressure. The expansive

cement, pozzolanic material, and geopolymer had very low porous structure, or the pores were not connected to transfer the fluid within the matrix. The second scenario can be complicated. If there are micro-paths formed along with the cement-casing interface and it is connected to the source of fluid, the fluid would flow through the path, even at very low differential pressure around the interface. However, one can assume a case where the micro-path is not fully developed, and it is blinded off at some distance from the fluid source. When increasing the differential pressure, the ability of a material to hold its bonding to the surrounding medium and prevent propagation of micro-path is expressed as hydraulic bond strength. Hydraulic bond strength is the function of fluid normal forces in the micro-annuli, size of the micro-annuli, chemical compatibility of the material with surrounding material, and mechanical properties of the barrier material and surrounding material.

5.4.3 *Steel – setting material interface*

As described in previous sections, the essence of interface properties between barrier materials and steel is not well understood. In this section, morphology and mineralogy at the interface of the setting materials after solidification were presented (VI). The polished steel surface, prepared as per Section 4.8, was considered as casing representative. The samples were cured for seven days at the equal condition as the SBS and hydraulic sealability test. The interface of the materials was separated accurately and coated with palladium plasma and placed under electron microscope for analysis.

The photos in Figure 5.12 and Figure 5.13 reveal the morphology of setting materials at the interface and the corresponding steel interface, respectively. Since the foremost intention of this test was to search for iron content at the interface, the microscope was set on the backscattered electron (BSE) mode to search for heavy elements accumulating on the surface by indicating brighter zones. The test was continued on the secondary electron (SE) that provides a better resolution on the

morphology of the materials. The porous structure on the surface of the neat class G cement (Figure 5.12. A) supports the poor hydraulic sealability results of the system. The surface is covered by a huge amount of hexagonal calcium hydroxide crystals, as well as calcium – silicate – hydrate (C-S-H) gels and needle shape ettringite. Generally, at the steel-cement interface, a higher concentration of alkaline pore solution (mainly $Ca(OH)_2$) acts as a buffer on the steel surface and protects it from destructive reactions (Page, 1975). Besides, higher concentration of $Ca(OH)_2$ at the interface increases calcium hydroxide (CH) crystal accumulation, which results in porous structure to form in this region (Horne et al., 2007). The SEM analysis on the neat class G – steel interface satisfies these statements as a porous structure with large crystals were observed on both cement and steel surfaces. The connectivity of these pores between CH crystals has negative impact on hydraulic sealability of class G cement.

Figure 5.12. B shows the surface of the expansive cement. The surface had a uniform structure that can be proof of its good hydraulic sealability. Apparently, the microsilica added to the mix design filled the pores and formed a dense C-S-H gel near surface compared to the neat class G cement. The ditch on the right side of the picture (see Figure 5.12. B) is the crystal of expanding agent added to the mix design to compensate for the shrinkage of the cement after solidification. However, positioning of expanding agent close to steel-cement interface can jeopardize hydraulic sealability of the system in long-term. These crystals can rupture the surface and rise toward the steel. Particle size of expanding agent and the final size of the corresponding crystal are parameters that must be considered for expansive cements. The steel surface connected to the expansive cement (Figure 5.13. B) is covered by wrinkles. The wrinkle shapes were concentric and branched from silicate and calcium-rich spots. Since the steel surface was prepared in the same procedure as for other materials, this pattern on the steel surface may be due to solidification reaction and the reason is still a remaining question.

Figure 5.12. C shows surface of the pozzolanic material. Although the surface has porous structure, the pores are not connected to each other and that is aligned with its good obtained hydraulic sealability. The bright spots are the unreacted ingredients of the material. The BSE scanning showed that the surface was full of heavy elements. But using EDS X-ray mapping, only a few points contained iron accumulation on the surface. The corresponding steel surface (Figure 5.13 C) was covered by the needle structures with the same composition of the pozzolanic material. The results from hydraulic bond and shear bond strength tests are evident that structure near the surface of the pozzolanic material can provide hydraulic sealability, while the structure is not strong enough to withstand the applied shear force.

Figure 5.12. D shows surface of the geopolymer. The surface structure was intact, similar to the expansive cement that endures the good hydraulic sealability results. The grain in the middle of the picture is an unreacted GGBFS. The UCS results in this study proved that the geopolymerization reaction continues over time and unreacted particles may react with the pore solution at a slower rate. Therefore, the matrix of geopolymers is continuously under development, which affects the mechanical properties as well as the structure at the interface. The BSE scanning of the geopolymer surface showed bright spots and the EDS X-ray mapping showed high iron concentration on that spot. Figure 5.13 D matches the steel surface connected to the geopolymer. The surface was covered with a dense fine structure separated from the geopolymer matrix. The profile of this structure on steel surface reveals a good grip between geopolymer and steel. The high shear bond strength supports the decent mechanical properties of the structure in this region.

Figure 5.12. E and Figure 5.13. E are SEM images of the thermosetting resin and the connected steel surface, respectively. Although the material failed to maintain hydraulic sealability due to its high coefficient of thermal expansion, it had a good bonding to the inner bar in the SBS test. Using BSE and EDS X-ray mapping, iron accumulation was

detected on the resin's surface. The spherical bright points in the picture are glass beads used in the mix as the weighting agent. Since there was only one iron-rich point observed on the resin's surface, it can be an error in sample preparation i.e., mill scale left on the surface during steel preparation. The SEM image of steel shows solidified resin adhered to the surface.

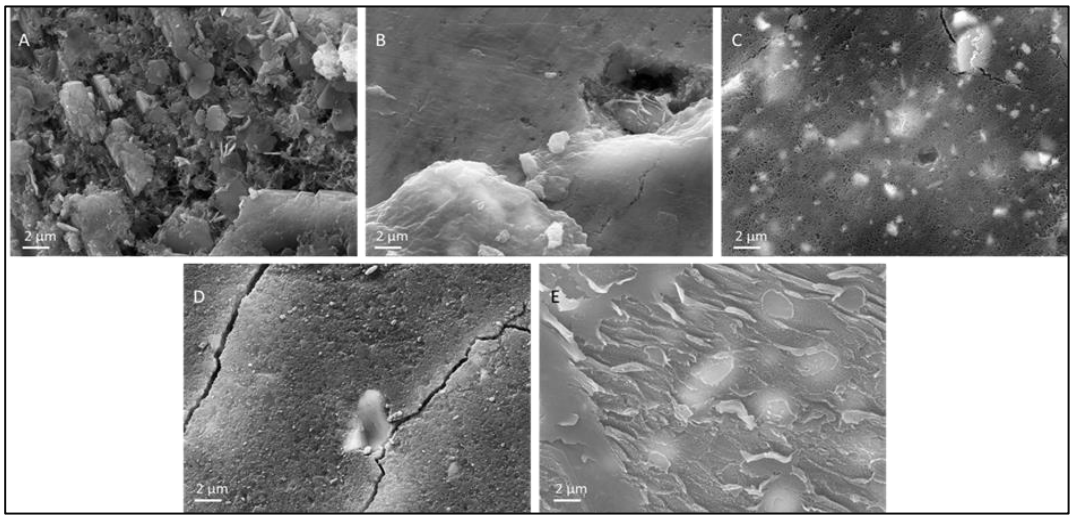

Figure 5.12. SEM images of the interface of setting materials with steel surface. A) neat class G, B) Expansive cement, C) Pozzolanic material, D) Geopolymer, and E) Thermosetting resin

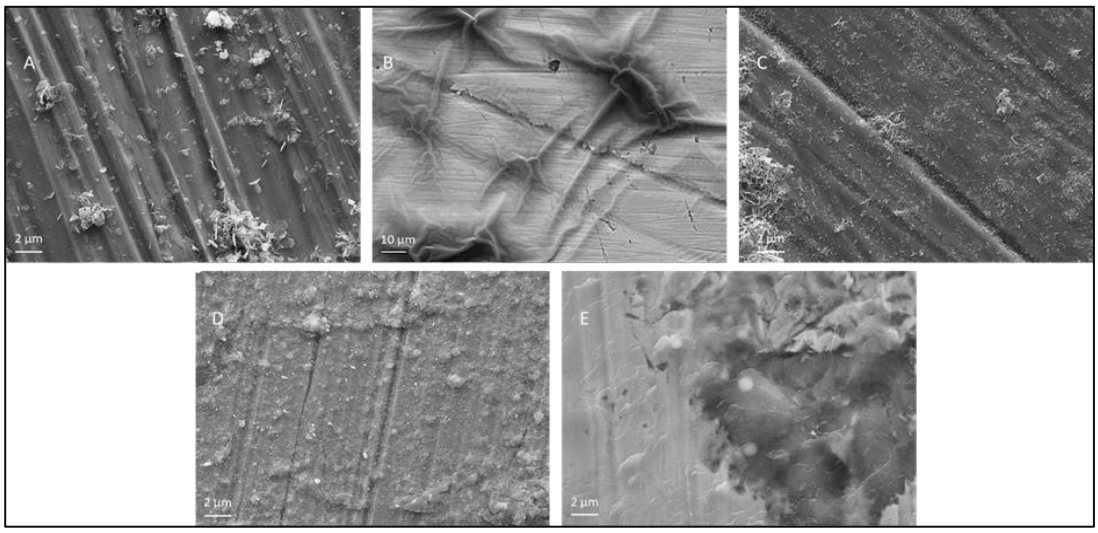

Figure 5.13. SEM images of steel surface connected to setting materials. A) neat class G cement, B) Expansive cement, C) Pozzolanic material, D) Geopolymer, and E) Thermosetting resin

Figure 5.14 shows the clean steel bars placed in the middle of SBS setup. The samples were left in the open air for a long time (the time is mentioned for each material). It is evident that the steel bars contacted with geopolymer and pozzolanic material remained clean, while those connected to cement systems were rusted. The neat class G cement had a permeable structure and therefore, air and humidity could transfer through the cement matrix. Although the expansive cement showed an impermeable structure during hydraulic sealability test, drying shrinkage could induce microcracks in the cement matrix facilitating humidity to reach the steel surface. The other root for crack could be uncontrolled crystal growth of expanding agents. Hence, the shear bond and hydraulic bond strength tests should be repeated after a longer curing period to confirm the workability of expanding agents.

The geopolymer structure remained impermeable after one year and the steel bar was protected from interaction with humidity. Depending on the mix design and ingredients, geopolymers have self-healing capability to some extent, which the cracks that formed due to drying shrinkage can

be healed after some time and under a specific environment (Liu et al., 2020). The steel bar connected to the pozzolanic material was removed six months earlier compared to other materials. But is expected to follow the same mechanism as the geopolymer.

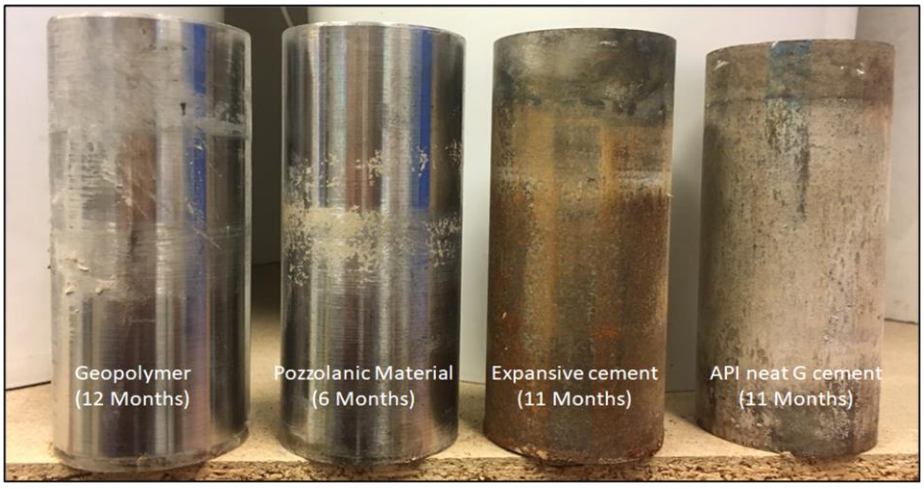

Figure 5.14. The steel bars placed in the SBS samples were removed. The samples were kept in the open air for different time intervals. The steels in geopolymer and pozzolanic material were still intact, while those which were inside the Portlandf based cement were rusted. The steel bar inside the thermosetting resin was difficult to remove and therefore, left inside the sample.

5.4.4 *Conclusion*

The bond strength test results can be affected by the difference in curing and testing temperature. It is due to the high coefficient of thermal expansion for some materials such as thermosetting resin.

1- The shear bond strength and hydraulic sealability have no correlation. One material can have high shear bond strength with a specific steel surface, while the interface could have a porous structure with high permeability.
2- On a rusty surface, the rust products can chemically interact in the solidification process and help to make a strong shear bond,

while the matrix has a high permeability that passes fluids within the structure.

3- For the geopolymer, although the rusty surface provided a higher shear bond strength, the possibility of chemical interaction between the rust product and the binder may for a stronger bonding to the steel. However, this zone may have permeable structure that negatively hydraulic sealability of geopolymer.

4- The expanding agents introduced in the expansive cement supported the material from leakage at the interfaces after one week. Since the mechanism of expansion is crystal growth, the chemical reaction of expanding agents should be monitored in longer period. Because uncontrolled crystal growth in long period at the circumferential regions pushes the cement from the steel surface and opens a gap at the interface.

5- The measurements at the steel – pozzolanic interface and steel – neat class G interface are good examples for concluding there is no correlation between shear bond and hydraulic sealability of barrier materials with steel casing.

6 Summary & Conclusion

In this study, selected candidate materials for cementing operation were evaluated at equal condition of pressure and temperature. The fluid-state properties and rheological behavior at the liquid phase were examined right after mixing and based on recommended procedures. The density, pH, and viscosity of the materials were within the requested operational range.

Thermosetting resin and pozzolanic material had lower gel strength compared to other materials, which may increase the risk of particle segregation before solidification depending on the ingredient's particle size. The expansive cement had a higher viscosity at low shear rates. Both cements and geopolymer developed stronger gel strength revealing their time-dependent rheological structure. For the recommended predefine bottom-hole circulation temperature, it is recommended that the slurries to be pumpable for more than four hours. The class G cement and geopolymer had a low pumpability compared to the expansive cement and thermosetting resin. The pozzolanic material did not develop gel after 28 hours using API consistometers. The expansive cement, pozzolanic material, and geopolymer revealed acceptable values for the static fluid loss test. The thermosetting resin was not bonded to the weighting agents, and blow-out occurred after about seven minutes.

Mechanical behavior of the materials was examined from one day to nine months curing time. The thermosetting resin showed the highest strength up to one month, and the mechanical properties retrograded afterward. The structure of this material could not hold any compression load after nine months. Mechanical behavior of the class G cement was stable for most of the test period. The structure of the material experienced retrogression between six and nine months which negatively affected the compressive strength of the material. The UCS of the expansive cement was slightly reduced during the test period; however, the reduction rate

was not as intensive as for the class G cement. The microsilica introduced to the slurry acted as an external silica source that can delay the strength retrogression.

The compressive strength of geopolymer was increased until six months curing time and then decreased after nine months. Geopolymerization reaction was delayed at earlier periods due to retarder introduced during mixing. The compressive strength of this material after six months of curing was 400 % higher than one-week-old samples. The compressive strength, tensile strength, and flexibility of cement-based systems and geopolymer were all in the same range after nine months. The pozzolanic material, although having a retarded strength development, had a constant strength during the curing period. The material had the lowest mechanical strength and the highest flexibility after nine months.

The shear bond strength and hydraulic sealability of barrier materials have no correlation with each other. The neat class G cement had high shear bond strength with a specific steel surface, while the interface was porous and had a high permeability. The rust product on the steel surface had a negative impact on the hydraulic sealability of pozzolanic material and geopolymer. The expansive cement had better hydraulic sealability with a rusted steel than the clean steel surface. The chemical composition of steel surface is important since the existing elements can chemically interact with the slurry during solidification process and form new minerals with different properties compared to the matrix of materials.

The interface analysis of materials on the polished steel surface provided a better understanding about the morphology of steel- steering material interface. The class G cement had a porous structure at its interface with steel. The expansive cement and geopolymer had an integrated surface due to ingredients introduced during mixing. The pozzolanic material had a zeolitic structure interface. The pores were not connected and fulfilled proper hydraulic sealability.

The main conclusion of this research study can be drawn as follows:

- The mechanical behavior of all tested materials highlights the importance of the long-term assessment of alternative barrier materials for cementing operations.
- There is no correlation between the tensile and compressive strengths of materials in the long term.
- The current mix design of geopolymer is not applicable for cementing operation as it has low pumpability and high wait on cement time.
- The retarder introduced to the geopolymer mix showed its impact on setting rather than gelation.
- The current mix design of pozzolanic material increases wait on cement time and nonproductive time of operation.
- Chemistry of the current mix design of thermosetting resin is not suitable for placing the slurry in this operating pressure and temperature. Zones with high permeable formation can separate the liquid resin and leave a fluid with higher density in the drilled hole.

Reference

Americal Petroleum Institute, A., 2010. API Spec 10A, Specification for Cements and Materials for Well Cementing, Specification for Cements and Materials for Well Cementing. API, Washington DC: API.

American Petroleum Institute, A., 2013. API RP 10B-2, Recommended Practice for Testing Well Cements, Washington, DC: API. API.

American Petroleum Institute, A., 2017. API TR 10TR7, Mechanical Behavior of Cement, Washington, DC: API. API.

American Society for Testing and Materials, A., 2015. ASTM-D695, Standard Test Method for Compressive Properties of Rigid Plastics. ASTM. doi:10.1520/D0695-15

Araújo, R.G.d.S., Freitas, J.C.d.O., Costa, B.L.d.S., Moreira, P.H.S.S., Silva, F.P.F.d. and Oliveira, Y.H.d., 2019. Alternative Material to be Applied in Oil Well Cementing Subjected to High Temperatures to Avoid Compressive Strength Retrogression, Offshore Technology Conference. OnePetro.

Bearden, W.G. and Lane, R.D., 1961. Engineered cementing operations to eliminate WOC time, Drilling and Production Practice. OnePetro.

Beharie, C., Francis, S. and Øvestad, K.H., 2015. Resin: An Alternative Barrier Solution Material, SPE Bergen One Day Seminar. Society of Petroleum Engineers.

Bensted, J., 1998. Special cements, LEA's Chemistry of Cement and Concrete. Elsevier, pp. 783-840.

Bullard, J.W., Jennings, H.M., Livingston, R.A., Nonat, A., Scherer, G.W., Schweitzer, J.S., Scrivener, K.L. and Thomas, J.J., 2011. Mechanisms of cement hydration. Cement and concrete research, 41(12): 1208-1223.

Chamssine, F., Khalifeh, M., Eid, E., Minde, M.W. and Saasen, A., 2021. Effects of Temperature and Chemical Admixtures on the Properties of Rock-Based Geopolymers Designed for Zonal Isolation and Well Abandonment, International Conference on Offshore Mechanics and Arctic Engineering. American Society of Mechanical Engineers, pp. V010T11A031.

Dahlem, J., Baughman, T., James, T. and Kelly Rives, R., 2017. Intervention and Abandonment-Riserless Productive Zone Abandonment Using Epoxy Resin, Offshore Technology Conference. Offshore Technology Conference.

Davidovits, J., 2013. Geopolymer cement. A review. Geopolymer Institute, Technical papers, 21: 1-11.

de Sena Costa, B.L., de Souza, G.G., de Oliveira Freitas, J.C., da Silva Araujo, R.G. and Santos, P.H.S., 2017. Silica content influence on cement compressive strength in wells subjected to steam injection. Journal of Petroleum Science and Engineering, 158: 626-633.

East, M., 2018. Technology Roadmap - Low Carbon Transition in the Cement Industy. , International Energy Agency.

Eid, E., Tranggono, H., Khalifeh, M., Salehi, S. and Saasen, A., 2021. Impact of Drilling Fluid Contamination on Performance of Rock-Based Geopolymers. SPE Journal: 1-8.

Fantilli, A., Mancinelli, O. and Chiaia, B., 2019. The carbon footprint of normal and high-strength concrete used in low-rise and high-rise buildings. Case Studies in Construction Materials, 11: e00296.

Gasda, S.E., Bachu, S. and Celia, M.A., 2004. Spatial characterization of the location of potentially leaky wells penetrating a deep saline aquifer in a mature sedimentary basin. Environmental geology, 46(6-7): 707-720.

Ghofrani, R. and Plack, H., 1993. CaO-and/or MgO-swelling cements: a key for providing a better annular sealing?, SPE/IADC Drilling Conference. Society of Petroleum Engineers.

Grinrod, M., Vassoy, B. and Dingsoyr, E., 1988. Development and use of a gas-tight cement, IADC/SPE Drilling Conference. OnePetro.

Hajimohammadi, A., Provis, J.L. and van Deventer, J.S.J., 2011. The effect of silica availability on the mechanism of geopolymerisation. Cement and Concrete Research, 41(3): 210-216.

Hodne, H., Saasen, A., O'Hagan, A.B. and Wick, S.O., 2000. Effects of time and shear energy on the rheological behaviour of oilwell cement slurries. Cement and concrete research, 30(11): 1759-1766.

Horne, A., Richardson, I. and Brydson, R., 2007. Quantitative analysis of the microstructure of interfaces in steel reinforced concrete. Cement and Concrete Research, 37(12): 1613-1623.

International Organization for Standardization, I., 2014. ISO/TS-16530, Well Integrity - part 1: Life Cycle Governance / Part 2: Well Integrity for Operational Phase.

Jafariesfad, N., Geiker, M.R. and Skalle, P., 2017. Nanosized magnesium oxide with engineered expansive property for enhanced cement-system performance. SPE Journal, 22(05): 1,681-1,689.

Karim, M., Hossain, M., Zain, M., Jamil, M. and Lai, F., 2017. Durability properties of a non-cement binder made up of pozzolans with sodium hydroxide. Construction and Building Materials, 138: 174-184.

Khalifeh, M., 2016. Materials for optimized P&A performance: Potential utilization of geopolymers.

Khalifeh, M., Hodne, H., Saasen, A. and Vralstad, T., 2013. Techniques and materials for north sea plug and abandonment operations, Offshore Technology Conference. Offshore Technology Conference.

Khalifeh, M. and Saasen, A., 2020a. Introduction to Permanent Plug and Abandonment of Wells. Springer Nature.

Khalifeh, M. and Saasen, A., 2020b. Types of Permanent Plugging Materials, Introduction to Permanent Plug and Abandonment of Wells. Springer, pp. 97-136.

Khalifeh, M., Saasen, A., Hodne, H. and Motra, H.B., 2019. Laboratory evaluation of rock-based geopolymers for zonal isolation and permanent P&A applications. Journal of Petroleum Science and Engineering, 175: 352-362.

Kiran, R., Teodoriu, C., Dadmohammadi, Y., Nygaard, R., Wood, D., Mokhtari, M. and Salehi, S., 2017. Identification and evaluation of well integrity and causes of failure of well integrity barriers (A review). Journal of Natural Gas Science and Engineering, 45: 511-526.

Liu, X., Nair, S.D., Aughenbaugh, K.L., Juenger, M.C. and van Oort, E., 2020. Improving the rheological properties of alkali-activated geopolymers using non-aqueous fluids for well cementing and lost circulation control purposes. Journal of Petroleum Science and Engineering, 195: 107555.

McCarthy, M.J. and Dyer, T.D., 2019. Pozzolanas and pozzolanic materials. Lea's Chemistry of Cement and Concrete: 363-467.

Nelson, E.B. and Guillot, D., 2006. Well Cementing. Schlumberger.

NORSOK-D-010, 2013. Well integrity in drilling and well operations. Standard Norway.

Oil&GasUK, 2015. Guidelines on Qualification of Materials for the Abandonment of Wells-Issue 2, OIL & GAS UK, London.

Page, C., 1975. Mechanism of corrosion protection in reinforced concrete marine structures. Nature, 258(5535): 514-515.

Paiva, M.D., Silva, E.C., Melo, D.M., Martinelli, A.E. and Schneider, J.F., 2018. A geopolymer cementing system for oil wells subject to steam injection. Journal of Petroleum Science and Engineering, 169: 748-759.

Panchmatia, P., Olvera, R., Genedy, M., Juenger, M.C. and van Oort, E., 2020. Shrinkage behavior of Portland and geopolymer cements at elevated temperature and pressure. Journal of Petroleum Science and Engineering, 195: 107884.

Papadakis, V.G., Fardis, M.N. and Vayenas, C.G., 1992. Hydration and carbonation of pozzolanic cements. Materials Journal, 89(2): 119-130.

Power, D. and Zamora, M., 2003. Drilling fluid yield stress: measurement techniques for improved understanding of critical drilling fluid parameters, AADE Technical Conference, Houston, pp. 1-3.

Provis, J.L. and van Deventer, J.S.J., 2009. Geopolymers: structures, processing, properties and industrial applications. Elsevier.

PSA, 2020. Trends in Risk Level in Norway's Petroleum Activity (RNNP) 2020, Petroleum Safety Authority Norway.

Rattanasak, U., Pankhet, K. and Chindaprasirt, P., 2011. Effect of chemical admixtures on properties of high-calcium fly ash geopolymer. International Journal of Minerals, Metallurgy, and Materials, 18(3): 364-369.

Saasen, A. and Ytrehus, J.D., 2018. Rheological Properties of Drilling Fluids: Use of Dimensionless Shear Rates in Herschel-Bulkley and Power-law Models. Applied Rheology, 28(5).

Saleh, F.K. and Teodoriu, C., 2017. The mechanism of mixing and mixing energy for oil and gas wells cement slurries: A literature

review and benchmarking of the findings. Journal of Natural Gas Science and Engineering, 38: 388-401.

Salehi, S., Khattak, J., Saleh, F.K. and Igbojekwe, S., 2019. Investigation of mix design and properties of geopolymers for application as wellbore cement. Journal of Petroleum Science and Engineering, 178: 133-139.

Sanabria, A., Knudsen, K. and Leon, G., 2016. Thermal activated resin to repair casing leaks in the Middle East, Abu Dhabi International Petroleum Exhibition & Conference. Society of Petroleum Engineers.

Taghavi, S., Alba, K., Moyers-Gonzalez, M. and Frigaard, I., 2012. Incomplete fluid–fluid displacement of yield stress fluids in near-horizontal pipes: experiments and theory. Journal of Non-Newtonian Fluid Mechanics, 167: 59-74.

Taylor, H.F., 1997. Cement chemistry, 2. Thomas Telford London.

Toby, B.H., 2006. R factors in Rietveld analysis: How good is good enough? Powder diffraction, 21(1): 67-70.

Todorovic, J., Raphaug, M., Lindeberg, E., Vrålstad, T. and Buddensiek, M.-L., 2016. Remediation of leakage through annular cement using a polymer resin: A laboratory study. Energy Procedia, 86: 442-449.

Trudel, E., Bizhani, M., Zare, M. and Frigaard, I., 2019. Plug and abandonment practices and trends: A British Columbia perspective. Journal of Petroleum Science and Engineering, 183: 106417.

Van, N.D., Choi, H. and Hama, Y., 2019. Modeling early age hydration reaction and predicting compressive strength of cement paste mixed with expansive additives. Construction and Building Materials, 223: 994-1007.

Vernon-Parry, K., 2000. Scanning electron microscopy: an introduction. III-Vs Review, 13(4): 40-44.

Vrålstad, T., Saasen, A., Fjær, E., Øia, T., Ytrehus, J.D. and Khalifeh, M., 2019. Plug & abandonment of offshore wells: Ensuring long-term well integrity and cost-efficiency. Journal of Petroleum Science and Engineering, 173: 478-491.

Zhan, P.-m. and He, Z.-h., 2019. Application of shrinkage reducing admixture in concrete: A review. Construction and Building Materials, 201: 676-690.

Appendices

Appendix 1 – Test Matrix

Tests		Neat class G	Expansive cement	Pozzolanic material	Geopolymer	Thermosetting resin
Viscosity		❋	❋	❋	❋	❋
Consistency	Atmospheric	❋	❋	❋	❋	❋
	Pressurized	❋	❋	❋	❋	❋
S Fluid Loss		❋	❋	❋	❋	❋
Gel Strength		❋	❋	❋	❋	❋
UCS (ATM)	1Day	❋	❋	❋	❋	❋
	3Day	❋	❋	❋	❋	❋
	5Day	❋	❋	❋	❋	❋
	7Day	❋	❋	❋	❋	❋
Tensile (ATM)	1Day	❋	❋	❋	❋	❋
	3Day	❋	❋	❋	❋	❋
	5Day	❋	❋	❋	❋	❋
	7Day	❋	❋	❋	❋	❋
UCS (PRS)	1Day	❋	❋	❋	❋	❋
	5Day	❋	❋	❋	❋	❋
	7Day	❋	❋	❋	❋	❋
	28Day	❋	❋	❋	❋	❋
	90Day	❋	❋	❋	❋	❋
	180Day	❋	❋	❋	❋	❋
	270Day	❋	❋	❋	❋	❋
Tensile (PRS)	1Day	❋	❋	❋	❋	❋
	5Day	❋	❋	❋	❋	❋
	7Day	❋	❋	❋	❋	❋
	28Day	❋	❋	❋	❋	❋
	90Day	❋	❋	❋	❋	❋
	180Day	❋	❋	❋	❋	❋
	270Day	❋	❋	❋	❋	❋
SSI Analysis	7Day	❋	❋	❋	❋	❋
SEM/XRD	7Day-9Month	❋	❋	❋	❋	❋
UCA	28Day	❋	❋	❋	❋	❋
Bond strength	7Day					
Shear bond	Clean steel	❋	❋	❋	❋	❋
	Rusted steel	❋	❋	❋	❋	❋
Hydraulic bond	Clean steel	❋	❋	❋	❋	❋
	Rusted steel	❋	❋	❋	❋	❋

Appendix 2 – Paper I

Materials for Well Integrity – Rheological Behavior Study

M. Kamali, M. Khalifeh, A. Saasen, L. Delabroy, R. Godøy

Paper SPE-209556-MS presented at SPE Norway Subsurface Conference, Bergen, Norway, 27th April 2022.

DOI: 10.2118/209556-MS

Appendix 3 – Paper II

Materials for Well Integrity – Short-Term Mechanical Properties of Cement Systems

M. Kamali, M. Khalifeh, A. Saasen, L. Delabroy

Paper SPE-200739-MS presented at the SPE Norway Subsurface Conference, Bergen, Norway, 2nd November 2020.

DOI: 10.2118/200739-MS

Appendix 4 – Paper III

Materials for Well Integrity: Characterization of Short-Term Mechanical Properties

M. Kamali, M. Khalifeh, A. Saasen, L. Delabroy

Paper OMAE2020-18623 presented at the 39th International Conference on Ocean, Offshore and Arctic Engineering OMAE2020, August 3-7, Virtual Online.

DOI: 10.1115/OMAE2020-18623

Appendix 5 – Paper IV

Alternative Setting Materials for Primary Cementing and Zonal Isolation – Laboratory Evaluation of Rheological and Mechanical Properties

M. Kamali, M. Khalifeh, A. Saasen, R. Godøy, L. Delabroy

Journal of Petroleum Science and Engineering, 2021.

DOI: 10.1016/j.petrol.2021.108455

Journal of Petroleum Science and Engineering 201 (2021) 108455

Contents lists available at ScienceDirect

Journal of Petroleum Science and Engineering

journal homepage: http://www.elsevier.com/locate/petrol

Alternative setting materials for primary cementing and zonal isolation – Laboratory evaluation of rheological and mechanical properties

Mohammadreza Kamali [a,*], Mahmoud Khalifeh [a], Arild Saasen [a], Rune Godøy [b], Laurent Delabroy [c]

[a] Department of Energy and Petroleum Engineering, University of Stavanger, 4036, Stavanger, Norway
[b] R&D Department, Equinor, 4035, Stavanger, Norway
[c] Aker BP ASA, 4020, Stavanger, Norway

ARTICLE INFO

Keywords:
Drilling operation
Zonal isolation
Primary cementing
Barrier materials
Cementing

ABSTRACT

Portland cement is the prime zonal isolation material used in hydrocarbon wells and its utilization has been extended to geothermal, carbon sequestration and gas storage wells. Despite the vast quantity of research activities and publications, well integrity reports show shortcomings associated with Portland cement at specific conditions of pressure, temperature, chemical environment and geographical locations. In this experimental study, four alternative barrier materials have been selected for further experiments at laboratory scale: an industrial class of expansive cement, a non-cement pozzolanic slurry, a rock-based geopolymer and an organic thermosetting resin. Neat class G cement was used as reference material for comparing the results.

The study includes the rheological behavior of the candidate materials, static fluid-loss and pumpability at both atmospheric and elevated pressures. All of the materials at the liquid phase showed an acceptable viscosity profile at the operational shear rates. The consistency curve of the slurries showed that the barrier materials are pumpable for the desired period with the right-angle set (RAS), except for the pozzolanic slurry, which was not able to make gel up to 24 h at dynamic conditions.

Mechanical properties of the candidate barrier materials including uniaxial compressive strength (UCS), modulus of flexibility, sonic strength development and tensile strength of the samples were characterized up to 28 days of curing. The UCS test results showed that the thermosetting resin has an extremely high compressive strength compared to the other materials, while the geopolymer and the pozzolanic slurry are more ductile. The tensile strength of the materials experienced no significant change over time; however, for the neat class G cement, it is reduced after 28 days.

1. Introduction

During zonal isolation operations, known as primary cementing, Portland cement is normally used as well barrier element to provide well integrity by preventing uncontrolled fluid flow behind the casing string. Portland cement serves the casing by anchoring and protection for a corrosive downhole environment. The barrier material is a key element to maintain well integrity, it should be able to meet a number of criteria necessary to achieve a safe operation during the life cycle of the well. According to the available guidelines (American Petroleum Institute, 2013; American Petroleum Institute, 2017; International Organization for Standardization, ISO, 2014; Norsok, 2013), candidate barrier materials have to make an integrated bonding with the casing pipe and formation to sufficiently seal the annular space between casing and formation or two casings. Additionally, the zonal isolation materials should be impermeable to prevent fluid migration within the barrier sheath. The bottom-hole corrosive environment shall not critically deteriorate the chemical and mechanical properties of the zonal isolation material. The intense mechanical loads are sometimes unavoidable; hence, it is essential that the barrier material has adequate mechanical strength and flexibility to withstand the downhole stresses caused by temperature and pressure changes. In addition, it is necessary to avoid the changes in the bulk volume of the barrier material. Severe shrinkage and expansion in the volume can damage the barrier sheath and consequently, results in loss of well integrity. Lastly, the compatibility of cementitious material and casing should be considered; any detrimental

* Corresponding author.
E-mail address: Mohammadreza.kamali@uis.no (M. Kamali).

https://doi.org/10.1016/j.petrol.2021.108455
Received 5 October 2020; Received in revised form 19 January 2021; Accepted 21 January 2021
Available online 27 January 2021

reaction at the interface can cause debonding and forming micro-annular paths.

Ordinary Portland cement (OPC) has been used extensively for primary cementing operations for many years (Nelson and Guillot, 2006). Therefore, its properties and behavior at various phases are well-known among engineers and academia. Along with its availability and reasonable market price, OPC has been a practical cementitious material for primary cementing, remedial activities and permanent plug and abandonment (P&A) (Le-Minous et al., 2017). However, over the years, a number of concerns related to short- and long-term utilization of OPC has been stated by operating companies and scientists (Jimenez et al., 2016). The industrial reports and academic publications have declared that a range of 2–45% of both production and injection wells, depending on the number of the wells per geographical location, suffer from well integrity issues (Davies et al., 2014; Vignes, 2011). They addressed the major shortcomings like low ductility and brittleness, bulk shrinkage while curing, low durability in a corrosive environment, and low thermal and chemical stability at elevated temperatures (Al Ramadan et al., 2019; Kiran et al., 2017; Vrålstad et al., 2018). Enormous research works have studied the effect of different additives intending to enhancing both rheological and mechanical properties of OPC and make it adaptable to drilling conditions (Jafariesfad et al., 2017a; Khalil et al., 2020; Mangadlao et al., 2015; Moreira et al., 2018). Despite all modifications and researches conducted on development of additives to well cements, the concerns are still valid as the main root of shortcomings is cement chemistry. Therefore, researchers have been searching for alternatives to Portland cement for field applications. Of these, one may refer to expansive cement, Pozzolanic based slurries, geopolymers and thermosetting resins (Abid et al., 2019; Beharie et al., 2015; Jafariesfad et al., 2017b; Khalifeh et al., 2018).

The current objective is to characterize rheological behavior and mechanical properties of the abovementioned materials at the equal downhole condition and presenting their shortcomings and advantages. The mechanical properties were measured in the short-term, and in a time span from 24 h after curing up to 28 days. The result for each test is compared with test results obtained with neat API class G cement, which is the prime material for the OPC. During this project, the bottom-hole circulating temperature (BHCT) was set to 65 °C, while the bottom-hole static temperature (BHST) was 90 °C. The pressure for curing the samples was equal to 17 MPa. This condition is applicable to the majority of the wells on the Norwegian Continental Shelf (NCS). Prior to discussing the experimental results, it is necessary to familiarize readers with barrier materials.

1.1. Expansive cement

Integrated bonding at cement-casing and cement-formation interfaces is crucial for achieving zonal isolation. Cement shrinkage is a result of chemical, autogenous and drying shrinkage phenomena. Hydration reaction of cement is associate with shrinkage as volume of the paste product is less than the reactants (Henkensiefken et al., 2009). The decrease in volume due to the hydration reaction is referred to as chemical shrinkage. The hydration reaction, however, continues as the slurry hardens. The unreacted cement in the system consumes the remaining water trapped in pores and leave the pores empty. The pore water drainage results volume reduction, which is caused by capillary pressure development and extra tension within the cement matrix. This process is simplified in Fig. 1. The volume change due to the pore water consumption is known as autogenous shrinkage. As the slurry solidifies, the change in volume is because of the autogenous shrinkage, which is lower compare to the chemical shrinkage (Henkensiefken et al., 2009). The shrinkage-induced tension can be intensified at the cement sheath inner and/or outer circumferences by external loads from pressure or temperature changes at nearby environment. If the summation of tensions exceeds the tensile strength of the cement, the risk of forming radial cracks or debonding from casing and formation increases significantly.

A proven approach of improving sealability and elimination of micro-annuli formation due to OPC volume shrinkage is the use of expansive zonal isolation materials, which expand upon setting (Baumgarte et al., 1999). The expanding agents act either by making crystals growing within the structure or by the controlled generation of gas bubbles within the cement matrix. Different mechanisms can be taken to acquire expansion within the cement system, and they are extensively reviewed in the literature (Nelson and Guillot, 2006; Santos et al., 2018; Thomas et al., 2014). Among all methodologies that have been investigated, the application of magnesium oxide (MgO) in well cements have revealed appropriate results. In civil and construction industry, where confining pressure may not exist, the amount of MgO is critically controlled to avoid cracks due to the expansion of the cement matrix. In the oil well, on the contrary, MgO can compensate shrinkage and maintain zonal isolation. The effectiveness of the expansive agent reaches a maximum when the corresponding expansion reaction takes place while the shrinkage arises. On one hand, the early expansion would not compensate for the long-term shrinkage in the cement matrix. Very late expansion may cause crack in the cement structure; hence, the expansive additives should be carefully engineered. Yet, the full control of the reaction and the effectiveness of the agent at different operational conditions are under investigation (Santos et al., 2020). The parameters such as expansive agent's particle size, and the dosage, time control of the reaction, and downhole pressure and temperature have a critical role in short- and long-term mechanical properties of the cement after solidification. The experimental observations show that hybrid use of nano-sized MgO with diverse reactivity levels can solve the issue of early expansion before solidification of the cement slurry (Jafariesfad et al., 2017b).

In this research work, a commercial industry expansive cement, which is extensively used for P&A operation is investigated for primary cementing operation and zonal isolation. The cement system has MgO as an expansive agent. This agent is dry blended with API class G cement.

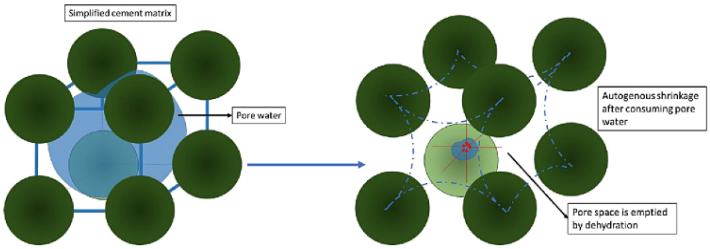

Fig. 1. Autogenous shrinkage of the cement-based materials during solidification.

1.2. Pozzolanic slurry

Some silica-rich materials, known as pozzolans, may not have cementitious properties on their own, but react with calcium hydroxide ($Ca(OH)_2$) in an aqueous environment and show cementitious properties (American Society for Testing and Materials, ASTM, 2013). Pozzolans are widely used as cement extender for cement and they are available in natural and artificial types. In the presence of pozzolans, the permeability of cement is significantly reduced and the silica reacts with undesirable side reaction products, $Ca(OH)_2$ in the system and form a stable and durable calcium – silicate – hydrate (C–S–H) compound. The microporous structural units broadly known as zeolites exist in pozzolanic materials. Zeolites can act as an ion-exchange component in a corrosive environment and maintain the cement properties (Papadakis et al., 1992).

In this study, a commercial pozzolan-based slurry is considered as a barrier material for primary cementing. It is a non-OPC material and it is primarily used as spacer fluid ahead of cement. Its rheological properties can be adjusted to the desired level and the slurry can set and develop strength at downhole conditions. No detailed information is available for the composition of this slurry. This material is used in the North Sea. Therefore, test results of this material are added for benchmarking its performance.

1.3. Geopolymer

Inorganic polymers, known as geopolymer, are a class of cementitious materials produced by mixing a liquid hardener with reactive aluminosilicate species (Davidovits, 2013). The tetrahedral long-chain molecules that consist of aluminum and silicate are formed during geopolymerization reaction and hence, no hydration takes place. The solid phase that is broadly known as geopolymeric precursor, may include low calcium fly ash, thermally activated clay (metakaolin) or naturally occurring rocks (Khalifeh et al., 2019; Liu et al., 2020; Salehi et al., 2019). The liquid phase is an alkali (normally sodium or potassium) silicate solution with an optimum modular ratio. The reaction is known as geopolymerization and it consists of three main mechanisms: the dissolution of aluminosilicate structure of the solid phase in presence of hydroxyls and creation of silanol groups (Si–O–H), orientation and reconnection of molecules due to an increase in the concentration of ions in the slurry and forming oligomers and finally, polycondensation by connecting oligomers and forming a long-chain structure of aluminosilicates.

The geopolymers are already used in civil industry, but the technology is still under development for oil and gas applications by adjusting the rheological and mechanical properties in accordance with downhole conditions. Previous research works confirmed that rheological behavior and mechanical properties of geopolymers are temperature-dependent (Khalifeh et al., 2018; Paiva et al., 2018). In the current work, a naturally occurring rock normalized with other aluminosilicate sources (Alvi et al., 2020) is mixed with potassium silicate solution to produce the rock-based geopolymers.

1.4. Thermosetting resin

Organic thermally activated resins, broadly known as thermosetting resin, can be solidified when exposed to a predesigned temperature. Thermosetting resins are considered as particle-free liquid polymers and this feature allows penetrating micro fractures and seal the leak paths by forming heavy-molecule solids (Beharie et al., 2015; Cestari et al., 2009). Therefore, they are mainly used for remediation jobs to seal the micro crack or defected annular cement. Temperature, pressure and the composition of the liquid resin are the main variables in the polymerization reaction. Glass transition temperature in thermosetting resins is defined as the maximum temperature after which, the solid material enters into the plastic region and rigid behavior is not available no longer (Montserrat, 1993). Therefore, it is critical to have full control over the mix design of resin, operational condition, and geological temperature gradients in the drilling environment.

Thermosetting resins have been studied for potential P&A applications and in remedial field operations (Al-Ansari et al., 2015; Todorovic et al., 2016). This class of organic materials has shown interesting mechanical properties. The compressive strength is considerably higher than the OPC while they are more ductile. However, their volume shrinkage and exothermic reaction during solidification can introduce mechanical and thermal stresses at specific circumstances and bring concerns (Vrålstad et al., 2018). In this study, glass beads are used to adjust density of the slurry; hence, our system is not considered as particle-free system.

2. Test material preparation and experimental procedure

In all experiments, the slurries were mixed using the raw materials delivered by the industrial service providers and the mixing procedure was followed in accordance with the provided instructions. The mixing procedure for each cementitious material is described as follows:

Neat class G cement – The neat API class G cement manufactured by Dyckerhoff was mixed with 44% deionized water. API high-speed mixer, Waring blender, was used to mix the slurry.

Expansive cement – The dry blended API class G cement (Dyckerhoff) with magnesium oxide as an expansive agent was delivered by the material supplier. Industrial chemicals were added to the slurry to tailor the rheological and mechanical properties of the slurry. The additives included in this study were retarders, fluid-loss controller, defoamer and cement particle dispersant. Microsilica solution with a mass fraction of 50% in water was recommended by the cement supplier to enhance performance of the material.

Pozzolanic slurry – Common industrial chemicals that usually are used for controlling cement properties were applied to mix the slurry. A chemical activator was introduced to the slurry before pre-conditioning. The pozzolanic slurry was mixed and delivered by the material supplier.

Geopolymer – The precursor was dry blended in accordance with the recommended procedure. The solid phase was an aluminosilicate rich naturally occurring rock normalized by adding active quenched blast furnace slag (BFS), which is an industrial waste, to achieve normalized chemical composition. Potassium silicate solution with a modular ratio of 2.49 was used as hardener and mixed with solid phase before pre-conditioning. API high-speed model, Waring mixer, was used to mix the slurry.

Thermosetting resin – The liquid pre-mixed resin based of vinyl toluene was provided by the material supplier. Glass beads were used to increase the mass density of the resin mixture and a viscosifier was added to control the rheological properties. The slurry was mixed at 600 RPM using Heidolph overhead stirrer model Heigh-TORQUE. The materials used in this study are summarized in Table 1.

Slurry preparation – All the laboratory experiments performed in a specific condition of pressure and temperature to simulate downhole conditions; where the bottom-hole circulating temperature (BHCT) and bottom-hole static temperature (BHST) were selected to be 65 and 90 °C, respectively. The downhole pressure is considered to be 172 bar. For all laboratory experiments, the mixed slurries were pre-conditioned for 30 min at the BHCT, in accordance with API 10B-2 (American Petroleum

Table 1
Mix design of the of candidate barrier materials used in this study.

	Solid phase				Liquid phase by weight of solid (BWS)				Additives (BWS)			
	Class G	Naturally occurring rock	Glass bead	Deionized water	Potassium silicate solution	Pre-mixed resin	Micro silica solution (50%)	Fluid-loss controller	Cement dispersant	Defoamer	Cement retarder	Viscosifier
Neat class G	790			44%								
Expansive cement	790			33%			11%	2.8%	0.5%	0.1%	0.6%	
Pozzolanic material	No information available.											
Geopolymer		700			44.5%							
Thermosetting resin			720			50%						1%

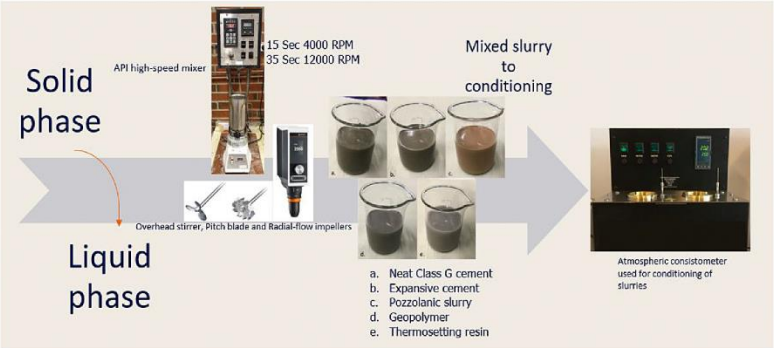

Fig. 2. Slurry sample preparation for laboratory tests.

Institute, 2013). The temperature ramp-up rate was 1 °C/min; after reaching the BHCT, the slurries were pre-conditioned for 30 min. Atmospheric consistometer, OFITE Model 60, was used for pre-conditioning of the slurries.

In Fig. 2, the slurry preparation up to conditioning before running laboratory experiments is shown graphically.

Viscosity measurement – Fann 35 rotational viscometer with configuration of R1-B1 was used for measuring the viscosity profiles. The viscometer cup was pre-heated to 65 °C for avoiding any thermal shock to the slurries. The test was performed following the API 10B-2 Recommended Practice (American Petroleum Institute, 2013). The average between the ramp-up and ramp down flow curves were used to calculate the viscosities at the different shear rates.

Static fluid-loss – The pre-conditioned slurries were transferred to the static fluid-loss test cell for measuring the performance of the slurries. The sampled fluid was measured at different time intervals, up to 30 min. For those slurries that experience break-through before 30 min, the following expression is used to report the API fluid-loss:

$$Fluid-loss = 2V_t\sqrt{\frac{30}{t}} \quad (1)$$

where V_t is total volume of the filtered liquid at the time of break-through, and t is the time in minute when the break-through occurs.

Pumpability – After loading the slurries in the relevant equipment, the temperature ramp-up rate was set equal to 1 °C/min until it reached to the BHCT and then the temperature was kept constant. Additionally, the consistency of the samples was measured at the elevated pressure of 172 bar with the pressure ramp-up of 17.2 bar/min. The equipment for measuring the consistency was OFITE Model 60 for atmospheric pressure and OFITE Model 2040 for elevated pressure. Both equipment sheared the slurries at 150 RPM; however, the paddles are different.

Uniaxial compressive strength (UCS) – The uniaxial compressive strength test was performed on samples cured at downhole condition of pressure and temperature after desired period of time. For UCS test, the specimens can be cured either in cubic forms with dimension of 50.8 mm (American Petroleum Institute, 2013) or in cylindrical mold with height to diameter (slenderness ratio) of 2.0 (American Petroleum Institute, 2017). The procedures for compressive strength test, and also non-destructive sonic strength development are described in API 10B-2. However, the test results only can be used to ensure that the cement has sufficient strength to resume drilling operation and they are not practically appropriate for annular cement integrity simulations (American Petroleum Institute, 2017). Hence, in this study, cylindrical specimens were considered to measure uniaxial compressive strength of the

materials. Two main reasonings for selecting cylindrical geometry are as following: a) the UCS test results can be more practical for cement sheath integrity simulations (American Petroleum Institute, 2017), b) practical issues such as design of the HPHT autoclave chambers used in this study.

Poly propylene plastic containers manufactured by VWR with diameter of 50 mm and height of 102 mm (see Fig. 4a) were used as mold. The molds can withstand the maximum temperature of 121 °C; therefore, they were applicable for curing the samples at 90 °C and under elevated pressure of 172 bar. After conditioning at BHCT, the slurries were poured in the molds and placed in the autoclaves for curing. Three samples were considered for each material and placed in the oven for different time intervals, 1-, 5-, 7- and 28-day (12 samples in total). Afterward, the hardened samples were removed from oven and gradually cooled down to ambient condition. Later, the samples were detached from the molds and both ends were flattened by using a cutting machine to eliminate the end effect during loading process (see Fig. 4b). Flattening both ends caused reduction in slenderness ratio below 2 that can overestimate the compressive strength of the barrier materials. Hence, the API 10TR7 for testing mechanical behavior of cement recommended correction factor that should be applied to each testing sample. For specimens with (l/d) < 2, API has referred to American Society for Testing and Materials, ASTM (2014) and correction factors can be either interpolating the range provided by Table 2, or using the polynomial equation in Fig. 3.

American Petroleum Institute (2017) recommends the constant compression stress rate in the range of 3.5 MPa/min to 14 MPa/min. However, due to technical limitations, the stress rate was selected equal to 35 MPa/min. According to a Cooperative Testing Results presented in Annex A, American Petroleum Institute (2017), the loading rate of 35 MPa/min results in lower compressive strength by 6% comparing to the loading rate of 14 MPa/min for the cylindrical specimens (American Petroleum Institute (2017)). The UCS machine used to conduct the tests was Toni Technik-H mechanical tester (see Fig. 4c).

Indirect tensile strength (Brazilian) – The same procedure as the UCS test was followed to cure the samples. Then, the cured samples were cut into the disc shapes with a thickness of about 30 mm and placed vertically between the curved jaws as shown in Fig. 4d. Zwick/Roell Z050 static material testing machine with a compression loading rate of 3 kN/min was employed to run the experiments (American Society for Testing and Materials, ASTM, 2016) and the tensile strength was calculated by the following equation.

$$\text{Tensile strength} = 1.2\frac{F}{\pi DL} \quad (2)$$

where F is the maximum tensile force, D is the diameter, and L is the thickness of the sample.

Sonic strength development – The pre-conditioned slurries were transferred to the ultrasonic cement analyzer (UCA) machine. The operational condition of temperature and pressure for the equipment was defined to be 90 °C and 172 bar, respectively. The temperature and pressure ramp-up rates were 1 °C/min and 17.2 bar/min. Chandler UCA Model 4265-HT was employed for this test. The machine is calibrated to test OPC, while for new materials, a novel algorithm must be provided and applied in the custom algorithm option.

Table 2
Correction factor of uniaxial compressive strength for specimens that have slenderness ratio below 2.

l/d	2	1.75	1.5	1.25	1
Correction factor	1	0.98	0.96	0.93	0.87

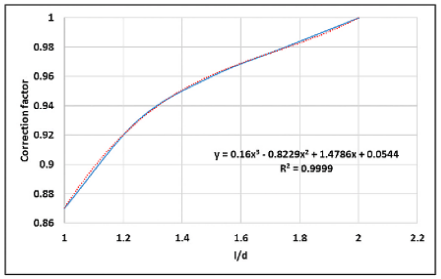

Fig. 3. Calculated correction factor by applying the polynomial equation for specimens with slenderness ratio less than 2.

3. Results and discussions

3.1. Rheological behavior and viscosity measurement

In this study, the viscosity of slurries was measured by the means of rotational viscometer. Fluid viscosity along with wellbore geometry (e.g. hole size, inclination and eccentricity) determines the frictional pressure losses and fluid displacement quality in the wellbore. Hence, accurate viscosity measurement and data fitted to an appropriate model are necessary. Among several suggested models for the drilling fluids, Herschel – Bulkley model is the simplest three-parameter model to describe the viscosity of non-Newtonian fluids over a range of shear rates (Herschel and Bulkley, 1926). In this model, shear stress (τ) at any shear rate ($\dot{\gamma}$) is presented as:

$$\tau = \tau_y + K\dot{\gamma}^n, \tau > \tau_y \quad (3)$$

$$\dot{\gamma} = 0 \quad \tau \leq \tau_y$$

where τ_y is the yield stress and n is the flow index, both are unique values and depending on the composition of the slurry. K is consistency factor and depends on the flow index. Hence, K cannot represent the properties of the fluid in fluid comparisons. Consequently, considering the Herschel – Bulkley approach and modelling the fluid behavior by curve fitting method may result in various combinations of K and n for the same data set. Saasen and Ytrehus (2018) re-arranged the Herschel – Bulkley model based on the suggested approach by Nelson and Eweoldt (2017) and introduced a surplus shear stress, τ_s and surplus shea rate, $\dot{\gamma}_s$, both are unique parameters for each fluid and the flow situation. The new model is defined as follows:

$$\tau = \tau_y + \tau_s\left(\frac{\dot{\gamma}}{\dot{\gamma}_s}\right)^n, \quad (4)$$

where $\tau_s = \tau - \tau_y$ at. $\dot{\gamma} = \dot{\gamma}_s$

The equation suggested by Power and Zamora (2003) provides an acceptable approximation for the yield stress:

$$\tau_y = 2\tau_3 - \tau_6 \quad (5)$$

The next step is to determine the surplus shear rate and the related surplus shear stress. Geometry of flow path is one of the effective parameters in shear rates. In primary cementing operation, the cement slurry flows in a pipe or in the annular area behind casing. Moreover, the flowrate at which the cement slurry is pumped can influence the shear rate. Usually, the shear rate of 102.2 s^{-1} (the pumping flow rate of about 1300 L/min in 9 5/8-in. to 12 ¼-in. annulus) is typical in cementing operations. This shear rate is equal to 60 RPM in bob and cylinder rotational viscometer. Subsequently, to determine the curvature

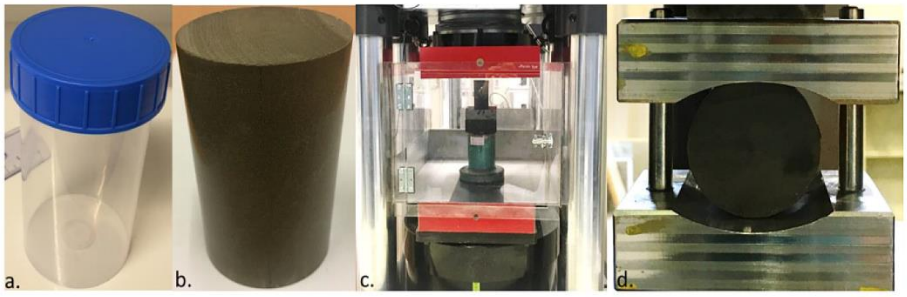

Fig. 4. a) The plastic mold used for curing the samples, b) Cured sample after flattened both ends, c) UCS test setup, d) Indirect tensile strength test setup.

Table 3
Density, pH, viscosity model parameters, fluid loss and consistency of the materials.

	Density (sg.)	pH	Gel Strength (Pa)		Viscosity model parameters				API Fluid Loss (ml)	Pumpability (min)	
			10-sec	10-min	ty	τ_s	n_{hs}	n_{hw}		ATM	PRS
Neat class G	1.9	13.6	11.75	69.5	6.13	31.68	0.98	0.29	821.04	132	96
Expansive cement	1.95	13.2	12.2	40.3	7.4	44.2	0.64	0.65	21	462.5	338.5
Pozzolanic material	1.68	13.3	3.57	5.11	2.04	26.65	0.72	0.70	18.8	N/A	N/A
Geopolymer	1.95	13.4	12.2	23	7.78	28.11	0.95	0.87	0	120	110
Thermosetting resin	1.65	N/A	3.5	19.4	3.32	38.58	0.844	0.82	183.76	293	263.5

N/A: Not Applicable

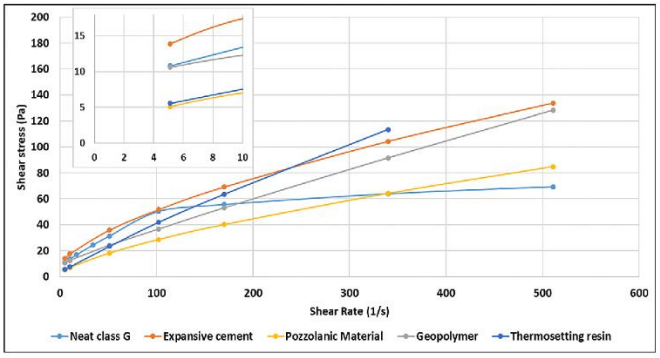

Fig. 5. Viscosity profile of the candidate barrier materials at 65 °C.

component in the model. Two different values can be estimated, one at shear rates below and one for the shear rates above the surplus shear rate, aiming to increase the accuracy of the prediction and they are labelled as n_{ls} and n_{hs}. The mentioned parameters can be calculated at 30 and 200 RPM as follows, respectively:

$$n_{ls} = \frac{\ln\left(\frac{\tau_{30} - \tau_s}{\tau_s}\right)}{\ln\left(\frac{\gamma_{30}}{\gamma_s}\right)} \quad (6)$$

$$n_{hs} = \frac{\ln\left(\frac{\tau_{200} - \tau_s}{\tau_s}\right)}{\ln\left(\frac{\gamma_{200}}{\gamma_s}\right)} \quad (7)$$

For all materials, the 10-sec and 10-min static gel strengths were measured at constant temperature of 65 °C and they are summarized in Table 3.

The viscosity profile of the barrier materials at 65 °C and atmospheric pressure, right after pre-conditioning is presented in Fig. 5. As all the slurries have yield stress and a flow index less than unity, they are non-Newtonian with a shear thinning behavior. They are pumpable at typical operational pumping rates. The static gel strength test was performed after 10 s and 10 min at 3 RPM. All the fluids develop gel strength during a static period. The yield stress for the thermosetting resin and pozzolanic material was less than the other materials, but the viscosity of the resin was higher at higher shear rates, which the dial

reading at 300 RPM was not achieved. The glass beads that added to the system as the weighting agent can have an influence on the fluid behavior and make a plug flow at higher shear rates. The same procedure was followed for the neat class G cement, where the measured shear stress at 102 s^{-1} for the neat class G was unexpectedly high. A possible human or equipment error was suspected. However, repeating the tests three times confirmed the accuracy of the observation. The operational shear rate for cementing operation barely passes 200 s^{-1} and it means that there will be no concern about the placeability of the slurries (Nelson and Guillot, 2006).

3.2. Static fluid-loss test

The static fluid-loss was measured by API recommended apparatus. In primary cementing operation, during placement and post-placement before the material solidifies, the formation can act as a filter and hydrostatic pressure above the slurry can squeeze slurry filtrate into the formation. The loss of liquid phase can result in building particle bridges across the annulus and, hence, reducing in hydrostatic pressure in the annulus and increasing the risk of reservoir fluid invasion into the barrier sheath. Such liquid may also have a critical role in the setting process and maintaining the desired mechanical properties for the life cycle of the well. Moreover, fluid-loss can also negatively affect the rheological properties and consequently, placeability of the slurry all the way up behind the casing as it becomes thicker when the liquid phase leaves the mixture. From the operational point of view, the cement slurry should be placed at the predesigned depth and with the predefined pumping rate and without significant change in the composition. Increasing the pump pressure to place a thick slurry that already lost a part of its liquid can accelerate the fluid loss and fracture formation. However, in remedial operations, a high slurry loss (i.e. including the liquid phase and particles) value is a benefit for cement squeezing, when the fluid loss can result in cement bridge-off to seal the leak path. The guidelines for fluid loss control have been developed based on the field experiences, not the theoretical models. Hence, the operators have different specification about the acceptable fluid loss and the value may vary depending on the drilling environment and formation, but the values below 50 ml per 30 min are favourable for primary cementing (Bensted, 1998).

The result of static fluid-loss of the slurries after 30 min preconditioning at 65 °C is presented in Fig. 6. The geopolymer slurry revealed no fluid-loss during the testing time, which means that there is no free fluid and the geopolymeric species present in the slurry are well attached to the hardener phase. Although the hardener composition has a crucial effect on the test results, literature shows that modification of particle size of geopolymeric precursors reduces the fluid loss by 100% comparing to the previous tests performed by Khalifeh et al. (2019). The pozzolanic slurry and expansive cement indicated an acceptable result, approximately 10 ml after 30 min. This is mainly due to particle size distribution and fluid-loss control agents used in these mixtures. The thermosetting resin, however, experienced break-through just 8 min after running the test. Although the glass beads were used as weighting agent and the system is not particle-free, they were not able to bond to the liquid resin during the mixing and pre-conditioning. Consequently, extensive fluid-loss was experienced. The loss of water from the neat G cement was intensive and the break-through occurred only 3 min after running the test. The API static fluid-loss values for the thermosetting resin and class G cement reported in Table 3 show higher than that of the liquid phase added to mix the slurry. The physical meaning of these values can be described as if the slurry is connected to the source of the liquid phase, the tabulated value can be passed as filtrate in 30 min.

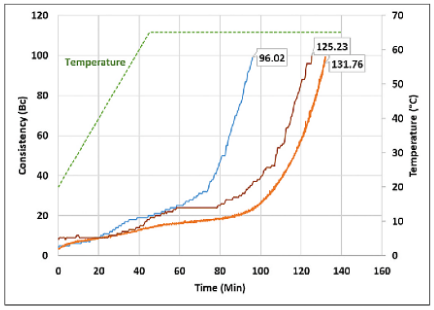

Fig. 7. The consistence of the neat class G cement slurry as function of time. Orange curve: Atmospheric consistometer. Brown curve: Pressurised consistometer at atmospheric conditions. Blue curve: Pressurised consistometer at elevated pressure. Numeric values are thickening time to 100 Bc (min). (For interpretation of the references to colour in this figure legend, the reader is referred to the Web version of this article.)

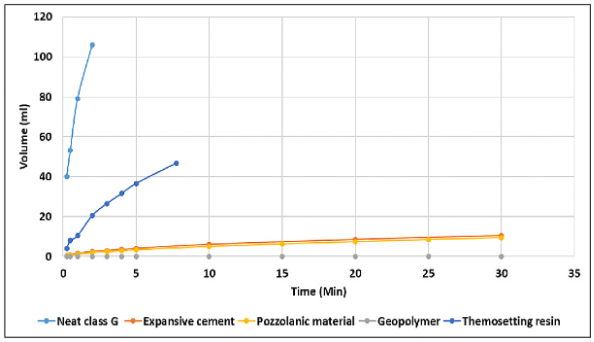

Fig. 6. Static fluid-loss of the barrier materials.

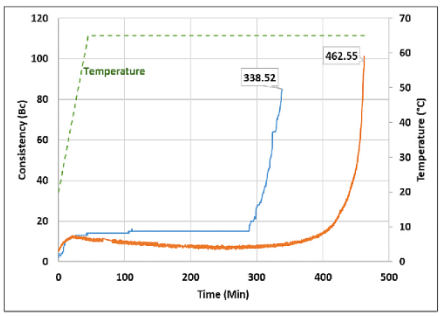

Fig. 8. The consistence of the expansive cement slurry as function of time. Orange curve: Atmospheric consistometer. Blue curve: Pressurised consistometer at elevated pressure. Numeric values are thickening time to 100 Bc (min). (For interpretation of the references to colour in this figure legend, the reader is referred to the Web version of this article.)

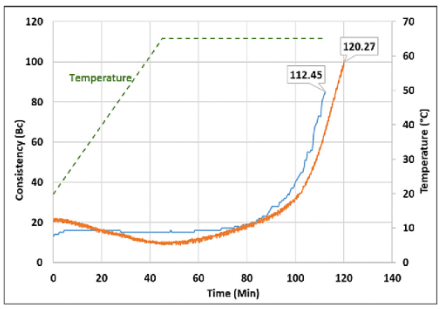

Fig. 10. The consistence of the geopolymer slurry as function of time. Orange curve: Atmospheric consistometer. Blue curve: Pressurised consistometer at elevated pressure. Numeric values are thickening time to 100 Bc (min). (For interpretation of the references to colour in this figure legend, the reader is referred to the Web version of this article.)

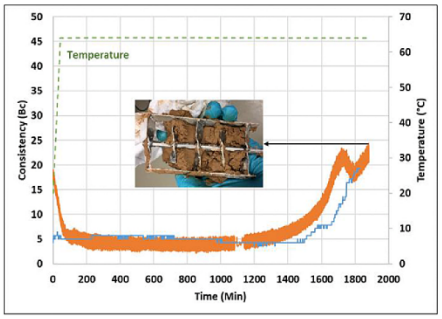

Fig. 9. The consistence of the pozzolanic material as function of time. Orange curve: Atmospheric consistometer. Blue curve: Pressurised consistometer at elevated pressure. (For interpretation of the references to colour in this figure legend, the reader is referred to the Web version of this article.)

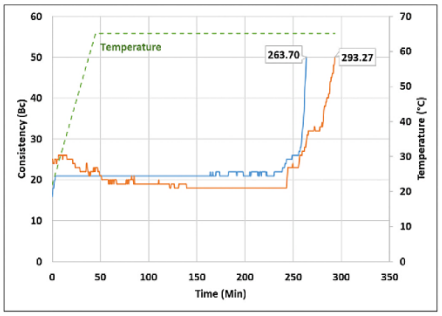

Fig. 11. The consistence of the thermosetting resin slurry as function of time. Orange curve: Atmospheric consistometer. Blue curve: Pressurised consistometer at elevated pressure. Numeric values are thickening time to 100 Bc (min). (For interpretation of the references to colour in this figure legend, the reader is referred to the Web version of this article.)

3.3. *Pumpability and consistency*

The pumpability of the cementitious slurries was measured by measuring the torque of spring connected to a paddle. The paddle stirred the slurry continuously. Considering the consistency of setting materials, one should differentiate between pumping time and setting. Setting time is the time required for the material to set from gel status. Pumping time, also known as workability, is a property of setting material indicating how long the slurry remains in the fluid phase before gelation occurs. The test is usually performed at the BHCT and the instrument measures the consistency of the slurry in Bearden units of consistency (Bc). Depending on the operator's criteria, the upper limit for the pumpability varies between 30 and 40 Bc and beyond that, the cement mixture is considered as unpumpable or risky fluid because the slurry becomes thick. However, it is recommended to continue the test until it reaches 100 Bc (American Petroleum Institute, 2013). The reason is that the trend of the curve from 40 Bc to 100 Bc can provide an estimation about the strength of gel so that gas should not be able to attack the slurry before it sets. A rapid increase in the consistency during this period is known as Right-Angle Set, where the transition from liquid to the solid phase happens quickly and it can significantly reduce the risk of formation fluid invasion into the cement sheath, especially in gas wells or oil wells with shallow gas. However, it may increase the risk of setting in drill string or setting at undesired depth before reaching the end station.

The consistency of the candidate barrier materials at atmospheric and elevated pressure of 172 bar is shown in Figs. 7–11. As two different

Fig. 12. The paddles that is used for shearing the mixed slurries in pressurised consistometer (upper device) and atmospheric consistometer (bottom device).

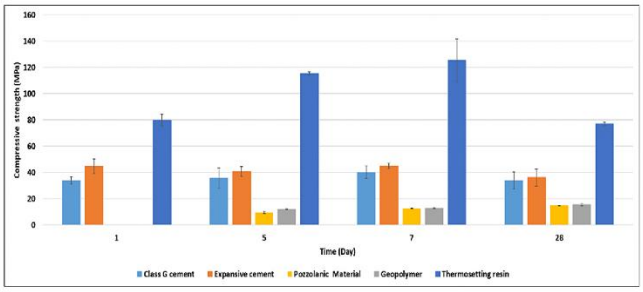

Fig. 13. Average compressive strength of the candidate barrier materials.

equipment were used to run the test at atmospheric and elevated pressure, an extra test was performed on the neat class G cement with the pressurised consistometer while the pressure was set at atmospheric level (brown curve). The reason was to test the reliability of the atmospheric consistometer and validity of the measurements. No significant difference was observed in the results; hence, the tests at atmospheric pressure were performed with atmospheric consistometer.

Increasing the pressure from atmospheric to 172 bar has an acceleration effect on the pumpability of all materiel to a different extent. For the neat class G cement, the acceleration effect was about 35 min which is about a 25% reduction in pumping time, while for the expansive cement the impact was slightly more pronounced. The expansive cement was pumpable for almost 7 h at atmospheric pressure and increasing the pressure reduced the pumpability to 5 h giving nearly a 26% reduction in pumping time. The kinetic of the governing chemical reactions and hydration of the components that exist in the chemical

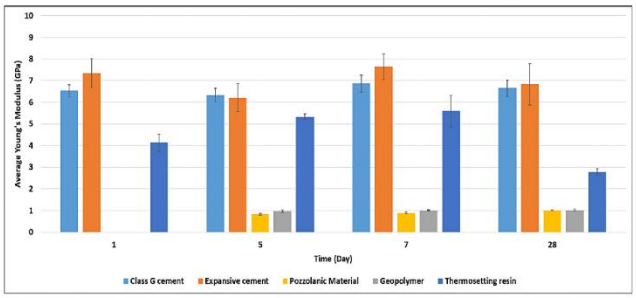

Fig. 14. Average Young's modulus of the barrier materials.

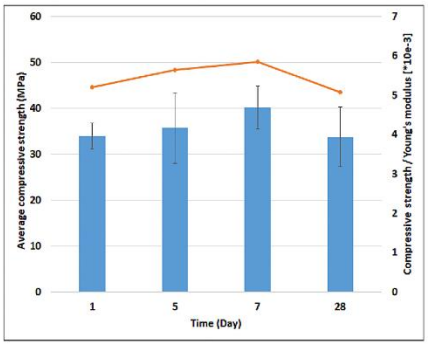

Fig. 15. Average uniaxial compressive strength (blue bars) and the compressive strength divided by Young's modulus (orange line) for the neat class G cement. (For interpretation of the references to colour in this figure legend, the reader is referred to the Web version of this article.)

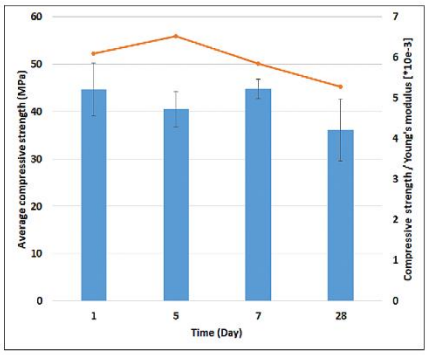

Fig. 16. Average uniaxial compressive strength (blue bars) and the compressive strength divided by Young's modulus (orange line) for the expansive cement. (For interpretation of the references to colour in this figure legend, the reader is referred to the Web version of this article.)

additives are likely pressure-sensitive (Wagh, 2016). These reactions have a significant influence on the formation of calcium-silicate-hydrate (C–S–H) gels and expedite gelation of the expansive cement. The consistency curve of the non-cement based pozzolanic slurry shows a constant trend up to 23 h after running the test. The curve reached a peak after 28 h and started to fluctuate. The test stopped at that stage and quick gelation happed only a few seconds after removing the sample from consistometers, Fig. 9. The test revealed how the static and dynamic condition affects gelation and setting time of the pozzolanic slurry. One may conclude that the physical damage to the gel structure of the material is the reason for having long thickening time. The geopolymer showed pressure independent pumpability. This has been confirmed by previous research conducted on the rock-based geopolymer (Khalifeh et al., 2019). Pumpability of the thermosetting resin was also pressure-dependent and it was reduced by 30 min by increasing the pressure, which is almost 10% reduction; however, the measured pumping time is still within the range recommended by operators. It might be valuable to study electrostatic forces between the particles or structure of solid phases for materials that showed pumping time-sensitive to pressure.

The expansive cement, geopolymer and thermosetting resin showed Right-Angle Set less than 15 min since the gelation phase started. Apart from the pressure as a variable in consistency tests, the effect of blade geometries of atmospheric and pressurised consistometers (see Fig. 12) is also recommended to be considered for future studies. The geometry of the paddle may affect the mixing energy or damaging the gel structures prior to the setting phase starts.

3.4. Uniaxial compressive strength (UCS) and flexibility

The average compressive strength of the barrier materials for the period of up to 28 days is presented in Fig. 13. The flexibility, compressive and tensile strength of the barrier material are linked together; increasing in ductility of the cementitious materials can result in a reduction of required compressive and tensile strengths (Jafariesfad et al., 2017a).

The average Young's modulus of each barrier material after curing the samples up to 28 days is shown in Fig. 14. The pozzolanic slurry and geopolymer were not able to develop early strength after 24 h curing under the bottom-hole condition. However, Young's modulus of these

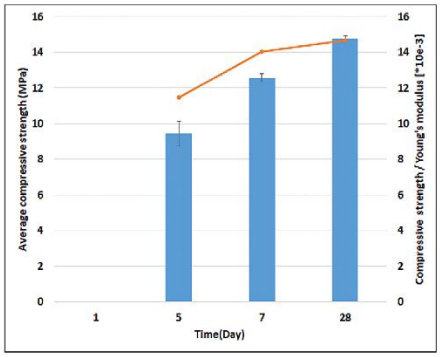

Fig. 17. Average uniaxial compressive strength (blue bars) and the compressive strength divided by Young's modulus (orange line) for the pozzolanic material. (For interpretation of the references to colour in this figure legend, the reader is referred to the Web version of this article.)

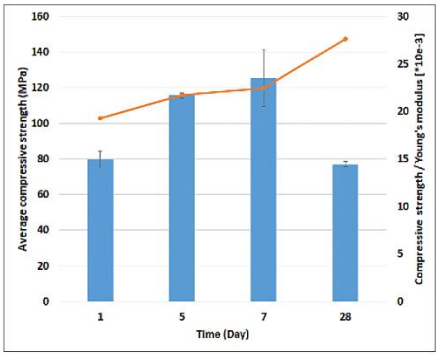

Fig. 19. Average uniaxial compressive strength (blue bars) and the compressive strength divided by Young's modulus (orange line) for the thermosetting resin. (For interpretation of the references to colour in this figure legend, the reader is referred to the Web version of this article.)

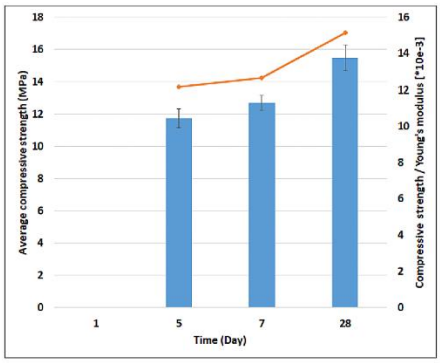

Fig. 18. Average uniaxial compressive strength (blue bars) and the compressive strength divided by Young's modulus (orange line) for the geopolymer. (For interpretation of the references to colour in this figure legend, the reader is referred to the Web version of this article.)

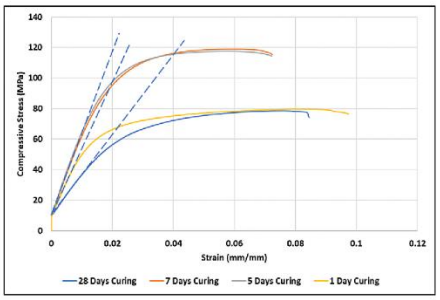

Fig. 20. Stress-strain curve for the thermosetting resin after curing at different time intervals.

materials after 5, 7, and 28 days of curing were significantly low, and the materials were extremely flexible. Both the neat cement and the expandable cement systems showed constant flexibility during 28 days of curing. The modulus of flexibility for thermosetting resin was dropped by almost 50% after 28 days of curing.

In Figs. 15–19, the average uniaxial compressive strength (UCS) (right vertical axis) and the ratio of the UCS to Young's modulus (UCS/E) (left vertical axis) of the barrier materials are presented. The compressive strength of the neat class G cement has a slight decrease during the period from 7 to 28 days. This provides a motivation to investigate the change in the compressive strength for even longer periods. The compressive strength of the expansive cement was slightly decreased at the end of the testing period comparing to the results after 1-day curing and it became more ductile. After 28 days, the pozzolanic slurry and the geopolymer reached to the compressive strength of 14 and 16 MPa, respectively, and their trend for strength development was increasing for both materials. Although the thermosetting resins are not as brittle as cement, their UCS test was performed as described in the previous section to provide equal testing conditions for comparison with the other investigated materials. Perhaps development of standards for characterization of mechanical properties of thermosetting resin-based materials for utilization as zonal isolation materials is a necessity. The stress-stain curve for the material showed elastic behavior at earlier stage of the loading, almost similar to the other materials, but it enters to a plastic region. In other words, the plastic region in stress-strain curve of thermosetting resin was extended comparing to the other materials. However, the thermosetting resin was also cracked at failure point. Fig. 20 shows the stress-stain curve for the thermosetting resin.

The strength development trend for the thermosetting resin was reached to the maximum value of 130 MPa after 7 days; almost three times greater than the neat class G cement, but the value was dropped by almost 40% to 80 MPa after 28 days. Nevertheless, the UCS/E parameter increased due to the ductility of the material in this period. In Fig. 21 it is provided a comparison of the UCS/E value for all the five barrier materials for the testing period. The observations in results of UCS tests and

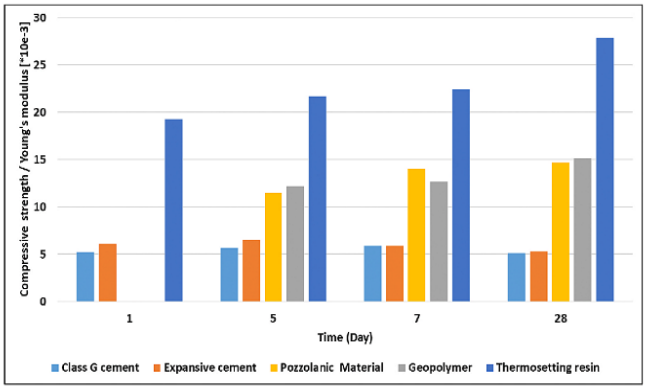

Fig. 21. The ratio of compressive strength to Young's modulus of the candidate barrier materials.

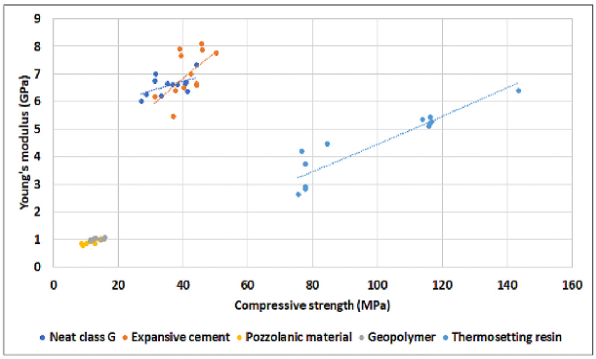

Fig. 22. Modulus of elasticity as function of compressive strength for five barrier materials.

Table 4
Young's modulus and compressive strength relationship equation parameters.

	Model parameters		Minimum WLS
	a	b	
Neat class G cement	2.560	0.2607	0.015
Expansive cement	0.701	0.6133	0.105
Pozzolanic material	0.732	0.1346	0.007
Geopolymer	0.544	0.2342	0.006
Thermosetting resin	0.015	1.2230	0.191

Table 5
Generated customised algorithm of the barrier materials for the UCA test based on data up to 28 days.

Material	Polynomial equation	R-square value
Class G cement	$y = 125.77x2 - 3701.1x + 226795$	0.9822
Expansive cement	$y = 190.85x^3 - 5281.6x + 35842$	0.9788
Pozzolanic material	$y = 365.82x^2 - 9880.6x + 65261$	0.9907
Geopolymer	$y = 28.662x^2 - 1310.9x + 12057$	0.995
Thermosetting resin	$y = 250.9x^3 - 9065.9x + 80945$	0.8502

the change in the ratio of UCS to Young's modulus have amplified the motivation to investigate the change in mechanical properties of all barrier materials in long-term. In addition, one needs to characterize the microstructure of these materials by the use of XRD and SEM techniques, to investigate any phase changes or transformation of the minerals.

3.4.1. Relationship between compressive strength and modulus of elasticity

Regularly the flexibility index is expressed in terms of compressive strength. Tomosawa and Noguchi (1993) analysed more than 3000 data of compressive strength for different types of heterogeneous concrete. They proposed a universal equation to estimate the structural deformation of concretes with compressive strength ranging between 20 and 160 MPa. The power-equation (Equation (8)) covers the compressive strength and mass density of the tested materials; besides, a correction factor takes into account the coarse aggregates and mineral admixtures in the concrete systems.

$$E = k_1.k_2.1486.\sigma_C^{\frac{1}{3}}.\gamma^2 \quad (8)$$

where E is the modulus of elasticity in MPa, k_1 and k_2 are the correction

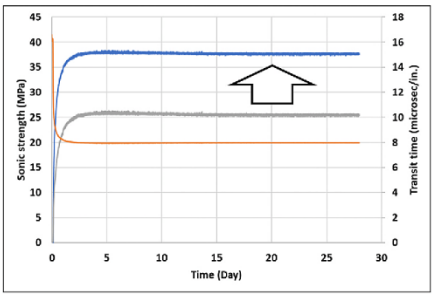

Fig. 23. Sonic strength development based on default algorithm of the equipment (grey line), Sonic strength development based on the generated algorithm (blue line) and the transit time (orange line) for the neat class G cement. (For interpretation of the references to colour in this figure legend, the reader is referred to the Web version of this article.)

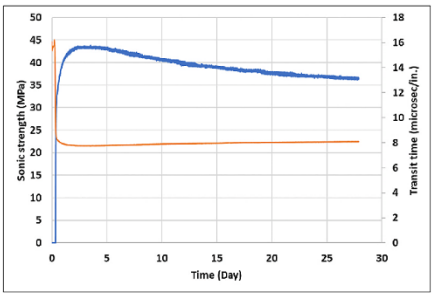

Fig. 24. Sonic strength development (blue line) and the transit time (orange line) for the expansive cement. (For interpretation of the references to colour in this figure legend, the reader is referred to the Web version of this article.)

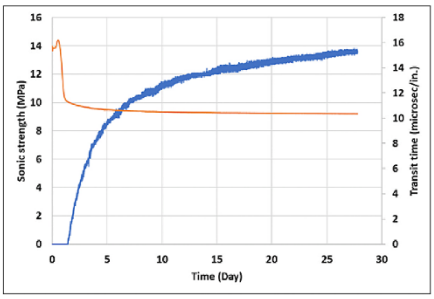

Fig. 25. Sonic strength development (blue line) and the transit time (orange line) for the pozzolanic material. (For interpretation of the references to colour in this figure legend, the reader is referred to the Web version of this article.)

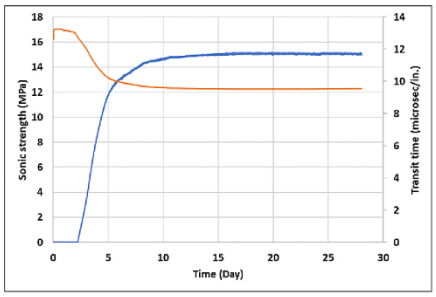

Fig. 26. Sonic strength development (blue line) and the transit time (orange line) for the geopolymer. (For interpretation of the references to colour in this figure legend, the reader is referred to the Web version of this article.)

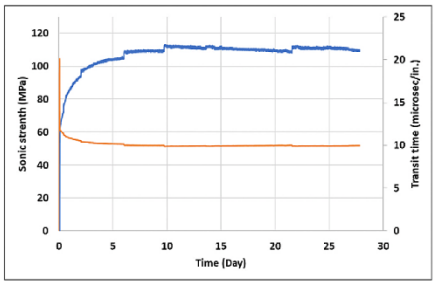

Fig. 27. Sonic strength development (blue line) and the transit time (orange line) for the thermosetting resin. (For interpretation of the references to colour in this figure legend, the reader is referred to the Web version of this article.)

factors defining the coarse aggregates and mineral admixtures, σ_C is the compressive strength in MPa, and γ is the mass density in Kg/l.

In this study, a regression analysis of over 12 crushed samples per each material was conducted based on the UCS test results, Fig. 22. Considering the universal equation suggested by Tomosawa and Noguchi (1993), a general equation was proposed to relate the short-term compressive strength of the materials as the explanatory variable and modulus of elasticity as the target variable. The suggested equations can predict the ductility of the materials with an acceptable accuracy at specific operational pressure and temperature in this project. All the slurries were mixed based on a fixed recipe; hence, the density of all materials is constant in the equation and can be neglected. Moreover, a homogeneous solid phase with constant mineralogy was used to mix and cure the barrier materials in entire tests. Consequently, the general equation can be simplified as a power function to the following form:

$$E = a.\sigma_C^b \quad (9)$$

In the equation above, the modulus of elasticity, E, is in GPa and σ_B is in MPa. Frequently, the least squares regression methodology is used to reduce the deviation between the model calculations and direct measurements. In this practice, the minimum weighted least squares (WLS) method is considered for finding the optimum values for a and b

constants in the general equation. The values for the constants are summarized in Table 4. The pozzolanic and geopolymeric materials showed the minimum WLS and it is an indication of homogeneity of the samples.

3.5. Sonic strength development

The ultrasonic cement analyser is able to estimate the strength development of the setting materials by measuring the sonic wave transit time through the slurries. Transit time of the sonic wave is a direct measurement by the equipment, and it is only dependent on the chemistry of the tested material. The software is programmed to convert the measured transit time to the compressive strength of the material based on a predefined algorithm introduced earlier to the system by the manufacturer. This algorithm is achieved based on previous experiments and it can provide a good estimation for the OPC. For setting materials other than OPC, the calculated compressive strength is not accurate, and a new algorithm should be introduced to the software. In this study, the UCS data were plotted versus the corresponding transit time measured by the equipment at the same period of curing time. Hence, four points were available for the neat class G, expansive cement and thermosetting resin while three points were available for the pozzolanic slurry and geopolymer. The generated algorithm for individual barrier material is presented in Table 5.

In Figs. 23–27, the sonic strength development (left vertical axis) and transit time (right vertical axis) for the candidate barrier materials are presented. The change in sonic strength development determined using the default algorithm for the neat class G cement is shown in Fig. 23. These values do not correspond with the crushing tests shown in Fig. 16. Hence, a new algorithm was made. The results from using this algorithm are shown by the blue curve in Fig. 23. The mechanical strength of the expansive cement started to decline 4 days after curing. A consecutive reaction corresponding to the chemical additives may cause a reduction in strength of the material. One possible scenario could be activation of the expansive agent that may create internal pressures. The trends of the pozzolanic material and geopolymer confirm that both materials had no strength up to 2 days after running the test, but the strength development was still ongoing after 28 days of the UCA test. The thermosetting resin was set fast at 90 °C and 2500 psi, but the corresponding plot shows a number of jumps in strength development trend. Coagulation of the weighting agents may be the reason for the sudden peaks in the trend; therefore, studying the non-zero zeta potential of the particles might explain the behavior of the material at this operational condition. Comparing the results from the UCA test with strength development in

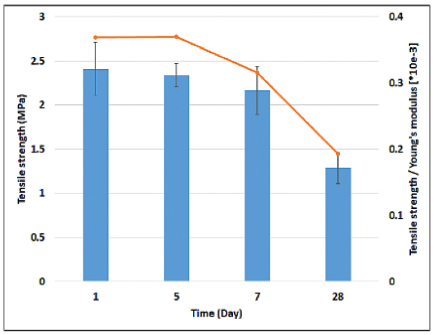

Fig. 29. Average tensile strength (blue bars) and the tensile strength divided by Young's modulus (orange line) for the neat class G cement. (For interpretation of the references to colour in this figure legend, the reader is referred to the Web version of this article.)

consistency curves can inform that how dynamic condition impacts the gelation of the materials, while its also essential to take into account the 25 °C difference in temperature in both tests, difference between BHST and BHCT. This effect on the thermosetting resin was intensive as static condition accelerates the gelation by 3 h. The dynamic condition effect was also observed for the pozzolanic material earlier in consistency test. A gap of 10-h is recognized between gelation and the strength development result of UCA test, which means that although the materials have formed gel after 28 h, it has not been set until about 40 h under 90 °C and static condition.

3.6. Indirect tensile strength (Brazilian) test

At downhole condition, the thermal and pressure loads occur during well completion and production period induce considerable tensions in complex directions to the cement sheath. These loads can arise well integrity challenges that may result in poor bonding of setting material to the casing/formation or the barriers with low tensile strength. The required tensile strength depends on the complex loadings on the barrier sheath as well as the mechanical properties of the nearby formation. Jafariesfad et al. (2017a) reviewed the typical loading modes and

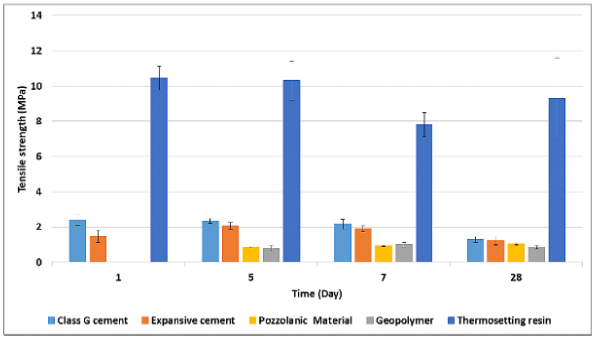

Fig. 28. Average tensile strength of the candidate barrier materials.

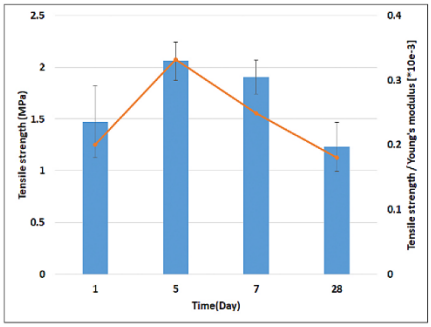

Fig. 30. Average tensile strength (blue bars) and the tensile strength divided by Young's modulus (orange line) for the expansive cement. (For interpretation of the references to colour in this figure legend, the reader is referred to the Web version of this article.)

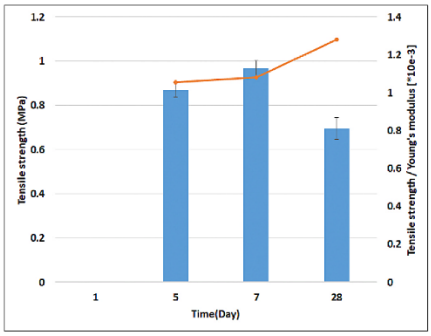

Fig. 31. Average tensile strength (blue bars) and the tensile strength divided by Young's modulus (orange line) for the pozzolanic material. (For interpretation of the references to colour in this figure legend, the reader is referred to the Web version of this article.)

minimum requirements to prevent the failure in barrier systems. They stated that for a different combination of radial and tangential stresses, Young's modulus affects the required tensile strengths to sustain zonal isolation and consequently, a higher ratio of tensile strength to Young's modulus is required.

In Fig. 28, it is shown the average tensile strength of the candidate barrier materials during a time span of 28 days. In Figs. 29–33, it is shown the average tensile strength (TS) (right vertical axis) and the ratio of tensile strength to Young's modulus (TS/E) (left vertical axis) of the barrier materials. All the candidate materials showed a decline in tensile strength between 7 days and 28 days of curing; except for the thermosetting resin, which experienced an increasing trend. The ratio of the tensile strength to Young's modulus of the cement system was declined after it reached a peak at 5 days. This parameter was almost constant for the pozzolanic material and geopolymer but for the thermosetting resin, it increased by more than 100% due to an increase in ductility and tensile strength. Fig. 34 provides a comparison of tensile strength over Young's modulus value for all five barrier materials for the testing period.

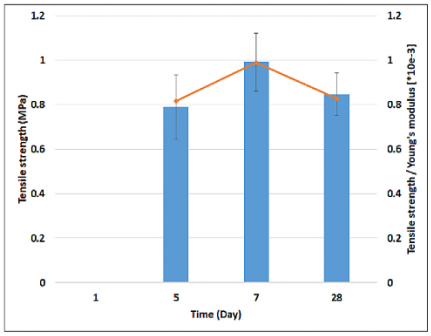

Fig. 32. Average tensile strength (blue bars) and the tensile strength divided by Young's modulus (orange line) for the geopolymer. (For interpretation of the references to colour in this figure legend, the reader is referred to the Web version of this article.)

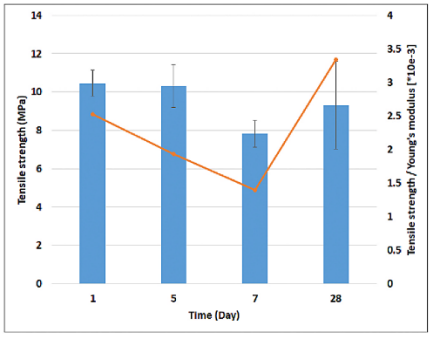

Fig. 33. Average tensile strength (blue bars) and the tensile strength divided by Young's modulus (orange line) for the thermosetting resin. (For interpretation of the references to colour in this figure legend, the reader is referred to the Web version of this article.)

In geomechanics, it is well-established that tensile strength and UCS is related (Nazir et al., 2013). Although direct measurement or laboratory tests of mechanical properties is the more reliable, estimations of USC/tensile strength based on available data can reduce the cost and save time. In this paper, a correlation between UCS and indirect tensile strength of the candidate barrier materials was investigated. The sample preparation for each test was followed the same procedure and both solid and liquid phases were homogeneous for each curing time. The average value of UCS and tensile strength was used to find the correlation.

The dispersion of average UCS and tensile strength tests results of the candidate barrier materials is shown in Fig. 35. The correlation coefficient was calculated for the mentioned parameters (see Table 6). The calculated correlation coefficients revealed that for the pozzolanic material, there is a strong positive relationship between the UCS and tensile strength. The coefficients for the expansive cement and neat class G cement indicated a fairly positive relation between the mentioned mechanical properties; but for the thermosetting resin, the value shows a

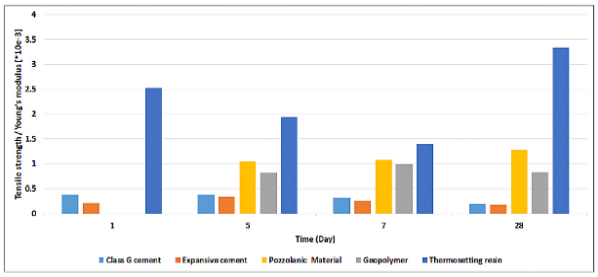

Fig. 34. The ratio of tensile strength to Young's modulus of the candidate barrier materials.

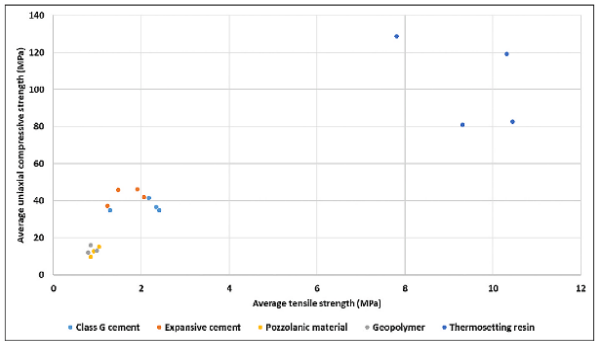

Fig. 35. Correlation between indirect tensile strength and UCS values for candidate barrier materials.

Table 6
Linear and power model parameters for the correlation between UCS and tensile strength of the barrier material.

	Power Model Parameters		Linear Model Parameters		Correlation coefficient	Power model Minimum WLS	Linear model Minimum WLS
	a	b	a	b			
Class G cement	33.52727	0.085083	1.52955	32.4155	0.294	0.016342	0.016744
Expansive cement	36.58101	0.234407	5.68501	31.58398	0.453	0.022118	0.023401
Pozzolanic material	13.9195	2.1149	28.14154	−14.1267	0.973	0.006746	0.005205
Geopolymer	13.2295	0.141667	1.812256	11.3871	−0.0003	0.03662	0.036794
Thermosetting resin	993.0011	−1.06013	−9.24029	179.9438	−0.5011	0.132749	0.141613

rather strong negative relationship. The calculated coefficient for the geopolymer was an indication of a weak relation between the UCS and tensile strength properties. Linear and power equations (Equation (10)) were considered to find an accurate relation between UCS and tensile strength and the minimum weighted least squares (WLS) method is considered for finding the optimum values for a and b constants in the general equation. The values for the constants are summarized in Table 6. The power model equation provides a better match based on available data, except for the pozzolanic material, which linear model fits better on the data set.

$$\sigma_C = a \times \sigma_T + b \quad \textit{Linear equation form}$$
$$\sigma_C = a \times \sigma_T^b \quad \textit{Power equation form} \qquad (10)$$

4. Conclusions

Rheological and mechanical performance of five different zonal isolation materials were examined at equal operational condition of pressure and temperature. Albeit shortcomings of the neat API class G cement, it was selected as reference in this experimental project due to its well-known chemistry and properties. Thermosetting resin and pozzolanic material showed lower yield stress comparing to the geopolymer and cement systems; however, the pozzolanic material appear more shear-thinning compared to thermosetting resin. Expansive cement exhibits higher viscosity in majority of shear rates. The expansive cement, neat class G cement and thermosetting resins developed strong 10-min gel structure, but the geopolymeric and pozzolanic

slurries showed less time-dependent gel structure.

All the materials except the pozzolanic material showed right-angle set pumping profile. The pozzolanic material remained in liquid state while sheared in the consistometers. Expansive cement, neat G cement and thermosetting resin showed pressure-dependent performance. Static fluid-loss and pumpability of the materials showed acceptable values for the expansive cement, pozzolanic slurry and geopolymer, while the thermosetting resin experienced early breakthrough. The glass beads used as weighting agent were not able to bond to the liquid resin to perform as a fluid-loss controller.

Considering compressive strength development of the neat class G cement, expansive cement and thermosetting resin, a consecutive reaction takes in place which results in retrogression of the strengths. Early strength development of the pozzolanic and geopolymeric slurries is a concern as they did not develop strength up to two days of curing. Tensile strength of the thermosetting resin is 11% of its compressive strength cured for 28 days, but tensile strength of the other materials ranged 3.5–5% of their compressive strengths. Ductility of the neat class G and expansive cements, pozzolanic and geopolymer materials do not experience significant change during this testing period; however, the thermosetting resin becomes more ductile. Calculated compressive to Young's modulus and tensile strength to Young's modulus values showed that the thermosetting resins are more flexible with higher strength, followed by the geopolymeric and pozzolanic materials, and lastly the expansive cement and neat G cement.

Credit author statement

Mohammadreza Kamali: Conceptualization, Methodology, Investigation, Data curation, Writing – original draft, Writing – review & editing, Mahmoud Khalifeh: Conceptualization, Methodology, Writing – review & editing, Investigation, Resources, Supervision, Project administration, Funding acquisition, Arild Saasen: Conceptualization, Methodology, Writing – review & editing, Investigation, Resources, Supervision, Rune Godøy: Conceptualization, Methodology, Writing – review & editing, Investigation, Laurent Delabroy: Conceptualization, Methodology, Writing – review & editing, Investigation.

Declaration of competing interest

The authors declare that they have no known competing financial interests or personal relationships that could have appeared to influence the work reported in this paper.

Acknowledgement

The authors would like to thank the Ministry of Education and Integration in Norway for funding this project. Moreover, the authors gratefully acknowledge Halliburton, WellCem AS and AlTiSS AS for their supports and sharing technical information. A special thanks goes to Salim Taoutaou for sharing operational experiences. The authors thank Aker BP and TOTAL for supporting part of the project through the SafeRock Project joint industrial project at UiS.

References

Abid, K., Gholami, R., Tiong, M., Nagaratnam, B., Sarmadivaleh, M., Mostofi, M., Bing, C. H., Muktadir, G., 2019. A pozzolanic supplementary material to reinforce class G cement used for drilling and completion operations. J. Petrol. Sci. Eng. 177, 79–92.

Al-Ansari, A., Al-Refai, I., Al-Beshri, M., Pino, R., Leon, G., Knudsen, K., Sanabria, A., 2015. Thermal activated resin to avoid pressure build-up in casing-casing annulus (CCA). SPE Offshore Europe Conference and Exhibition. Society of Petroleum Engineers.

Al Ramadan, M., Salehi, S., Teodoriu, C., 2019. Robust Leakage Modeling for Plug and Abandonment Applications, International Conference on Offshore Mechanics and Arctic Engineering. American Society of Mechanical Engineers. V008T11A054.

Alvi, M.A.A., Khalifeh, M., Agonafir, M.B., August 2020. Effect of nanoparticles on properties of geopolymers designed for well cementing applications. J. Petrol. Sci. Eng. 191, 107128.

American Petroleum Institute, 2013. API RP 10B-2, Recommended Practice for Testing Well Cements. API, Washington, DC.

American Petroleum Institute, 2017. API TR 10TR7, Mechanical Behavior of Cement. API, Washington, DC.

American Society for Testing and Materials, ASTM, 2013. ASTM C311, Standard test methods for sampling and testing fly ash or natural pozzolans for use in portland-cement concrete. ASTM.

American Society for Testing and Materials, ASTM, 2014. ASTM-C39, Standard test method for compressive strength of cylindrical concrete specimens. ASTM.

American Society for Testing and Materials, ASTM, 2016. ASTM D3967-16, Standard Test Method for Splitting Tensile Strength of Intact Rock Core Specimens. American Society for Testing and Materials.

Baumgarte, C., Thiercelin, M., Klaus, D., 1999. Case studies of expanding cement to prevent microannular formation. SPE Annual Technical Conference and Exhibition. Society of Petroleum Engineers.

Beharie, C., Francis, S., Øvestad, K.H., 2015. Resin: an Alternative Barrier Solution Material, SPE Bergen One Day Seminar. Society of Petroleum Engineers.

Bensted, J., 1998. Special Cements, LEA's Chemistry of Cement and Concrete. Elsevier, pp. 783–840.

Cestari, A.R., Vieira, E.F., Tavares, A.M., Andrade Jr., M.A., 2009. An oilwell cement slurry additivated with bisphenol diglycidil ether/isophoronediamine—kinetic analysis and multivariate modelings at slurry/HCl interfaces. J. Hazard Mater. 170 (1), 374–381.

Davidovits, J., 2013. Geopolymer Cement. A Review, vol. 21. Geopolymer Institute, pp. 1–11. Technical papers.

Davies, R.J., Almond, S., Ward, R.S., Jackson, R.B., Adams, C., Worrall, F., Herringshaw, L.G., Gluyas, J.G., Whitehead, M.A., 2014. Oil and gas wells and their integrity: implications for shale and unconventional resource exploitation. Mar. Petrol. Geol. 56, 239–254.

Henkensiefken, R., Bentz, D., Nantung, T., Weiss, J., 2009. Volume change and cracking in internally cured mixtures made with saturated lightweight aggregate under sealed and unsealed conditions. Cement Concr. Compos. 31 (7), 427–437.

Herschel, W., Bulkley, R., 1926. Measurement of consistency as applied to rubber-benzene solutions. Am. Soc. Test Proc 621–633.

International Organization for Standardization, ISO, 2014. ISO/TS-16530, Well Integrity - part 1: Life Cycle Governance / Part 2: Well Integrity for Operational Phase. ISO.

Jafariesfad, N., Geiker, M.R., Gong, Y., Skalle, P., Zhang, Z., He, J., 2017a. Cement sheath modification using nanomaterials for long-term zonal isolation of oil wells. J. Petrol. Sci. Eng. 156, 662–672.

Jafariesfad, N., Geiker, M.R., Skalle, P., 2017b. Nanosized magnesium oxide with engineered expansive property for enhanced cement-system performance. SPE J. 22 (05): 1,681-1,689.

Jimenez, W.C., Urdaneta, J.A., Pang, X., Garzon, J.R., Nucci, G., Arias, H., 2016. Innovation of annular sealants during the past decades and their direct relationship with on/offshore wellbore economics. In: SPE Bergen One Day Seminar. Society of Petroleum Engineers.

Khalifeh, M., Saasen, A., Hodne, H., Godøy, R., Vrålstad, T., 2018. Geopolymers as an alternative for oil well cementing applications: a review of advantages and concerns. J. Energy Resour. Technol. 140 (9), 092801.

Khalifeh, M., Saasen, A., Hodne, H., Motra, H.B., 2019. Laboratory evaluation of rock-based geopolymers for zonal isolation and permanent P&A applications. J. Petrol. Sci. Eng. 175, 352–362.

Khalil, M., Amanda, A., Yunarti, R.T., Jan, B.M., Irawan, S., 2020. Synthesis and application of mesoporous silica nanoparticles as gas migration control additive in oil and gas cement. J. Petrol. Sci. Eng. 107660.

Kiran, R., Teodoriu, C., Dadmohammadi, Y., Nygaard, R., Wood, D., Mokhtari, M., Salehi, S., 2017. Identification and evaluation of well integrity and causes of failure of well integrity barriers (A review). J. Nat. Gas Sci. Eng. 45, 511–526.

Le-Minous, J.C., Mutti, D., Bonvet, A., Unamue-Rodriguez, I., Chang, A., Massie, I., Xiao, E., Schnell, E., 2017. Permeability study of API class G and B cements considering seawater and WBM contamination. In: SPE/IADC Drilling Conference and Exhibition. Society of Petroleum Engineers.

Liu, X., Nair, S.D., Aughenbaugh, K.L., Juenger, M.C., van Oort, E., 2020. Improving the rheological properties of alkali-activated geopolymers using non-aqueous fluids for well cementing and lost circulation control purposes. J. Petrol. Sci. Eng. 195, 107555.

Mangadlao, J.D., Cao, P., Advincula, R.C., 2015. Smart cements and cement additives for oil and gas operations. J. Petrol. Sci. Eng. 129, 63–76.

Montserrat, S., 1993. Calorimetric measurement of the maximum glass transition temperature in a thermosetting resin. J. Therm. Anal. 40 (2), 553–563.

Moreira, P.H.S.S., de Oliveira Freitas, J.C., Braga, R.M., Araújo, R.M., de Souza, M.A.F., 2018. Production of carboxymethyl lignin from sugar cane bagasse: a cement retarder additive for oilwell application. Ind. Crop. Prod. 116, 144–149.

Nazir, R., Momeni, E., Armaghani, D.J., Amin, M.M., 2013. Correlation between unconfined compressive strength and indirect tensile strength of limestone rock samples. Electron. J. Geotech. Eng. 18 (1), 1737–1746.

Nelson, A.Z., Ewoldt, R.H., 2017. Design of yield-stress fluids: a rheology-to-structure inverse problem. Soft Matter 13 (41), 7578–7594.

Nelson, E.B., Guillot, D., 2006. Well Cementing. Schlumberger.

Norsok, D., 2013. Well integrity in drilling and well operations, 010 Standards Norway, Rev 4.

Paiva, M.D., Silva, E.C., Melo, D.M., Martinelli, A.E., Schneider, J.F., 2018. A geopolymer cementing system for oil wells subject to steam injection. J. Petrol. Sci. Eng. 169, 748–759.

Papadakis, V.G., Fardis, M.N., Vayenas, C.G., 1992. Hydration and carbonation of pozzolanic cements. Materials Journal 89 (2), 119–130.

Power, D., Zamora, M., 2003. Drilling Fluid Yield Stress: Measurement Techniques for Improved Understanding of Critical Drilling Fluid Parameters. AADE Technical Conference, Houston, pp. 1–3.
Saasen, A., Ytrehus, J.D., 2018. Rheological properties of drilling fluids: use of dimensionless shear rates in herschel-bulkley and power-law models. Appl. Rheol. 28 (5).
Salehi, S., Khattak, J., Saleh, F.K., Igbojekwe, S., 2019. Investigation of mix design and properties of geopolymers for application as wellbore cement. J. Petrol. Sci. Eng. 178, 133–139.
Santos, L., Dahi Taleghani, A., Li, G., 2018. Smart expandable polymer cement additive to improve zonal isolation. In: SPE/AAPG Eastern Regional Meeting. Society of Petroleum Engineers.
Santos, L., Dahi Taleghani, A., Li, G., 2020. Smart expandable fiber additive to prevent formation of microannuli. SPE Drilling & Completion.
Thomas, J., Musso, S., Catheline, S., Chougnet-Sirapian, A., Allouche, M., 2014. Expanding cement for improved wellbore sealing: prestress development, physical properties, and logging response. In: SPE Deepwater Drilling and Completions Conference. Society of Petroleum Engineers.
Todorovic, J., Raphaug, M., Lindeberg, E., Vrålstad, T., Buddensiek, M.-L., 2016. Remediation of leakage through annular cement using a polymer resin: a laboratory study. Energy Procedia 86, 442–449.
Tomosawa, F., Noguchi, T., 1993. Relationship between compressive strength and modulus of elasticity of high-strength concrete. In: Proceedings of the Third International Symposium on Utilization of High-Strength Concrete. Norwegian Concrete Assn Lillehammer, Norway, pp. 1247–1254.
Vignes, B., 2011. Contribution to Well Integrity and Increased Focus on Well Barriers in a Lifecycle Aspect. University of Stavanger.
Vrålstad, T., Saasen, A., Fjær, E., Øia, T., Ytrehus, J.D., Khalifeh, M., 2018. Plug & abandonment of offshore wells: ensuring long-term well integrity and cost-efficiency. J. Petrol. Sci. Eng.
Wagh, A.S., 2016. Chemically Bonded Phosphate Ceramics: Twenty-First Century Materials with Diverse Applications. Elsevier.

Appendix 6 – Paper V

Experimental Study of Hydraulic Sealability and Shear Bond Strength of Cementitious Barrier Materials

M. Kamali, M. Khalifeh, E. Eid, A. Saasen

Journal of Energy Resources Technology, 2021

DOI: 10.1115/1.4051269

Experimental Study of Hydraulic Sealability and Shear Bond Strength of Cementitious Barrier Materials

Mohammadreza Kamali[1]
Department of Energy and Petroleum Engineering,
University of Stavanger,
Stavanger 4036, Norway
e-mail: mohammadreza.kamali@uis.no

Mahmoud Khalifeh
Department of Energy and Petroleum Engineering,
University of Stavanger,
Stavanger 4036, Norway
e-mail: mahmoud.khalifeh@uis.no

Elsayed Eid
Department of Energy and Petroleum Engineering,
University of Stavanger,
Stavanger 4036, Norway
e-mail: e.eid@stud.uis.no

Arild Saasen
Department of Energy and Petroleum Engineering,
University of Stavanger,
Stavanger 4036, Norway
e-mail: arild.saasen@uis.no

In this experimental study, two different cementitious materials, including (i) a class of expansive cement currently used for plug and abandonment (P&A) operations and (ii) a non-cement-based naturally occurring rock, known as geopolymer, are selected to examine the hydraulic bond strength and shear bond strength. Clean machined steel and rusty corroded steel were selected to represent the casing. The test samples were cured at 90 °C considered as bottom-hole static temperature (BHST) and under elevated pressure of 17.2 MPa for 1 week. The hydraulic sealability of the barrier materials tested up to 3.4 MPa of differential pressure. The results indicated that additives used in slurry preparation impact the hydraulic sealability of the material. Additionally, the rusty corroded steel provided a better hydraulic sealability comparing to the clean machined steel for the same cementitious material. The shear bond strength test was performed by running the push-out test. According to the present test observations, no correlation was found between the shear bond and hydraulic bond strength of different barrier materials. The geopolymer showed the lowest shear bond strength, while it provided the highest hydraulic sealability.
[DOI: 10.1115/1.4051269]

Keywords: petroleum engineering, cementing operations, petroleum wells-drilling/production/construction

1 Introduction

In drilling operation and well construction, a cementitious slurry is pumped into the wellbore and placed behind the casing. The slurry is solidified and acts as a barrier to seal the annular space between the casing and formation and provide zonal isolation. The barrier material facilitates well construction and production by preventing formation fluid migration between different strata, holding the casing in place, and protecting it from corrosion. Consequently, the cementitious barrier material must be impermeable and be able to make a sufficient bonding to the casing to achieve integrated hydraulic sealability [1].

Ordinary Portland cement (OPC) is the leading material for primary cementing and plug and abandonment (P&A) operations. The chemistry of OPC is well-documented for both operating engineers and scientists, and the material is commercially available. Various chemical additives are introduced to the cement system to improve its performance at downhole conditions [2]. However, OPC is found to have shortcomings after setting including, but not limited to thermal instability, retrogression of mechanical properties due to contamination by drilling mud, low ductility, and shrinkage. Shrinkage of the cement bulk due to the hydration reaction can increase the risk of micro-path formation at the cement–casing and cement-formation interfaces. Besides, poor mud removal, improper cement placement due to eccentricity of casing and wellbore geometry, and gas channeling in the cement sheath can have a detrimental effect on zonal isolation and accelerate well integrity failure. Moreover, the cyclic change in pressure and temperature over the lifespan of the well implies a lot of compaction and tension of the cementitious barrier materials. Such condition requires sufficient flexible cement system with high tensile strength to Young's modulus and compressive strength to Young's modulus ratios. The OPC-based system is brittle in nature and may show a weak performance at downhole condition by forming radial cracks when it is subjected to an excessive load [3–5]. Therefore, researchers and technology providers continuously attempt to improve the quality of set cement and the cementing operation by either new cementing techniques or introducing alternative cementitious materials for the situations that OPC has limitations [6,7].

In zonal isolation and well abandonment operation, shear bond and hydraulic bond strength are two parameters, which contribute to effective hydraulic sealability at the interface of zonal isolation material and its adjacent medium [8]. The shear bond strength represents how strong the bonding is to prevent the movement of casing/cement sheath in the wellbore, and it is quantified as the minimum required force to move the casing within the cement sheath or the cement sheath within the formation. The hydraulic bond strength is the maximum hydraulic force induced by the formation fluid to initiate debonding at the interface. This parameter can be determined by continues pumping fluid at the boundaries until the leakage occurs. The shear bond strength and the hydraulic bond strength at the interface of barrier material and casing are discussed and reviewed in detail in Sec. 1.1. Figure 1 shows a schematic of the wellbore, including formation, casing, and the cement sheath.

1.1 Shear Bond and Hydraulic Bond Strengths. The shear bond strength effectively resists shear displacement and is expressed as the minimum required force to initiate movement at the interface of two materials, and it is an important indication of the cement ability to support casing string in wellbore [9] mechanically. On the laboratory scale, the shear bond strength between the cementitious material and casing pipe or formation is measured by placing the casing pipe (or a rod with few centimeters in diameter) inside the zonal isolation material or curing the zonal isolation

[1]Corresponding author.

Contributed by the Petroleum Division of ASME for publication in the JOURNAL OF ENERGY RESOURCES TECHNOLOGY. Manuscript received March 17, 2021; final manuscript received May 16, 2021; published online June 7, 2021. Assoc. Editor: Saeed Salehi.

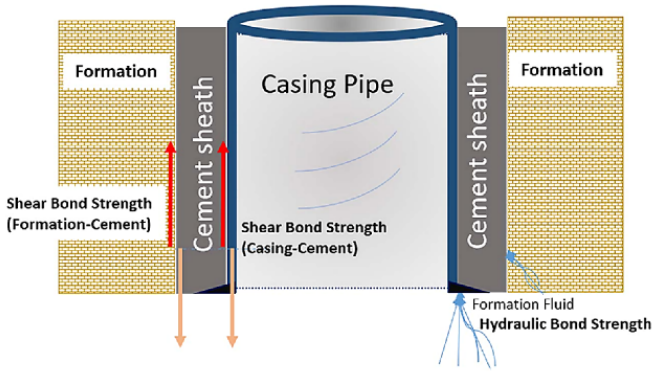

Fig. 1 Schematic of the wellbore including the formation, casing, and the cement sheath. The shear and hydraulic bond strengths are illustrated at the cement–casing and cement-formation interface.

material inside the formation outcrop. Then, a loading frame applies an axial load until debonding occurs, and the inner material starts to slip. One of the early shear bond strength experimental studies was performed by Evans and Carter [10]. The shear bond of different cement systems was investigated with casing and two types of formation, including sandstone and limestone. They reported the shear bond strength between 0.07 and about 2.76 MPa. They stated that shear bond strength depends on curing conditions, including but not limited to curing pressure and temperature, casing surface roughness, drilling fluid existence, and size of specimens. Kakumoto et al. [11] studied the effect of confining pressure on push-out test samples. They applied effective confining pressure of 1.5 and 3 MPa and compared the results with the ambient effective pressure of 0 MPa. The test result shows that increasing the confining pressure around the testing specimens contributes to escalated shear bond strength, depending on the pipe roughness. The authors also showed when the samples reach a maximum load (i.e., maximum load before debonding occurs), the applied load can enter a fluctuation zone. They revealed that it is the effect of stick-slip at the interface of the samples.

Lavrov et al. [12] investigated the effect of casing size on the shear bond strength. The authors studied 37 testing samples with pipe outer diameter (OD) of 10, 21, and 33 mm and height of 30 mm. The samples were cured at 80 °C and under elevated pressure. The tests were performed at displacement control mode with a rate of 0.5 mm/min. The test result shows the same oscillation behavior for the samples caused due to the selected mode of testing. They experimentally proved that the shear bond strength declines by about 36% with an increase in pipe diameter for the selected range of 10–33 mm. One of the limitations of running laboratory experiments is downscaling the real condition to the smaller size, particularly when the materials will go under mechanical loads. One important observation on Lavrov et al.'s test results is the large standard deviation from the mean values of the shear bond strength, which might be due to the small size of the tested samples or inconsistency in the sample preparation. They claimed that bonding strength is not an intrinsic parameter of cement–casing systems and should not be applied to field conditions directly. Using finite-element simulations, they concluded that the normal stress caused by cement shrinkage is reduced at the interface of larger diameters, and it results in less friction resistance of casing and cement. Thus, less push-out strength. In an earlier study conducted by Lavrov et al. [13], they attempted to measure the tensile bond strength between cement and steel using a three-point bending test. They prepared bi-material beams with the dimension of 60 × 5 × 5 cm—30 × 5 × 5 cm cement and 30 × 5 × 5 cm steel—and cured the specimens for 1 month at ambient pressure and temperature. The samples, however, were not able to be retrieved for testing as all samples were broke at the interface of steel–cement. Hence, they concluded that the push-out test represents friction and mechanical interlock between casing and cement, rather than providing information about adhesion between two materials [12].

In another experimental study, Khalifeh et al. [14] investigated the bond strength of Portland cement with six different pipe materials, including steel (reference material), titanium, two different grades of uncoated aluminum, and two different types of nano-coated aluminum pipes. They prepared the test specimens by curing cement around 50 mm pipes at an elevated temperature of 70 °C and atmospheric pressure for 7 days. The test results revealed that uncoated aluminum pipes provided poor shear bond strength, which is rooted in the detrimental reaction at the interface of the cement–aluminum. On the other hand, the titanium pipes were found to have stronger shear bond strength with Portland cement by 5% greater compared with the cement–steel system. The nano-coated aluminum pipes showed strong shear bond strength compared with the uncoated aluminum pipes. Even, the strength was 13% higher than the cement–steel system. Their study highlighted the possible chemical interaction between cement and the different casing materials.

The characterization of bond strength of geopolymers was studied by Zhang et al. [15] at ambient and elevated temperatures. Their research study included 18 different combinations of metakaolin and fly ash as a solid phase. They tested the shear bond strength in the temperature range of 20–300 °C and concluded that increasing temperature has an adverse effect on the bond strength of geopolymers. The test results also indicated that the chemical composition such as Si/Al ratio, SiO_2/K_2O ratio, and solid/liquid ratio of alkali-activated material significantly impact bond strength. In another study about the characterization of geopolymers for oil and gas applications, Salehi et al. [16] investigated the shear bond strength of class F fly ash geopolymers. In this study, sodium hydroxide (NaOH) with the concentration of 8 M, 10 M, and 12 M was used as a hardener. The experiments were performed at 65 and 93 °C, and the results showed that for mentioned specific fly ash-based system, there is an optimum value for the sodium hydroxide concentration. The maximum bond strength was achieved with 10 M NaOH. It was concluded that an increase in the concentration up to 10 M of alkali hydroxide hardener

accelerates the polymer gel formation, which is responsible for bond strength and compressive strength of geopolymers. Increasing the concentration beyond 10 M for this system affects gel formation and strength development of the slurry and resulting in weaker bonding between the geopolymer and the casing metal. Comparing the test results of fly ash geopolymers with the API class H Portland cement shows slightly higher bond strength for the geopolymers. The researchers highlighted a parameter "fracture energy" accountant for shear bond strength of considered materials. Fracture energy is described as the ability of materials with crack to resist fracture. In this study, this parameter was higher for the geopolymer than the class H cement. In another study about alternative materials for OPC in the oil and gas industry, Khalifeh et al. [17] tested the shear bond strength of a rock-based geopolymer. They used potassium silicate solution as a hardener with SiO_2/K_2O of 2.28 and cured the samples at 70 °C for 7 days. The measured shear bond strength was about 1.3 MPa, which is 3.6% less than the class G cement tested at the same condition. The authors concluded that the hardener modular ratio (SiO_2/M_2O) affects the bond strength of geopolymers (M is an alkali metal, potassium, or sodium).

The principle of shear bond strength is needed to be thoroughly understood. Shear bond strength at the interface of casing and cement can be the summation of (a) friction at the interface of different materials, (b) mechanical interlock due to surface roughness, (c) inward tension at the surface resulting from cement shrinkage, and (d) bonding as a result of chemical interaction between cementitious material and minerals exist at casing surface. However, the latter is a subject of debate.

It is insufficient to have a strong bonding to achieve proper zonal isolation; a cementitious material can have severe adhesion to the casing material, while pathways exist at the interfaces and formation fluid can easily penetrate through micro-channels. Hence, hydraulic bond strength is more critical in terms of zonal isolation, and it should be further investigated [18].

Hydraulic bond strength characterizes the interface between casing and cement material to resist the hydraulic fluid penetration, and it can be considered as a direct measurement of hydraulic sealability and providing zonal isolation [19]. The hydraulic bond strength is defined as minimum pressure induced by an injection fluid to make debonding or initiating flow at cement–casing/formation interface.

Several experimental studies investigated hydraulic bond strength of cement–casing or cement-formation interface at both small- and large-scale [10,14,20]. The experiments were conducted by continuous injection of gas or liquid at the interfaces, and the pressure development and/or the flowrate during the test were monitored. Chemistry and proper placement of the cementitious barrier material, and the pipe surface properties are critical parameters to have integrated hydraulic sealability. The compatibility of the casing material and the cementitious slurry is a necessity. In an earlier experimental study conducted by Khalifeh et al. [14], incompatibility of aluminum pipe and the API neat class G cement was highlighted. Steel pipes are common materials for casing the borehole. For situations that alternative material is required for cementing operation or a new additive is introduced to the cement slurry, it is inevitable to test the system's compatibility and performance.

The output results of hydraulic bond strength tests are relevant for a qualitative comparison between the casing and cementitious materials for both academia and field engineers. The quantitative information, however, includes the non-negligible scaling effect of the test setup. As discussed in the literature [9,12], the small-scale test results provide no guarantee for the exact observation in the field-scale setup. Nonetheless, studying the hydraulic bond strength requires thorough details about micro-path development, size, structure, and direction at the interfaces from a purely academic point of view. Fluid flow through a degraded cement sheath was studied through the visualization of the micro-annuli employing computational fluid dynamics (CFD) and X-ray computed tomography (CT) [21]. Researchers used pressure- and thermal-cycling to mimic real downhole conditions in drilling operations and visualized the fluid flow through the micro paths with the cement sheath and cement–casing interfaces. They concluded that the flow in the macro annuli is a complex phenomenon as it depends on the size and shape of the flow path and the magnitude of degradation of the cement sheath.

1.2 Cementitious Materials. It is crucial to have integrated bonding at the cement–casing or cement-formation interfaces to achieve proper zonal isolation in the well construction. OPC experiences autogenous shrinkage during solidification [22]. In the hydration reaction, the calcium-rich cement powder consumes the water and forms calcium–silicate–hydrate (C–S–H) groups, which are accountable for strength development. When the reaction proceeds, the unreacted cement particles consume free water within the cement matrix and empty the pores. This phenomenon results in autogenous shrinkage and applies internal tensile stress in solidified cement. For situations that the cement sheath has no access to external humidity, the autogenous shrinkage can be extensive and cause radial cracks. Therefore, in oil and gas applications, particularly when the cement slurry is placed between two casings, a higher water to cement ratio is considered [23].

Expansive agents are one of the additives that can compensate the shrinkage to some extent, where the expanding agent can make crystals or generate gas bubbles during the solidification process [24]. The effectiveness of expansive cement for oil and gas applications increases if the expansion reaction occurs at the right time—when the shrinkage starts. Early expansion reaction would not effectively compensate for the long-term shrinkage. While very late expansion can cause cracks in cement structure, it is essential to engineer the chemical reactivity of expanding agents in cement.

Geopolymers are inorganic materials that are produced by mixing a reactive aluminosilicate species with a liquid hardener and make a slurry with cementitious properties [17,25]. In this class of material, the geopolymerization reaction occurs instead of hydration and forms long-chain molecules in tetrahedral orientation, including aluminate and silicate. The solid phase may include low calcium fly ash, metakaolin, or naturally occurring rock. The liquid phase is an alkali silicate solution (potassium or sodium) with an adjusted modular ratio. The geopolymerization reaction proceeds in three main steps: (a) the aluminosilicate structures are dissolved and the silanol groups (Si–O–H) are created, (b) the single groups are oriented and reconnected to form oligomers as the ion concentration increases in the slurry, and finally, (c) the long-chain structure of aluminosilicates is formed through polycondensation and by connecting oligomers. Although geopolymers are used in the civil industry, the technology is still at the research stage for oil and gas application by engineering the properties based on downhole conditions.

In this research work, an expansive commercial cement used for plug and abandonment operation and a rock-based geopolymer are applied, as zonal isolation material, to study shear bond and hydraulic bond strengths of the casing. This study aims to investigate the performance of a different class of materials at similar operational conditions of pressure and temperature and generate a data set including the test results of neat materials. The neat API class G cement was also selected to make the results reproducible as a non-commercial reference. The common additives may also be different depending on material suppliers all around the world.

2 Material Preparation and Experimental Procedures

2.1 Slurry Preparation and Mixing. For all samples, the slurries were mixed using the raw materials, including solid and liquid phases and additives that were delivered by the industrial service providers. The mixing procedure was followed in accordance with the provided instructions by material suppliers and described in detail in the following. The recipes were designed and suggested based on bottom-hole circulation temperature (BHCT) of 65 °C and bottom-hole static temperature (BHST) of

90 °C, and the pressure of 170 bar. This is the condition for majority of wells in North Sea, and it is recommended by operating companies. The rheological properties and pumpability of materials at BHCT, and mechanical properties of materials after solidification up to 28 days of curing were tested and published [26]. All materials used for hydraulic bond strength tests were mixed using the API high-speed mixer Waring blender. The mixer starts to mix the slurry for 15 s at 4000 rpm and continues mixing for 35 more seconds at 12,000 rpm. The shear bond strength specimens needed a higher volume of cementitious slurry; therefore, the API high-speed mixer was not applicable due to its small capacity. Hobart N50-60 commercial blender was used to mix the slurry for the shear bond strength test. The mix design of each material was upscaled and sheared for 30 min, while the mixer speed was fixed at level 2. The mixing procedure and components for each type of barrier material are described as follows:

Neat class G cement—The solid phase consists of only neat API class G cement manufactured by Dyckerhoff. It was mixed with 44% by weight of cement (BOWC) de-ionized water.

Expansive cement—The solid phase was dry blended class G cement with magnesium oxide as an expansive agent, and it was delivered by the material supplier. Industrial chemicals were added to the de-ionized water and formed the liquid phase. The material supplier recommended additives were to tailor the rheological and mechanical properties of the slurry. The additives included in this study were retarder, fluid-loss controller, defoamer, and cement particle dispersant. Microsilica solution with a mass fraction of 50% in water was recommended by the cement supplier to enhance the performance of the material.

Geopolymer—The slurry was mixed based on an in-house recommendation. The solid phase that also known as precursor was dry blended by hand mixing and shaking in a sealed bucket. The precursor was an aluminosilicate-rich naturally occurring rock normalized by active quenched blast furnace slag (BFS), an industrial waste, to achieve normalized chemical composition. In this study, the potassium silicate solution with a modular ratio of 2.49 was used as a hardener mixed with the precursors.

2.2 Molding, Curing, and Running Test. *Shear bond strength*—The shear bond strength test was performed by conducting the push-out test. The specimen consists of

(a) Inner pipe: A metal bar with a diameter of 51 mm and a height of 120 mm, which represents casing material.
(b) Outer pipe with an inner diameter of 150 mm: The outer pipe is functioned to hold the cementitious slurry during the curing period and as a casing material to measure the shear bond strength. Therefore, the shear bond strength for each sample of barrier material was measured twice; once, at the interface of a small bar with a diameter of 51 mm and next time, at the interface of the outer casing with an inner diameter of 150 mm.
(c) Stainless-steel bottom-cap: It has a hole with a diameter of 51.5 mm in the center to fix the metal bar. The bottom-cap also has a circular groove to hold the outer pipe. Plastic cellophane was placed on the bottom-cap to avoid any bonding between the slurry and the cap during the curing period. The bottom-cap was removed before running the shear bond strength rest.
(d) Stainless-steel top-cap: It is similar to the bottom-cap, but with two extra holes with a diameter of 20 mm, one for filling the cell and the other one for observing the level of liquid slurry inside the mold.

The whole system was assembled using silicon glue 1 day before mixing the slurry. The system was cured at 90 °C, corresponding to bottom-hole static temperature. However, the pressure for curing shear bond strength test specimens could not be increased above 500 psi due to safety issues and limitations with the curing chamber. After 7 days of curing, the samples were prepared for the push-out test to measure the shear bond strength test in short-term. The specimens were cooled down to the ambient temperature in 9 h to avoid thermal shock to the system. The bottom- and top-caps were removed slowly, and the samples were placed on a stand for applying loading rate. The stand was designed to only hold the cement sheath. Both the middle bar and outer pipe are free to move during loading. Initially, the bar was pushed until the bonding was broken. At this point, the bar started to move within the cement sheath. In the next step, the loading rate was applied to the outer pipe until it was debonded at the interface with the cement sheath. A universal testing machine (Zwick/Roell Z050) that is normally used for the compressive/tensile strength test was used as equipment to apply load on samples. Loading regime to push the bars and pipers may have an impact on the results, and it also depends on the sensitivity of the equipment. The equipment was programmed on load control mode rather than position control, and the loading rate of 50 N/s was selected. The reason for considering load control is presented in detail under Sec. 4. The whole process of sample preparation is illustrated graphically in Fig. 2.

Hydraulic bond strength—After mixing by API high-speed Waring blender, the barrier materials were transferred to the atmospheric consistometer and conditioned for 30 min at bottom-hole circulation temperature of 65 °C. The temperature controller was functioned to increase the temperature by 1 °C/min. After conditioning, the slurry was poured inside the casing pipes. The 120 mm casing pipe has an inner diameter of 37 mm and a thickness of 7 mm. Three holes are established at the center of the body with an orientation of 120 deg for pump connection and fluid injection. The pipes used for the hydraulic bond strength test were the same in composition and material as the solid bars used for the shear bond strength test. The samples were placed inside cylindrical autoclaves in the oven to be cured for 7 days. The temperature for curing was 90 °C, and a pump provided the pressure of 2500 psi in autoclaves. Three specimens were provided per barrier material with casing to minimize the possible errors in running the tests. After 7 days, the samples were cooled down slowly and connected to an ISCO pump for hydraulic testing and fluid injection. De-ionized water was used as an injection fluid. There is no common standard to evaluate the hydraulic bond strength of barrier materials for oil and gas applications. The pump was programmed to increase the pressure gradually in the following steps:

(1) From atmospheric to 100 psi in 1 min and hold at 100 psi for 10 min.
(2) From 100 to 150 psi in 1 min and hold at 150 psi for 10 min.
(3) From 150 to 200 psi in 1 min and hold at 200 psi for 5 min.

The neat class G cement was the first material to test the hydraulic bond strength. It was observed the samples start to lose their hydraulic sealability at 200 psi. It was not applicable to increase the differential pressure due to high fluid leak in specimens. However, the expansive cement and geopolymer showed no leakage and no sign of failure until 200 psi. Therefore, it was decided to increase the differential pressure up to 500 psi in following the steps:

(a) From 200 to 300 psi in 1 min and hold at 300 psi for 5 min.
(b) From 300 to 400 psi in 1 min and hold at 400 psi for 5 min.
(c) From 400 to 500 psi in 1 min and hold at 500 psi for 15 min.

The test stopped at 500 psi due to safety issues. Figure 3 graphically shows the setup for hydraulic bond strength. To avoid drying shrinkage, all testing samples for shear bond and hydraulic bond strength test were kept under water after removing the oven and running the experiments.

3 Experimental Results

3.1 Shear Bond Strength Test. The samples after 7-day curing were placed under compression load to run the push-out

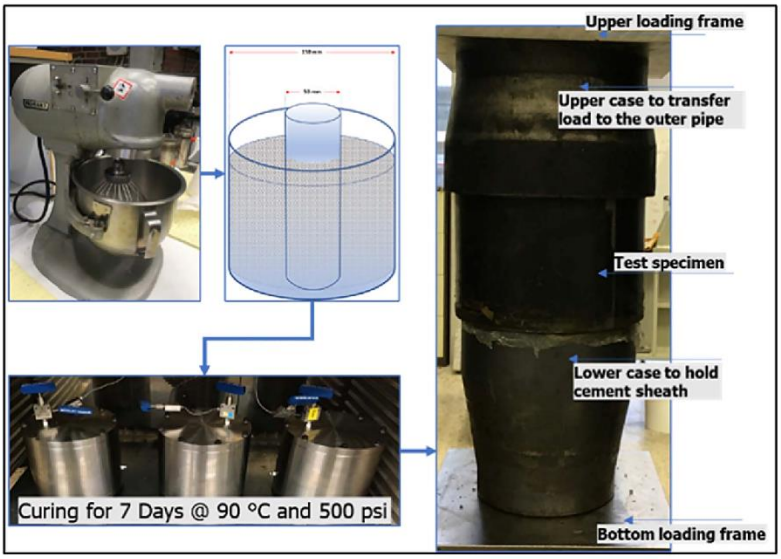

Fig. 2 The sample preparation process for the shear bond strength test, including mixing, molding, curing, and testing

Fig. 3 The sample preparation and test setup for the hydraulic bond strength test

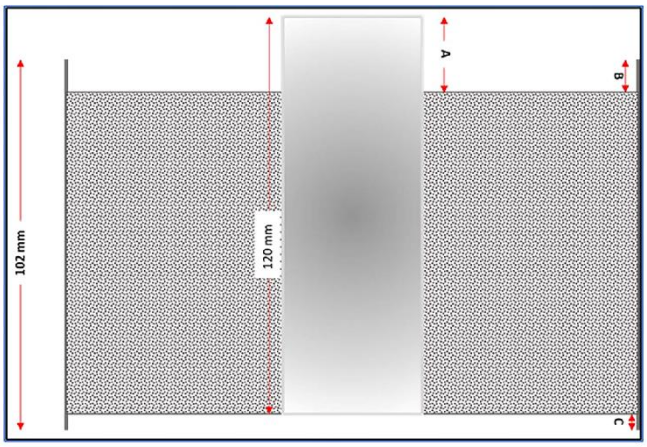

Fig. 4 The cross section of a shear bond strength test sample. A, B, and C should be measured for each specimen.

test. For every sample, the contact area of barrier material with the inner bar and the outer pipe was estimated before loading the specimen. The contact area was calculated by extracting A, B, and C for each sample as illustrated in Fig. 4.

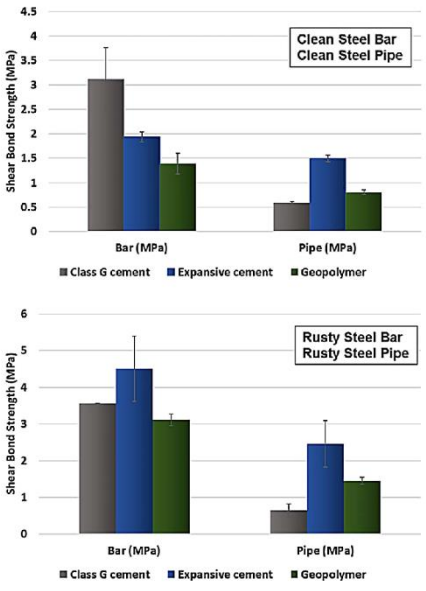

Fig. 5 Shear bond strength at the interface of solid bar and outer pipe for API neat class G cement, expansive cement, and geopolymer

Figure 5 shows the shear bond strength for the candidate barrier materials with both clean and rusty steels. The bond strength for all samples with rusty steel is increased. However, the bond strength of neat class G cement has less increase, by about 10% for both rusty bar and pipe steel compared with the clean steel surfaces. The reason for this lesser increase is not known. The shear bond strength of class G cement at the pipe interface was only 17% of the bond strength with the bar. In another study with the same cement and similar grade of steel bar in the middle, Khalifeh et al. [14] reported the shear bond strength of 1.3 MPa, which is 58% lower than the current measured strength. Following sample preparation procedure but increasing temperature by 20 °C and curing under elevated pressure of 3.4 MPa has positively impact shear bond strength.

The shear bond strength of expansive cement experienced about 100% increase when the rusty steel was considered, both at the pipe and bar interface. The shear bond strength at the bar interface was reached to the average value of 4.5 MPa, and at the pipe interface, the bond strength was measured 2.5 MPa, which is 55% of the bond strength at the bar interface.

The shear bond strength for the geopolymer was increased by 100% at both rusty bar and pipe interfaces. The shear bond strength of the geopolymer at the pipe surface was about 50% of strength at the bar interface for both clean and rusty boundaries.

The difference in shear bond strength of geopolymer and expansive cement with neat class G cement at outer pipe can be either related to the shrinkage of class G cement or chemical interactions between the barrier materials and surface minerals in the interface transition zone (ITZ). However, the chemical interaction between rust and different cementitious materials is not yet well understood.

3.2 Hydraulic Bond Strength Test. The hydraulic bond strength test goal was to qualitatively evaluate the hydraulic sealability at the interface of the barrier material and casing systems. The hydraulic bond strength test results for selected barrier materials and clean machined steel are shown in Fig. 6. The figure includes the flowrate (ml/min), cumulative injected fluid by the pump during the test period (ml) and pressure (psi). The neat class G cement–steel pipe system was considered as a reference in this study.

The high initial flowrate refers to the fluid to fill and pressurize the connected pipes to the samples, and it can be ignored. The

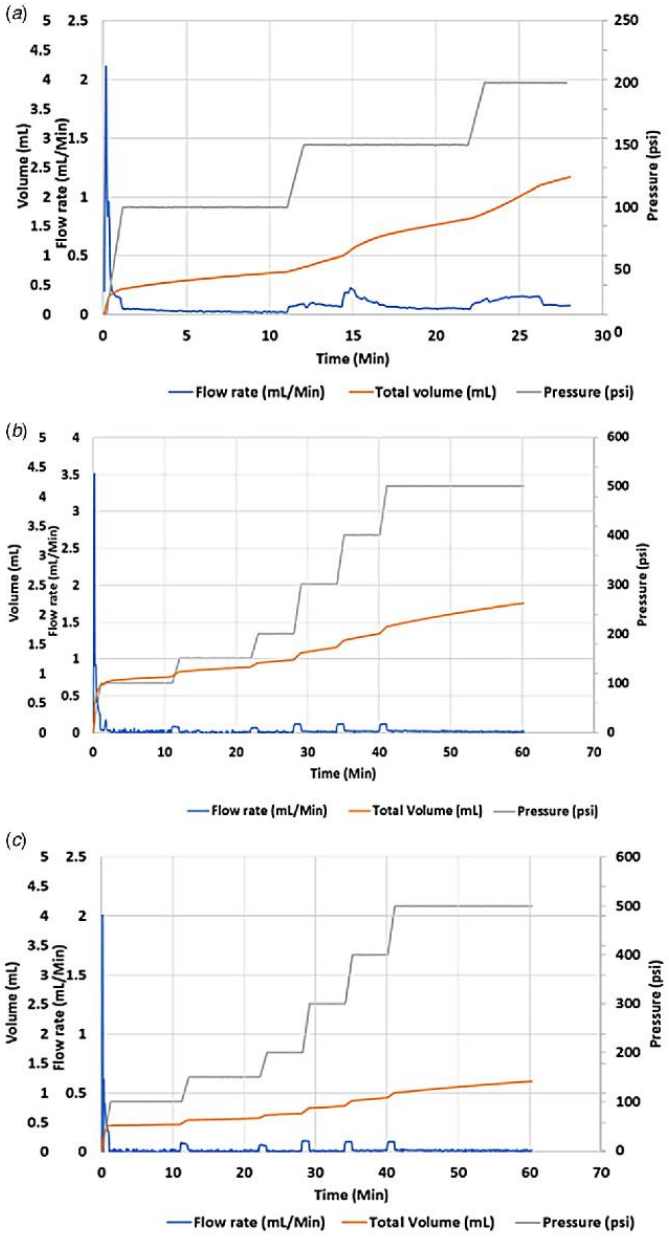

Fig. 6 Hydraulic bond strength test results for clean machined steel including the flowrate in ml/min, cumulative volume of injected fluid in ml, and pressure in psi for (*a*) API neat class G cement, (*b*) expansive cement, and (*c*) geopolymer

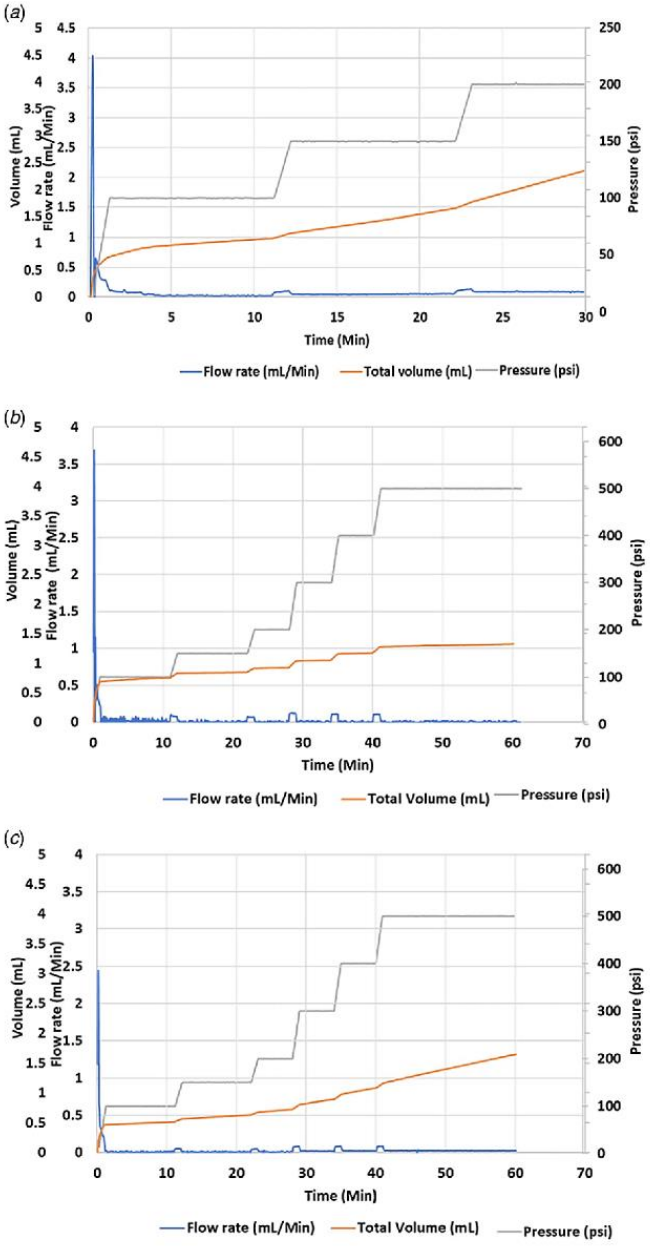

Fig. 7 Hydraulic bond strength test results for rusty steel including the flowrate in ml/min, cumulative volume of injected fluid in ml, and pressure in psi for (*a*) API neat class G cement, (*b*) expansive cement, and (c) geopolymer

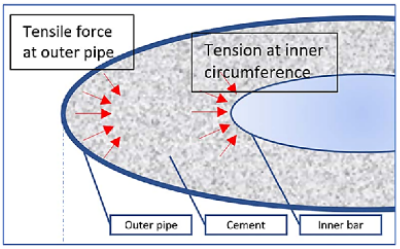

Fig. 8 Tensile loads due to cement shrinkage at outer and inner circumference of the cement sheath

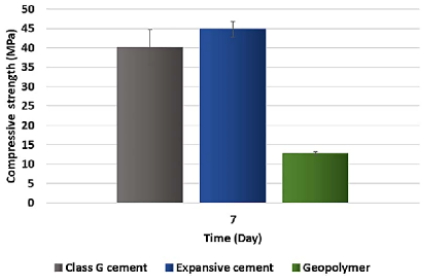

Fig. 9 Uniaxial compressive strength of barrier materials up to 7 days

small humps in the flowrate trend during the test are also referred to the increase in differential pressure. A relatively high flowrate was expected for the neat class G cement due to the autogenous shrinkage. The test was only continued up to differential pressure of 200 psi due to high leakage at the interfaces between pipe and cement and also cement matrix. Expansive cement and geopolymer could provide sealability up to 200 psi. The logged pump flowrate was negligibly low, compared with that of the neat class G cement (Fig. 6). Therefore, no fluid leak was observed at the interfaces and material matrices when the tests were continued up to 500 psi. Both expansive cement and geopolymer systems provided appropriate sealability comparing to the neat class G cement. The test results for the cementitious materials and rusty corroded steel are shown in Fig. 7. Similar to the clean steel test results, the samples followed almost the same trend. The geopolymer showed a minimum flowrate compared with the other systems. The hydraulic sealability of the expansive cement system was also in the same range of geopolymer.

4 Discussions

Shear bond strength—The shear bond strength of different barrier materials was measured at the inner and outer surfaces of the set barrier materials and steel. The shear bond strength test's main goal in the present work was predicting the pure shear force that is required to make a movement at the interface of the steel and barrier material by reducing the possible uncertainties. This is the main reason to consider a relatively thick sheath of barrier materials (about 50 mm) for molding and sample preparation. Thinner thicknesses could result in radial cracks due to the almost 70 °C difference between curing and testing temperatures. However, the samples were cooled down gradually for 9 h, but the difference in the thermal expansion coefficient of barrier materials and steel could cause radial cracks [27].

Additionally, the outer pipe was carbon steel grade S235JRH (roughness: 2.1, chemical composition: 2% carbon, 1.4% manganese, and 0% silicon), while the inner bar was chromium-rich grade 4140 (roughness: 2.07, chemical composition: 1.06% chromium, 0.91% manganese, 0.41% carbon, and 0.3% silicon). Suppose any possible chemical interaction affects bonding between the barrier material and the steel pipe. In that case, the chemical composition, and minerals at the surface of both barrier material and metal are the key parameters. Consequently, the effect of pipe diameter in the shear bond strength test is irrelevant in this study. Moreover, shrinkage due to the hydration reaction and chemistry of cement slurries is well-known. When the cement-based slurries are placed in a circular geometry, such as specimens that are provided for the shear bond strength test, cement shrinkage implies inward tension to the convex interface consisting of the interface between cement and middle bar. At the concave interface, the interface between cement and outer pipe, it is opposite. The interface of the cement and concave metal experiences a tension from the pipe-cement interface heading inward [27]. Figure 8 graphically illustrates the possible shrinkage tension regime that exists in a circular geometry. This can be an explanation for higher shear bond strength at the bar's interface (convex surface) compared with the outer pipe (concave surface).

Despite the shear bond strength test result reported by the previous literature, no fluctuation was observed in results after debonding occurred at the interface [11]. The loading mode applied by the equipment in the push-out test is an important parameter and may impact shear bond strength test results. The previous studies have selected position control to apply load on the samples. Generally, it is believed that for the compression tests of cementitious materials to measure uniaxial compressive strength, the control mode—position or load control—has no effect on stress–strain curves at the linear elastic range. In contrast, for the plastic range, the loading rate will be much lower than the load control, or the beginning of the position control [28]. By considering the displacement control mode selected by previous researchers for testing the samples, the fluctuation in the results may be due to the equipment adjustments to meet the selected testing mode. When the pipe starts to move within the cement sheath, dynamic friction exists at the interface of both materials. The equipment intends to meet the specified displacement rate; hence, it suddenly stops/reduces the loading rate on the sample. The dynamic friction coefficient changes to the static friction coefficient, which is greater than the dynamic one. Consequently, a more loading rate is required to push the pipe and reach the defined displacement rate, and the force starts to rise again. This oscillation behavior will repeat at entire time of the test after debonding occurs.

Evans and Carter found a correlation between compressive strength and shear bond strength of cement [10]. They showed a direct relationship between compressive strength and shear bond strength of the cement systems and stated that the supporting ability of cement could be determined if its compressive strength is available. The uniaxial compressive strength of the barrier materials was tested for up to 7 days of curing slurries under elevated temperature and pressure. The results are presented in Fig. 9 [26]. However, the mentioned relation between compressive strength and shear bond strength is only valid for the barrier materials and inner rusty bar. Still, for the outer pipe, the compressive strength was inversely proportional to the shear bond strength when geopolymer and cement systems are compared. Therefore, the correlation can be updated by including the different classes of barrier materials and the position of the casing pipe (inside or outside of the barrier material).

Hydraulic bond strength—Generally, as the curing condition is different from the testing conditions in the laboratory, the provided results cannot be extended to the real field application due to the

Fig. 10 Top: API neat class G samples started to leak both at interface and within the bulk at 100 psi of differential pressure. Middle: Expansive cement at 500 psi of differential pressure. Bottom: Geopolymer at 500 psi of differential pressure. Both expansive cement and geopolymer revealed no fluid leakage within the bulk.

uncertainties. Therefore, it is recommended to consider the results to make only a qualitative comparison between different casing materials and cementitious barrier materials.

The curing condition, samples preparation, casing material, and the casing inside diameter were the same for different cementitious materials. Hence, any difference in hydraulic sealability can be divided into two sections:

(1) At the casing-barrier material's interface, either by possible constructive reactions between the components of the set barrier material and the casing to form a tight and integrated sealing at the interfaces, and shrinkage compensation of the cementitious material. The neat class G cement is expected to experience an autogenous shrinkage due to the hydration reaction, which applies extra tension at the interfaces. The

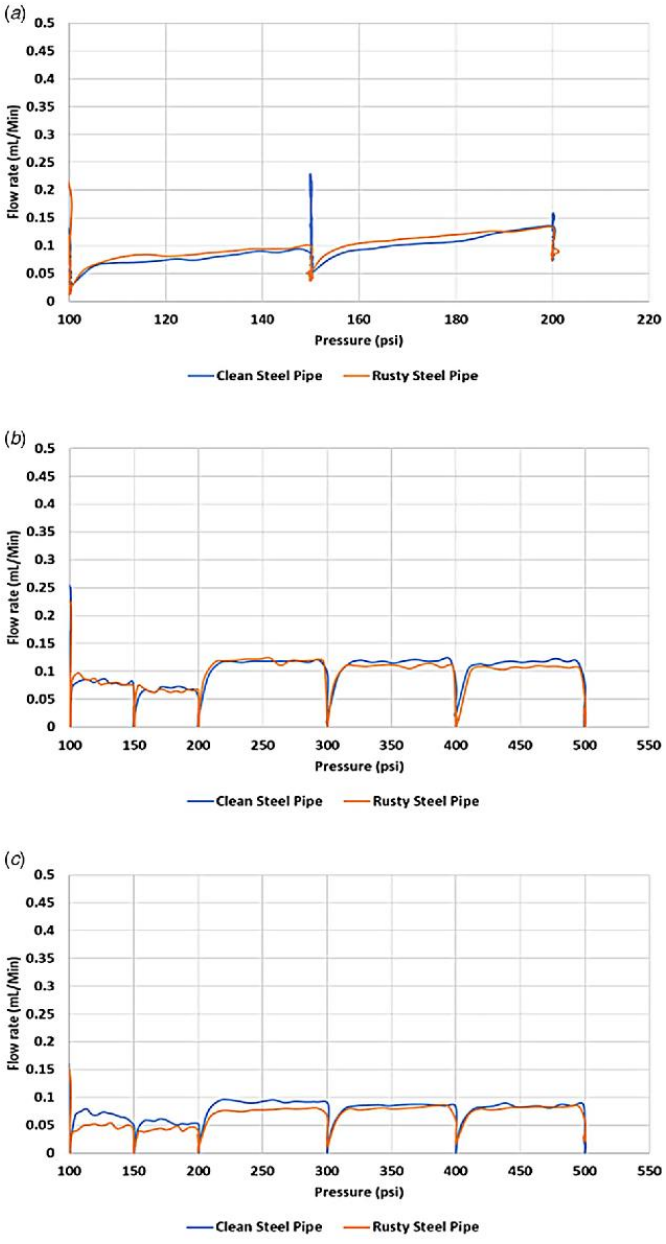

Fig. 11 The injection flowrate as function of differential pressure for clean steel pipe and rusty steel pipe for (*a*) API neat class G cement, (*b*) expansive cement, and (*c*) geopolymer

role of chemical additive and expansive agent in the expansive cement was brilliant in the test results. Although the geopolymer slurry follows a different reaction path for solidification, similar chemical components responsible for shrinkage compensation in expansive cement exist in geopolymer slurry. The BFS used in the geopolymer precursor significantly contributes to both shear and hydraulic bond strengths. The slag can develop internal stresses caused by densified microstructure. This feature can later result in rebonding and healing performance at the interface [29].

(2) Within the matrix of the barrier material. During the hydraulic bond strength test for the neat class G cement, it was observed that the injected fluid not only leaked at the cement–casing interface but also found its way through the cement matrix due to higher permeability comparing to expansive cement and geopolymer. Figure 10 clearly shows the fluid penetration and at the API net class G's surface. Accordingly, the additives used in expansive cement and the chemical composition of geopolymer improved the hydraulic sealing capability by providing a less permeable structure for the materials.

Except for the neat class G cement system, the results from rusty steel pipes comparing to the clean steel pipes showed that the rusted steel had provided a slightly better sealing capability for the same barrier material, as presented in Fig. 11. This observation may reveal that the rough surface at the interface can disconnect possible macro paths or more meandrous micro paths, which take for time for the fluid to move at the interface. A similar observation was reported by other researchers [30]. Running CFD analysis and X-ray CT techniques can help to understand the micro annular path's direction and size.

5 Conclusion

Two alternative barrier materials, including expansive cement and geopolymer, were highlighted, and shear bond and hydraulic bond strengths were tested. The neat API class G cement was also selected as a noncommercial reference. The shear bond strength of barrier materials and steel casing summarizes different parameters such as surface geometry, chemical and mechanical characteristics of both barrier material and casing. The mineralogy of materials at the contact interface can influence the bonding in the short- and long-term. Therefore, the interface transition zone of the barrier material and metal should be studied in detail. The strong shear bond strength may not be representative of good zonal isolation individually; hence, the mechanical properties of the materials, such as compressive and tensile strengths and modulus of flexibility, should also be included to evaluate the performance of the whole system.

The hydraulic sealability of the zonal isolation materials with clean and rusty steel was tested by continuously injecting water at the barrier material-casing interface. Both expansive cement and geopolymer showed sealing capability during the test period and up to 0.34 MPa (500 psi) of differential pressure. The injection flowrate can be considered as a function of possible micro annular paths at the interfaces. The rusty steel pipes showed slightly better hydraulic sealability, which can be due to the tortuous flow path formation. The chemical interaction between cement and rusty steel or clean steel at the interface transition zone remains a question. The difference in curing condition of pressure and temperature with the testing condition at room temperature and pressure is non-negligible; thus, further studies are required to extend the field application results.

Acknowledgment

The authors would like to thank Halliburton and AITiSS AS for their supports and for sharing technical information. A special thanks go to Johannes Steinnes Jensen and Emin Ahmadov for preparing the test setup for curing samples. The authors also thank Aker BP and TOTAL for supporting part of the project through the SafeRock Project joint industrial project at the University of Stavanger (UiS).

Conflict of Interest

There are no conflicts of interest.

Data Availability Statement

The datasets generated and supporting the findings of this article are obtainable from the corresponding author upon reasonable request. The authors attest that all data for this study are included in the paper. Data provided by a third party are listed in Acknowledgment.

Funding Data

- Research Council of Norway (KD) through the Department of Energy and Petroleum Engineering (IEP), University of Stavanger (UiS).

References

[1] Vrålstad, T., Saasen, A., Fjær, E., Øia, T., Ytrehus, J. D., and Khalifeh, M., 2019, "Plug & Abandonment of Offshore Wells: Ensuring Long-Term Well Integrity and Cost-Efficiency," J. Pet. Sci. Eng., **173**, pp. 478–491.
[2] Alvi, M. A. A., Khalifeh, M., and Agonafir, M. B., 2020, "Effect of Nanoparticles on Properties of Geopolymers Designed for Well Cementing Applications," J. Pet. Sci. Eng., **191**, pp. 107–128.
[3] Opedal, N., Todorovic, J., Torsæter, M., Vralstad, T., and Mushtaq, W., 2014, "Experimental Study on the Cement-Formation Bonding," SPE International Symposium and Exhibition on Formation Damage Control, Lafayette, LA, February, Society of Petroleum Engineers.
[4] Skadsem, H. J., and Kragset, S., 2021, "Effect of Buoyancy and Inertia on Viscoplastic Fluid–Fluid Displacements in a Regular and an Irregular Eccentric Annulus," ASME J. Energy Resour. Technol., **143**(6), p. 062101.
[5] Jafariesfad, N., Geiker, M. R., Gong, Y., Skalle, P., Zhang, Z., and He, J., 2017, "Cement Sheath Modification Using Nanomaterials for Long-Term Zonal Isolation of Oil Wells," J. Pet. Sci. Eng., **156**, pp. 662–672.
[6] Kimanzi, R., Wu, Y., Salehi, S., Mokhtari, M., and Khalifeh, M., 2020, "Experimental Evaluation of Geopolymer, Nano-Modified, and Neat Class H Cement by Using Diametrically Compressive Tests," ASME J. Energy Resour. Technol., **142**(9), p. 092101.
[7] Khalifeh, M., Saasen, A., Hodne, H., Godøy, R., and Vrålstad, T., 2018, "Geopolymers as an Alternative for Oil Well Cementing Applications: A Review of Advantages and Concerns," ASME J. Energy Resour. Technol., **140**(9), p. 092801.
[8] Khalifeh, M., and Saasen, A., 2020, *Introduction to Permanent Plug and Abandonment of Wells*, Springer Nature, The Hague.
[9] Opedal, N., Cerasi, P., and Vrålstad, T., 2019, "Cement Bond Strength Measurements," International Conference on Offshore Mechanics and Arctic Engineering, Glasgow, Scotland, UK, November, American Society of Mechanical Engineers.
[10] Evans, G. W., and Carter, L. G., 1962, "Bounding Studies of Cementing Compositions to Pipe and Formations," Presented at the Drilling and Production Practice, New York, January, American Petroleum Institute.
[11] Kakumoto, M., Yoneda, J., Tenma, N., Miyazaki, K., Aoki, K., and Itoi, R., 2012, "Frictional Strength Between Casing and Cement Under Confining Pressure," The Twenty-Second International Offshore and Polar Engineering Conference, Rhodes, Greece, June, International Society of Offshore and Polar Engineers.
[12] Lavrov, A., Bhuiyan, M., and Stroisz, A., 2019, "Push-Out Test: Why Bother?" J. Pet. Sci. Eng., **172**, pp. 297–302.
[13] Lavrov, A., Gawel, K., Stroisz, A., Torsæter, M., and Bakheim, S., 2017, "Failure Modes in Three-Point Bending Tests of Cement-Steel, Cement-Cement and Cement-Sandstone Bi-Material Beams," Constr. Build. Mater., **152**, pp. 880–886.
[14] Khalifeh, M., Hodne, H., Saasen, A., Dziekonski, M., and Brown, C., 2018, "Bond Strength Between Different Casing Materials and Cement," SPE Norway One Day Seminar, Bergen, Norway, April, Society of Petroleum Engineers.
[15] Zhang, H. Y., Kodur, V., Qi, S. L., and Wu, B., 2015, "Characterizing the Bond Strength of Geopolymers at Ambient and Elevated Temperatures," Cem. Concr. Compos., **58**, pp. 40–49.
[16] Salehi, S., Khattak, M. J., and Bwala, A. H., 2017, "Characterization, Morphology and Shear Bond Strength Analysis of Geopolymers: Implications for Oil and Gas Well Cementing Applications," J. Nat. Gas Sci. Eng., **38**, pp. 323–332.

[17] Khalifeh, M., Saasen, A., Hodne, H., and Motra, H. B., 2019, "Laboratory Evaluation of Rock-Based Geopolymers for Zonal Isolation and Permanent P&A Applications," J. Pet. Sci. Eng., **175**, pp. 352–362.
[18] Ytrehus, J. D., Lund, B., Taghipour, A., Kosberg, B. R., Carazza, L., Gyland, K. R., and Saasen, A., 2021, "Hydraulic Behavior in Cased and Open-Hole Sections in Highly Deviated Wellbores," ASME J. Energy Resour. Technol., **143**(3), p. 033008.
[19] Bybee, K., 2005, "The Cement-to-Formation Interface in Zonal Isolation," J. Pet. Technol., **57**(08), pp. 41–44.
[20] Lecampion, B., Bunger, A., Kear, J., and Quesada, D., 2013, "Interface Debonding Driven by Fluid Injection in a Cased and Cemented Wellbore: Modeling and Experiments," Int. J. Greenhouse Gas Control, **18**, pp. 208–223.
[21] De Andrade, J., Sangesland, S., Skorpa, R., Todorovic, J., and Vrålstad, T., 2016, "Experimental Laboratory Setup for Visualization and Quantification of Cement-Sheath Integrity," SPE Drill. Eng., **31**(04), pp. 317–326.
[22] Henkensiefken, R., Bentz, D., Nantung, T., and Weiss, J., 2009, "Volume Change and Cracking in Internally Cured Mixtures Made With Saturated Lightweight Aggregate Under Sealed and Unsealed Conditions," Cem. Concr. Compos., **31**(7), pp. 427–437.
[23] Nagelhout, A., Bosma, M. G., Mul, P., Krol, G., van Velzen, H., Joldersma, J., James, S. G., Dargaud, B., Schreuder, R., and Théry, F., 2010, "Laboratory and Field Validation of a Sealant System for Critical Plug-and-Abandon Applications," SPE Drill. Eng., **25**(03), pp. 314–321.
[24] Thomas, J., Musso, S., Catheline, S., Chougnet-Sirapian, A., and Allouche, M., 2014, "Expanding Cement for Improved Wellbore Sealing: Prestress Development, Physical Properties, and Logging Response," SPE Deepwater Drilling and Completions Conference, Galveston, TX, September, Society of Petroleum Engineers.
[25] Salehi, S., Khattak, M. J., Ali, N., Ezeakacha, C., and Saleh, F. K., 2018, "Study and Use of Geopolymer Mixtures for Oil and Gas Well Cementing Applications," ASME J. Energy Resour. Technol., **140**(1), p. 012908.
[26] Kamali, M., Khalifeh, M., Saasen, A., Godøy, R., and Delabroy, L., 2021, "Alternative Setting Materials for Primary Cementing and Zonal Isolation—Laboratory Evaluation of Rheological and Mechanical Properties," J. Pet. Sci. Eng., **201**, p. 108455.
[27] Torsæter, M., Todorovic, J., and Lavrov, A., 2015, "Structure and Debonding at Cement–Steel and Cement–Rock Interfaces: Effect of Geometry and Materials," Constr. Build. Mater., **96**, pp. 164–171.
[28] American Petroleum Institute, 2017, *API TR 10TR7, Mechanical Behavior of Cement*, API, Washington, DC.
[29] Blanco, A., Colina, A., Rodriguez, W., and Bolivar, R., 1999, "Effective Pay Zone Isolation of Steam Injection Wells," Latin American and Caribbean Petroleum Engineering Conference, Caracas, Venezuela, April, Society of Petroleum Engineers.
[30] Corina, A. N., Skorpa, R., Sangesland, S., and Vrålstad, T., 2020, "Simulation of Fluid Flow Through Real Microannuli Geometries," J. Pet. Sci. Eng., **196**, p. 107669.

Appendix 7 – Paper VI

Bonding Mechanism of Zonal Isolation Materials to Casing and Pipe Materials

M. Kamali, M. Khalifeh, A. Saasen

SPE Journal, 2022

DOI: 10.2118/209812-PA

This paper is not available due to copyright

Appendix 8 – Paper VII

Long-Term Mechanical Properties Of Barrier Materials For Cementing Operations – Analysis Of Morphology And Micro-Structure

M. Kamali, P. Moreira, M. Khalifeh, A. Saasen

Paper OMAE2022-78634 accepted at the 41st International Conference on Ocean, Offshore and Arctic Engineering OMAE2022, June 5-10, Hamburg, Germany.